Analysis of homogeneous film flows on inclined surfaces and on corrugated sheet of packing using CFD

By the Faculty of Mechanical, Process and Energy Engineering of the
Technische Universität Bergakademie Freiberg

approved

Thesis

to attain the academic degree

Doktor-ingenieur

(Dr. – Ing.)

submitted

by **M.Sc., Kumar Subramanian**
born on 11th April.1982 in Mayiladuthurai (India)

Reviewers: **Prof. Dr. -Ing. habil. Jens-Uwe Repke**
Prof. Dr. -Ing. habil. Günter Wozny

Date of the award : 16th May 2014

ACKNOWLEDGEMENTS

It is my great pleasure to express my gratitude to Prof. Dr. -Ing. habil. Jens-Uwe Repke and Prof. Dr. -Ing. habil. Günter Wozny for giving me an opportunity to perform my doctoral thesis under their guidance. I am very grateful to Prof. Repke for his technical inputs to take my thesis in the right direction.

At this moment, I would also like to extend my thanks to my colleagues Steve and Martin for sharing their technical ideas in the same research area and for helping me out during the experiments. I am also thankful to Mrs. Marita Skupin for assisting during laboratory works.

I would like to thank Stan and Tunc for giving me inputs on CFD simulations especially on meshing and performing post processing of the results. I am very grateful to Dr. Wolfgang Baumann, CFD consultant from ZIB, Berlin for assisting me throughout my thesis during parallel computing in HLRN. I am also thankful to Mr. Thomas Eppinger, License manager for CFD software for assisting me with the license.

I would like to extend my sincere gratitude to the management committee Evonik Stiftung for providing financial assistance for three years during my thesis. Especially my sincere thanks to Mrs. Susanne Peitzmann for assisting me throughout the period with all the kind help possible.

I am also thankful to Mrs. Inge Habisreitinger and Mr. Daniel Weißmann for helping me in official formalities and with technical problems related to computer and network.

I cannot be without expressing my sincere thanks to my colleagues and friends Stan, Hamid, Daniel, Shankui, Lukasz and Song for making the working atmosphere livelier and hear me all the time venting out my happiness and worries. My life in Berlin would not have moved so peacefully without my friends Ananth, Sivanesan, Silvia, Maalolan, Purv and Tamil whom I can rely on during my bad times. I am very grateful to Siva, Tamil, Murali, Susan, Markus and Isabella for reading my thesis and helping me to improve it better. I am also thankful to my cousin Sriram who is one big reason for me to be in Germany and keep on guiding me throughout both professionally and personally. I would like to thank Markus for translating the abstract to German.

Last but not least, I am very much grateful to my dad, mom, brother and Mano for having confidence in me and encouraging me throughout my stay in Germany. I would like to dedicate my thesis to them.

April 15, 2015 **Kumar Subramanian**

ABSTRACT

The key to success in separation of liquid mixtures is the efficient creation and utilization of vapour-liquid contact area. By packing the column with gas-liquid contact devices such as structured packing, the vapour-liquid contact area can be increased. However, the efficiency of these packed columns depends strongly on the local flow behaviour of the liquid and vapour phase inside the packing.

The aim of this work was to develop three-dimensional CFD models to study the hydrodynamic behaviour on the corrugated sheets of packing. Different approaches are possible to simplify the problem and to extend it for more complex flow scenarios. In this work, three-dimensional CFD simulations were performed to study the complete fluid-dynamic behaviour. This was performed in two steps.

As a first step, the developed model was validated with experimental studies using a simplified geometry i.e., an inclined plate. The three-dimensional Volume-of-Fluid (VOF) model was utilized to study the flow behaviour of the gas-liquid countercurrent flow. The influence of the liquid surface tension was taken into consideration using the Continuum Surface Force (CSF) model. The wetting characteristics of liquids with different viscosity (1 and 5 mPas) and contact angle (70° and 7°) were studied for different flow rates. Three different mixtures (water, water-glycerol (45 wt. %) and silicon-oil (DC5)) were considered. Initially, the rivulet width of experiments and simulations were compared and an error of 5 % maximum was determined. The results were also in good agreement with earlier studies. The percentage of wetting due to changes in flow rate, viscosity and contact angle was compared and discussed. For all tested systems, excellent agreement between the experiments and simulation studies was found. In addition, profiles of the velocity in the film at film flow conditions over a smooth inclined plate obtained from simulations were compared with experimental profiles obtained using a μPIV technique. A detailed sensitivity study was also performed in order to understand the changes in the velocity profiles due to small change in liquid flow rate, temperature and inclination angle.

As a next step, the developed model was extended to geometries resembling real corrugated sheets of packing used in industrial applications. In earlier numerical studies of structured packing, geometries were simplified to enable easy meshing and faster computation. In this work, the geometries of corrugated sheets of packing were developed without any

simplification and the flow behaviour was studied using the model validated in the first step. The flow behaviour on sheets with different geometrical modifications such as smooth and triangular crimp surfaces as well as perforations on the sheets were numerically studied and quantitatively compared with experimental studies for the three different fluid test systems. The agreement between the simulations and experiments was within an acceptable range for all system. The difference in the interfacial area between the corrugated sheets of a packing with and without perforation was analyzed and the prediction ability of different empirical correlations for the interfacial area available in literature was also compared and discussed.

Furthermore, the numerical study was extended to understand the influence of the second corrugated sheet. Studying the flow behaviour between two sheets experimentally is very challenging, especially inside opaque packing. The model proved to be a very suitable tool to study the hold-up of the liquid between two sheets, the change in wetting behaviour due to small change in liquid inlet position. The results are also in good agreement with the earlier experimental studies, where researchers measured the liquid hold-up mainly in the region where two corrugated sheets touch each other.

The three-dimensional CFD model was validated to study the flow behaviour on corrugated sheets of packing. The results from the simulations agree very well with findings from the experimental studies in terms of wetting and hold-up.

ZUSAMMENFASSUNG

Der Schlüssel zum Erfolg bei der Trennung von Flüssigkeitsgemischen ist die Ausbildung von Dampf-Flüssig-Kontaktflächen und deren Nutzung. Durch die Installation von Einbauten zur Gas-Flüssig-Kontaktierung in Kolonnen, wie beispielsweise strukturierte Packungen, kann die Kontaktfläche vergrößert werden. Zusätzlich hängt die Trenneffizienz jedoch stark von dem Fließverhalten der Dampf- und Flüssigphase in der Packung ab.

Das Ziel dieser Arbeit war die Entwicklung dreidimensionaler CFD-Modelle, um das hydrodynamische Verhalten von Flüssigkeiten in Packungen, bestehend aus Wellblechen, zu untersuchen. Verschiedene Ansätze sind möglich, um das Problem zunächst zu vereinfachen und dann für komplexe Strömungsszenarien zu erweitern. In dieser Arbeit wurden dreidimensionale CFD-Simulationen durchgeführt, um das komplette fluiddynamische Verhalten zu studieren. Dies erfolgte in zwei Schritten.

Im ersten Schritt wurde das entwickelte Modell anhand experimenteller Studien unter Verwendung einer geneigten Platte als vereinfachte Geometrie validiert. Das dreidimensionale Volume-of-Fluid-Modell (VOF) wurde verwendet, um das Strömungsverhalten im Gas-Flüssig-Gegenstrom zu untersuchen. Der Einfluss der Oberflächenspannung wurde anhand des Continuum Surface Force Modells (CSF) berücksichtigt. Die Benetzungseigenschaften von Flüssigkeiten unterschiedlicher Viskosität (1 und 5 mPas) und Kontaktwinkel (70° und 7°) wurden für verschiedene Fließgeschwindigkeiten untersucht. Drei verschiedene Testmischungen (wasser, wasser-glycerin und silikonöl) wurden betrachtet. Zunächst wurde die Rinnsalbreite von Experiment und Simulation verglichen, wobei der Fehler bei maximal 5 % lag. Die Ergebnisse sind in guter Übereinstimmung mit früheren Studien. Der Benetzungsgrad in Abhängigkeit von Durchfluss, Viskosität und Oberflächenspannung wurde verglichen und diskutiert. Für alle Testsysteme wurde eine sehr gute Übereinstimmung zwischen Experiment und Simulation festgestellt. Zusätzlich wurden simulierte Geschwindigkeitsprofile in den Flüssigkeitsfilmen auf einer glatten geneigten Platte mit denen verglichen, die mittel µPIV-Technik experimentell ermittelt wurden. Eine detaillierte Sensitivitätsstudie wurde ebenfalls durchgeführt, um die Änderung im Geschwindigkeitsprofil aufgrund kleiner Änderungen in der Durchflussrate, der Temperatur und dem Neigungswinkel besser zu verstehen.

Im nächsten Schritt wurde das entwickelte Modell auf Geometrien erweitert, die Wellblechen realer Packungen in industriellen Anwendungen ähnlich sind. In früheren numerischen Studien

zu strukturierten Packungen wurde deren Geometrie vereinfacht, um die Gittergenerierung zu erleichtern und Simulationsrechnungen zu beschleunigen. In dieser Arbeit wurde die Geometrie der Wellbleche ohne jegliche Vereinfachung implementiert und das Fließverhalten anhand der vorher validierten Modelle untersucht. Das Strömungsverhalten bei unterschiedlichen geometrischen Modifikationen, wie beispielsweise glatter und dreieckig gewellter Oberflächen sowie mit Perforationen wurde mithilfe von Simulationen untersucht und quantitativ mit experimentellen Studien für drei verschiedenen Testsystemen verglichen. Die Übereinstimmung zwischen Simulationen und Experimenten war in einem akzeptablen Bereich für alle Testsysteme. Der Unterschied in der Grenzfläche zwischen den gewellten Packungslagen mit und ohne Perforation wurde analysiert und die Vorhersagefähigkeit von empirischen Korrelationen aus der Literatur verglichen und diskutiert

Darüber hinaus wurden die numerischen Studien erweitert, um den Einfluss einer zweiten gewellten Lage zu verstehen. Die experimentelle Untersuchung des Fließverhaltens zwischen zwei Lagen ist aufgrund der fehlenden optischen Zugänglichkeit sehr schwierig. Das Modell erweist sich hier als sehr hilfreiches Tool, um die Änderungen in der Mikro-Skala Ebene und auch den Einfluss auf Benetzungsverhalten, Geschwindigkeitsprofile und Veränderungen in der Strömung zu studieren, wenn die Flüssigkeit durch die Kontaktpunkte der zwei welligen Packungslagen fließt. Die Ergebnisse sind in guter Übereinstimmung mit früheren experimentellen Studien, in denen die meisten Flüssigkeitsanteile in den Regionen festgestellt wurden, an denen sich die beiden Lagen berühren.

Das dreidimensionale CFD-Modell wurde validiert, um das Fließverhalten auf Wellblechen von Packungen zu untersuchen. Die Ergebnisse der Simulationen sind in sehr guter Übereinstimmung mit experimentellen Daten zur Benetzung und zum Holdup.

TABLE OF CONTENTS

TABLE OF FIGURES

LIST OF TABLES

LIST OF SYMBOLS

Latin symbols

$\bar{u}$	Average velocity	m/s
$\dot{V}$	Volumetric flow rate	m^3/s
U_f^n	Volume flux through the face	-
d_{eq}	Equivalent diameter	m
f_i	Interfacial friction factor	-
m_{pq}	Mass transfer from phase p to phase q	-
m_{qp}	Mass transfer from phase q to phase p	-
$\hat{n}$	Unit normal	-
a_{eff}	Effective interfacial area	m^2
a_p	Packing area	m^2
B	Length of the base side of the corrugation	m
D_h	Hydraulic diameter	m
F	F factor	$Pa^{0.5}$
F_{SE}	Surface enhancement factor	-
F_{vol}	Force at the surface as volume force from divergence theorem	
g	Acceleration due to gravity	m/s^2
H	Height of the corrugation	m
h_L	Liquid hold-up	-
N	Surface normal to interface	-
P_{op}	Operating Pressure	bar
Q	Fraction of area covered by specific material (Eq. 2.11)	-
R	Roughness factor	-
S	Length of corrugation side of the corrugation	m
$S_{\alpha q}$	Source term for each phase	-
T	Specific Load	m^3/m^2h
u	Velocity	m/s
U_f	Volume flux through the face based on normal velocity	
u_{max}	Maximum velocity	m/s
V	Volume of the cell	m^3
w	Width of the plate	m
z_1,z_2,z_3,z_4,z_5	Dimensionless constant (Eq. 2.18)	-
Δt	Time step for simulation	s
Δx	Dimension of the cell in direction x	m

Greek Symbols

$\beta_{L,e}$	Effective Liquid flow angle	°
∇	Divergence operator	-
α	Corrugation angle	°
α_q	Volume fraction of the phase q	-
β	Inclination angle	°
β_w	Discount factor as a function of liquid rate	-
δ	Film thickness	m
δ^*	Dimensionless ratio of film thickness	-
ε	Void fraction	-
ε_{fh}	Void fraction of the packing surface	-
θ'	Contact angle for heterogeneous surface (Eq. 2.11)	°
θ_1	Maximum possible contact angle	°
θ_2	Minimum possible contact angle	°
θ_w	Wenzel contact angle	°
θ_y	Young's contact angle	°
κ	Curvature	-
κ	Curvature for free surface	-
μ	Dynamic viscosity	kg/m.s
ν	Kinematic viscosity of the Liquid	m^2/s
ρ	Density	kg/m^3
σ	Surface tension	N/m
σ_{LG}	Surface tension of liquid-gas interaction	N/m
σ_{SG}	Surface tension of solid-gas interaction	N/m
σ_{SL}	Surface tension of solid-liquid interaction	N/m
ω	Mole fraction in liquid phase	-
Ω	Fraction of packing surface occupied by holes	-

Dimensionless constants

A, B	Constants depending on packing type (Eq. 2.17)	-
Fi	Film number	-
Fr	Froude number	-
Ka	Kapitza number	-
Ma	Maragoni number	-
N	Dimensionless constant (Eq. 3.14)	-
Re	Reynolds number	-
We	Weber number	-

Abbreviations

µPIV	Particle Image Velocimetry	-
CA	Contact Angle	°
CFD	Computational Fluid Dynamics	-
CSF	Continuum Surface Force	-
HA	Hydrodynamic Analogy	-
HETP	Height Equivalent to Theoretical Plates	-
HLRN	High performance computing network of Northern Germany	-
HTU	Height of Transfer Units	-
LDV	Laser Doppler Velocimetry	-
REU	Representative Element Units	-
UDF	User Define Function	-
UV	Ultravoilet	-
VOF	Volume of Fluid	-

Subscripts

1,2	Phase 1 and Phase 2	-
eff	Effective	-
g	Gas phase	-
L	Liquid phase	-
Op	Operating	-
q	q^{th} phase	-

1 INTRODUCTION

The key to success in separation of liquid mixtures by distillation depends on the creation and utilization of vapour-liquid contact area. The three major types of distillation equipment's are: Trays, Random packing and Structured packing. Structured packing increased its market share rapidly during the last two decades. Even though the first generation of structured packing was introduced as early as 1940s, it was not used more in industrial applications. The second generation of structured packing began in late 1950s and started penetrating into market by claiming its advantages of low pressure drop per theoretical stages (Kister, 1992). However, their high cost, high sensitivity to solids and low capacity hindered its application in industry. The corrugated-sheet of packing, introduced in the late 1970s, became competent by claiming higher capacity and lower sensitivity to solids while retaining the high efficiency. Therefore, by 1980s, the corrugated sheet of structured packing have drawn accelerated rise in industry (Kister, 1992). The reason for the improvement in efficiency with structured packing is reported as increase in interfacial area created by liquid spreading over the packing surface which is available for mass transfer. Even though the structured packing is well established, the local flow behaviour inside the packing is still not yet well understood. Various efforts have been undertaken by researchers around the world with different approaches to understand more about the local flow behaviour which helps to design the packed column and to increase their efficiency.

The efficiency of the packed column strongly depends on the local flow behaviour of the liquid inside the packing. Since the flow can rapidly change due to the small changes in dimensions of corrugated sheets, it is reasonable to consider the local flow behaviour as a major factor (Repke and Wozny, 2002). Most of the efficiency criteria for structured packing are not known, as the supplier of the packing does not disclose any technical data. Researches were conducted in a different dimension to understand the flow behaviour in micro scale, macro scale and in large scale. Few researchers concentrated on the material of the packing based on the application. Some of the examples of non-metallic packings are ceramic, polymers, gauze packing and SiC packing (Ivanova et al., 2007). Many researchers focused on the geometrical features of the structured packing to improve their performance. To improve the capacity of packing, inclination angle of 60° was proposed (Olujic et al., 2004). Various small changes in the geometry, such as straight edges in the bottom of packing element or in the top of packing element or in both the side of packing element were proposed (Bender and Moll, 2003). The change in efficiency due these modifications was studied in detail and recommendations were made for further studies. Detailed theoretical review of state of the art will be presented in Chapter 2. To increase the wetting characteristics, the surface of the packing was roughened using microstructures (Kister, 1992). Initially, the surface was roughened using two dimensional structures and later it was further extended to three dimensional structures. A detailed analysis of the influence of the size of the microstructures on transport phenomena was presented recently (Kohrt et al., 2011). As discussed above, various efforts have been undertaken to understand the flow in structured packing and to increase their capacity.

Due to the recent improvement in computational power, Computational Fluid Dynamics has been used to calculate the flow behaviour in these structured packing (van Baten et al., 2001a). CFD is foreseen as one of the major tools to complement the experimental efforts. Also, various computational tools help us to understand the flow behaviour in microscopic scale. On the other hand, even this enormous improvement in computational power is not sufficient to study the flow behaviour in whole column as in real industrial applications. Hence, various theories have been presented to simplify and understand the problem better with available computational facility. However, the computational results need to be validated with experimental studies. To understand the hydrodynamics of the liquid-phase flow in structured packing filled with catalyst pellets resembling KATAPAK-S, a Toblerone model was presented and a detailed CFD study was performed to understand the transversal dispersion in structured packed bed. Similarly, efforts have been extended to study the radial and axial liquid phase dispersion and liquid and gas-phase mass transfer within the sandwich structures (Higler et al., 1999;van Baten et al., 2001b;van Baten et al., 2001a;van Baten and Krishna, 2002;van Baten and Krishna, 2001).

The primary aim of this work is to develop a computational model to understand the flow behaviour in corrugated sheet of packing with countercurrent gas flow and to validate it experimentally. To validate the model, initially a simple geometry of smooth inclined plate was used and then the model was further extended to the complex corrugated sheet of packing.

Outline of this thesis

In Chapter 2, theoretical background and various dimensionless correlation used in this work are presented. Various parameters like contact angle and their influence on wetting area and detailed literature review of different hypothesis available for contact angle is presented. Various empirical correlations are available in the literature to determine the effective interfacial surface area. Different approaches proposed by other researchers and the approach used in this work are also discussed. Extensive literature review of experimental and CFD studies contributed to the study of flow behaviour of liquid and gas phase are presented in detail.

In Chapter 3, various geometries resembling the corrugated sheet of packing used in this work are shown along with model equations and their corresponding boundary conditions.

In Chapter 4, the fluid dynamic behaviour of different liquids on the inclined plate is discussed and compared with experimental studies. The hydrodynamics of the inclined plate is studied in two different ways. First, wetting studies for different testing mixtures and secondly, detailed analysis of velocity profiles using μPIV method. The comparisons between experimental and simulation studies are presented and the agreement is found to be very good. The detailed sensitivity analysis was performed to understand the change in velocity profile due to change in flow rate, temperature and inclination angle. Furthermore, the model was also extended to study the influence of the countercurrent flow in the velocity profile.

The model developed in Chapter 4 was extended to study the flow behaviour on corrugated sheet of packing which is presented in Chapter 5. While studying the hydrodynamics of corrugated sheets of packing, different geometrical modifications are considered and studied using simulations. The influence in the flow behaviour due to the modification of triangular and smooth crimp and the changes in wetting due to the presence of perforations were discussed. Various empirical correlations presented in literature for predicting the effective interfacial area was compared and analyzed. Furthermore, the change in liquid flow, hold-up and wetting due to the presence of second corrugated sheet was also discussed. In Chapter 6, some conclusions were presented based on this work and outlook was presented for further studies.

The model developed and utilized in this work serves as a good basis for experimental validation to study the flow behaviour in corrugated sheets of packing. This will help to reduce the experimental effort and to understand the change in fluid-dynamic and in transport phenomena in micro and macro level.

2 THEORETICAL BACKGROUND

2.1 Different flow regimes

The flow of thin liquid layer along the wall with a thickness in the range of 1 mm is known as liquid film. Based on the formation of liquid film, it can be categorized as falling films, shear-driven films, condensing films and impinging jets (Dietze, 2010). Such flows are complex as depicted in Fig. 2.1 and can happen in many of industrial applications including nuclear reactors, condensers, gas turbines, etc. In distillation and absorption columns equipped with structured packing, more such complex flows appear where the liquid film does not develop smooth interface.

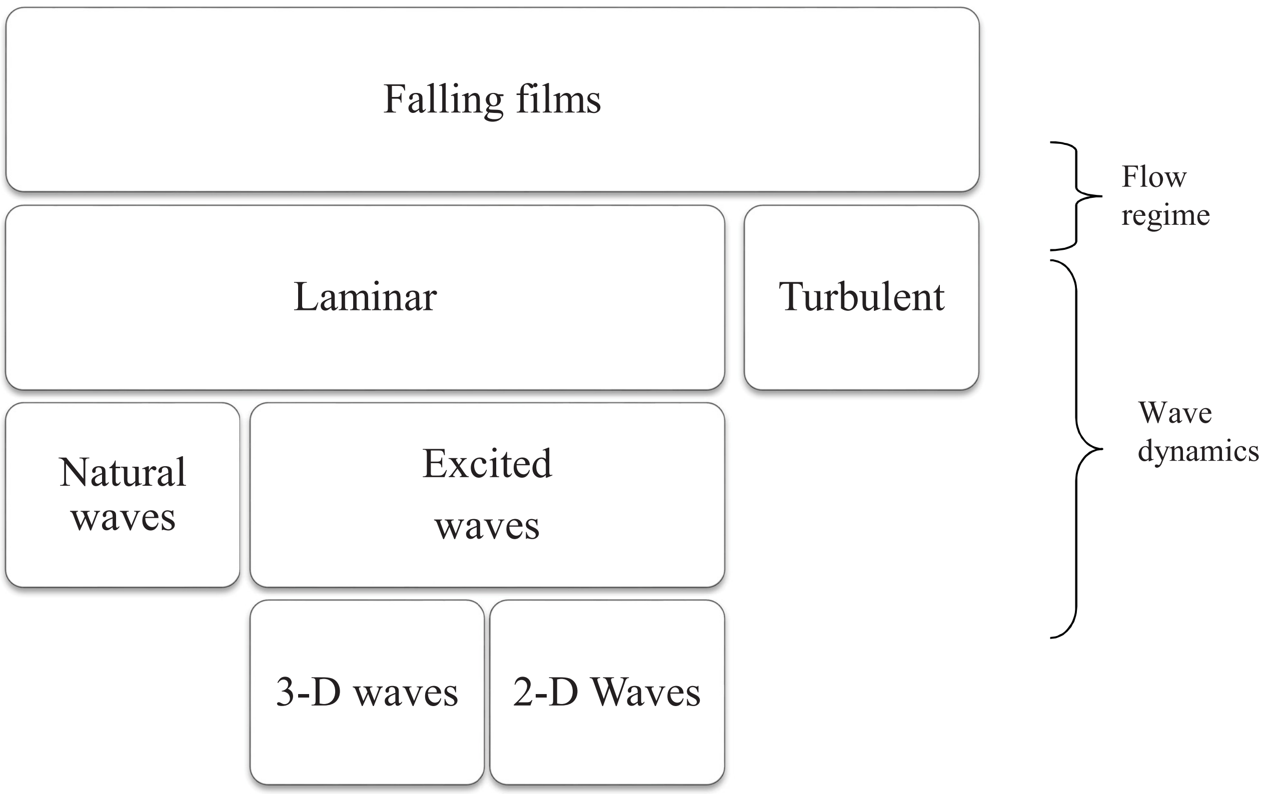

Figure 2.1 Classification of different flow regimes.

Flow regimes can be classified as laminar and turbulent. When the liquid load is very low, it forms a very thin film near the wall and the clear interface between the gas and liquid phase can be seen. With increasing liquid load, the film translates to small waves of the same amplitude in the transient region and develops further to turbulent region where strong waves with different amplitudes arise. As described in Fig. 2.2, the flows in laminar region are considered within the scope of this thesis. Flow regimes can be described using the dimensionless Reynolds number, which is a function of liquid load ($\dot{V}$), kinematic viscosity (ν) and width of the plate (*w*). Reynolds number is defined as follows:

$$Re = \frac{\dot{V}}{w \cdot \nu} \tag{2.1}$$

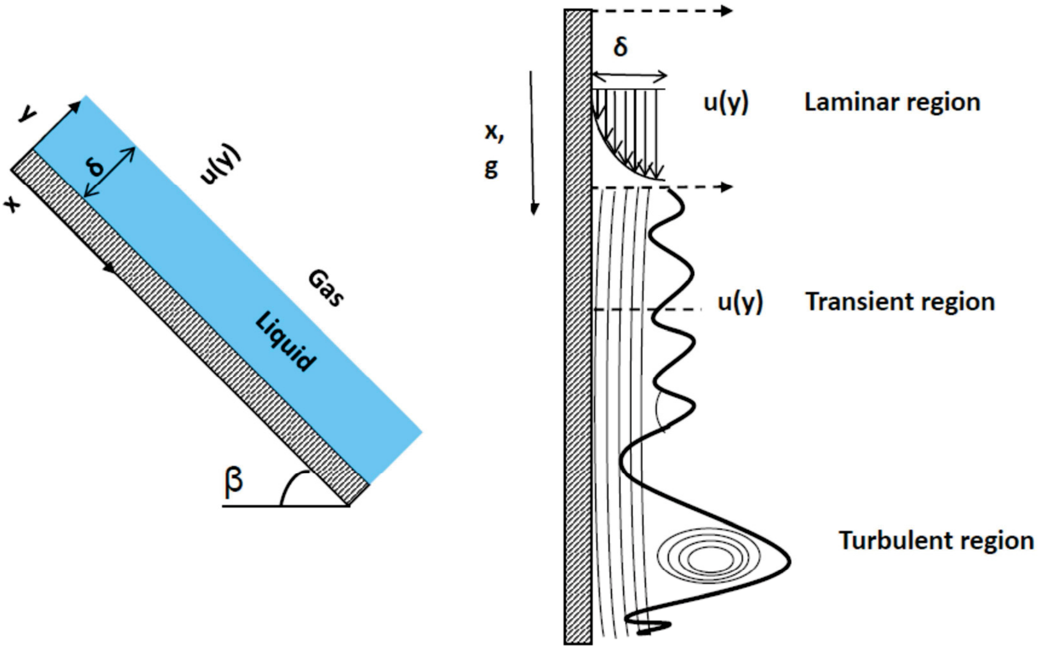

Figure 2.2 Schematic representation of different flow regimes.

Nusselt theory (Nusselt, 1916a;Nusselt, 1916b) defined velocity u(y) as a parabolic profile for laminar flow with wall y = 0 to film thickness of y = δ. (Brauer, 1971) included the influence of inclination angle β to the gravity term. So the velocity profile can be written as

$$u(y) = \frac{g\sin(\beta)\delta^2}{\nu}\left(\frac{y}{\delta} - \frac{1}{2}\left(\frac{y}{\delta}\right)^2\right) \tag{2.2}$$

The film thickness can be calculated using the equation

$$\delta = \left(\frac{3\dot{V}\nu}{g\sin(\beta)\cdot w}\right)^{1/3} \tag{2.3}$$

With the average velocity of

$$\bar{u} = \left(\frac{g\sin(\beta)\nu}{3}\right)^{1/3} \cdot Re^{2/3} \tag{2.4}$$

and maximum velocity of

$$u_{max} = \frac{3}{2}\,\bar{u} \tag{2.5}$$

Where, g is the acceleration due to gravity (9.81 m/s^2), *w* is the width of the plate and $\dot{V}$ is the volumetric flow rate (m^3/s).

Other dimensionless numbers were also used while describing the film flow behaviour. To describe the gravity driven flow, Froude number (Fr) is used which is defined as

$$Fr = \frac{\bar{u}^2}{g.\,\delta} \tag{2.6}$$

Another number utilized while analyzing the interface between two phases in multiphase flows and in the flow where surface tension plays a vital role is Weber number (We). Weber number can be defined as

$$We = \frac{\rho_L u^2 \delta}{\sigma} \tag{2.7}$$

Kapitza number is used to describe the film flow behaviour with waves by including the influence of the surface tension. It is defined as

$$\frac{1}{Ka} = \frac{\rho\sigma^3}{g\,\mu^4} = \frac{Re^4 Fr}{We^3} \tag{2.8}$$

where, Ka is Kapitza number.

2.2 Approach to the problem

Due to the very complex geometry and big size, it is very tedious to study the flow behaviour inside the packed columns directly. It is also very complicated and tedious to understand the flow behaviour in the whole column. However, it is very important to understand the local flow behaviour inside the small packing structure and then to use the results for further scale up studies. Recent improvement in computational speed is also not enough to measure the behaviour inside a completely packed column.

The approach utilised in this work is shown in Fig. 2.3. To simplify the problem, 3D smooth inclined plate will be initially used to study the flow behaviour using a CFD model (Fig. 2.3) and validate it with experimental studies using µPIV method. Further, the validated model can be extended to real industrial corrugated sheets of packing that resembles the packing used in industrial applications.

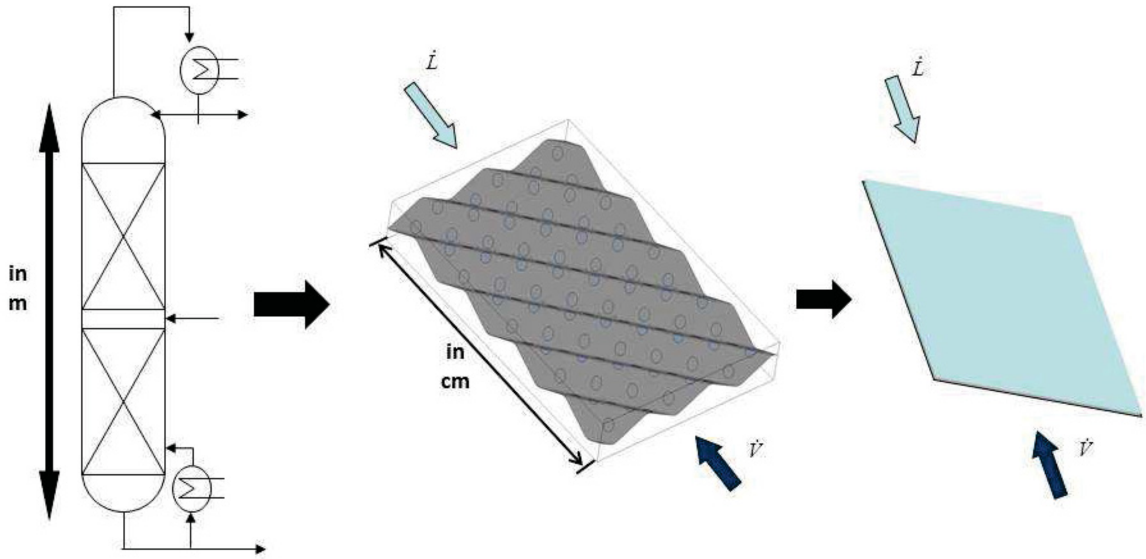

Figure 2.3 Approach adapted in this work to study the flow behaviour.

2.3 Wetting/Contact Angle

2.3.1 Contact angle

Wetting is the ability of the liquid to maintain contact with a solid surface, resulting from intermolecular interaction between the solid surface and the liquid. The force balance between adhesive and cohesive forces determines the degree of wetting as shown in Fig. 2.4. The wetting phenomenon can be explained in terms of contact angle. The contact angle θ_y is the angle in which the liquid-vapour interface meets the solid-liquid interface. Young (Young, 1805) defined the contact angle as the ratio between difference to the surface tension of solid-gas and solid-liquid interaction and surface tension of liquid-gas interaction. Young's contact angle is shown in Eq. (2.9)

$$cos\,\theta_y = \frac{\sigma_{SG} - \sigma_{SL}}{\sigma_{LG}} \tag{2.9}$$

Where, θ_y = Young contact angle.

σ_{SG} = surface tension of solid-gas interaction.

σ_{SL} = surface tension of solid-liquid interaction.

σ_{LG} = surface tension of liquid-gas interaction.

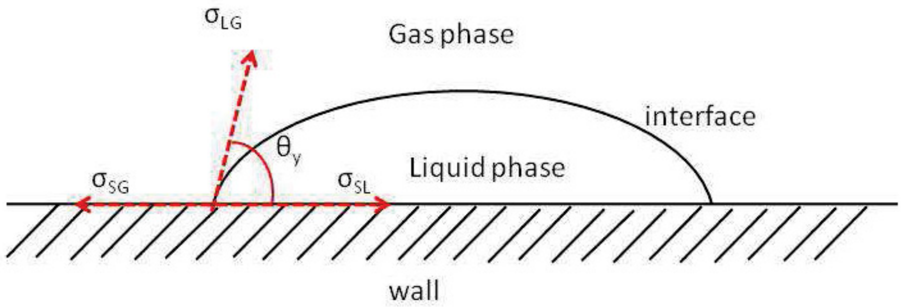

Figure 2.4 The pictorial representation for the contact angle measurement.

A contact angle less than 90° (low contact angle), the fluid will spread over a large area of the surface, and the wetting will be high. Contact angles greater than 90° (high contact angle) generally means that wetting of the surface is unfavorable so the fluid will minimize the contact with the surface and form a compact liquid droplet.

Table 2.1 The various degrees of wetting and their strength of solid-liquid and liquid-vapour interactions with respect to contact angle (Young, 1805)

Contact Angle	Degree of Wetting	Strength of	
		Solid-liquid interaction	Liquid-vapour interaction
θ_y = 0	Perfect wetting	Strong	Weak
0° < θ_y < 90°	High wetting	Strong	Strong
		Weak	Weak
90° < θ_y < 180°	Low wetting	Weak	Strong
θ_y = 180°	No wetting	Weak	Strong

Young's contact angle measurements were performed on smooth surface. However, in most of the practical circumstances, liquid interacts with a rough surface that causes deviation of the contact angle (Wenzel, 1936). Wenzel was the first researcher to express the influence of roughness on contact angle. He defined the contact angle including roughness factor R.

$$\cos\theta_w = R\cos\theta_y \tag{2.10}$$

where, θ_w = Wenzel contact angle (rough surface)

θ_y = Young contact angle (smooth surface)

R = Roughness factor; ratio of effective surface to the geometric surface.

(Cassie and Baxter, 1944) later studied in detail the influence of roughness on contact angle. (Cassie, 1948) defined contact angle θ' for heterogeneous surface as

$$\cos\theta' = Q_1\cos\theta_1 + Q_2\cos\theta_2 \tag{2.11}$$

Where θ_1 and θ_2 are the maximum and minimum possible angles and Q_1 is the fraction of the surface having contact angle θ_1 and Q_2 is the fraction having angle θ_2.

The influence of surface tension gradients on the performance of a small distillation column was studied in detail (Zuiderweg and Harmens, 1958). A 'positive system' as a binary one in which the liquid surface tension increases as the volatile component is removed from the liquid mixture. A 'negative system' would show the reverse effect. Thus, for a positive system, transfer to the vapour phase of a low-surface-tension component would locally increase the surface tension such that liquid from elsewhere would be attracted to that place, causing better liquid spreading and increased mass transfer area. Conversely, loss of a high surface tension component would cause liquid to flow away from that spot, possibly leaving dry patches.

A series of theoretical studies on the effect of roughness on wetting of an idealized sinusoidal surface were published (Johnson and Dettre, 1964a;Johnson and Dettre, 1964b;Dettre and Johnson, 1964;Dettre and Johnson, 1965). A hypothesis of advancing angle and receding angle was proposed and confirmed that roughening a surface increases the advancing angle and decreases the receding angle.

(Ponter et al., 1967) studied the effect of different wetted wall lengths and surface roughness during absorption. After a series of studies, they reported that increase of surface roughness increases the wetting and along with surface roughness, texturing of surface can improve wetting.

(Oliver et al., 1980) studied the influence of liquid spreading for different surface roughness experimentally. The hysteresis was observed in all the surface roughness studies. Defining a single contact angle for all these different situations was questioned.

(Ponter and Au-Yeung, 1984) studied the influence of liquid viscosity on effective interfacial area in packed columns and compared with other theoretical correlations present in the literature. High order of disagreement was observed between each method.

After extensive experimental study, (Shi and Mersmann, 1985) developed a correlation for the effective interfacial area in packed columns taking into account the influence of liquid properties like surface tension, contact angle and viscosity. They have studied eight different materials from stainless steel to different polymers, 4 different liquids ranging in viscosity from 1 to 21 cP and surface tension of 23 to 72 mN/m. They have reported the strong influence of contact angle on the effective interfacial area and the fact that these properties change considerably during long-time operation of the distillation column, which may be problematic for the column designers.

(McGlamery, 1988), in his studies on film flow characteristics on textured metal surfaces, measured the contact angles of water, ethylene glycol and ethanol in the presence of carbon dioxide or oxygen. Eight different types of textured surfaces were tested and concluded that roughness (grooves) parallel to the direction of spreading decreases the apparent contact angle, whereas roughness normal to the direction of spreading has the reverse effect.

(Stoter et al., 1993) studied the maldistribution of structured packing. In their work, they discussed the wetting characteristics of structured packing and the influence of liquid properties on wetting. Different testing mixtures were selected in order to study the influence of surface tension, viscosity and wetting tests on the effective area. They developed discrete cell model based on average mass, momentum and energy equations which enables the prediction of velocity profiles.

The flow behaviour of liquid on textured surfaces especially considering the influence of contact angle was studied experimentally. Both smooth and corrugated surfaces were used and the contact angle was measured using the Wilhelmy plate method by (Shi and Mersmann, 1985). They reported the hysteresis effect on measuring contact angle similar to the report of (Shi and Mersmann, 1985) and (McGlamery, 1988). They also compared the wetting behaviour of liquids with similar surface tension and different viscosities. It was observed that a contact angle decreases with an increase in surface roughness or surface texturing which is in accordance to Wenzel Equation (Nicolaiewsky and Fair, 1998).

The influence of surface tension on the performance of packing was reported as the change in effective packing area. When the surface tension was increased, the fractional area decreases by approximately a factor of 2 on going from 250Y to 500Y packing. The similar tests at reduced surface tension showed that the area of 250Y was unchanged, whereas that of 500Y increased by 50%. This indicates that, at high surface tension, access to the surface of the 500Y packing was being inhibited and lowering the surface tension served to maximize the effective area of the packing (Tsai et al., 2008).

There is a gap in predicting the wetting behaviour on corrugated sheets of packing by taking surface tension, contact angle and other material properties into account. This will be addressed in next sections.

2.3.2 Effective Interfacial area

The effective interfacial area (a_{eff}) is the surface area available for mass transfer and can be related to the magnitudes of both individual mass transfer coefficients and liquid holdup. This is also related to the total packing surface area per unit volume, a_p.

For completely wetted surface, (Bravo et al., 1985)

$$a_p = a_{eff} \tag{2.12}$$

For partially wetted packing eg., gauze packing (Fair and Bravo, 1990)

$$a_p = \beta_w a_p \tag{2.13}$$

where, β_w is the discount factor that is the function of liquid rate and surface wettability.

β_w = 0.1 – 0.3 , for poorly wetted surface.

β_w = 0.8 – 1.2 , for well wetted surface.

An interfacial area in the case of structured packing was found to be relatively independent of gas flow rate but highly dependent on the liquid flow rate (Rocha et al., 1993).

The effective interfacial area was modelled as the primary function of total packing area a_p, and the contact angle between the liquid-solid interface based on the fluid hydraulics over an inclined plane. (Shi and Mersmann, 1985). Equation 2.14 was given by (Rocha et al., 1996).

$$\frac{a_{eff}}{a_p} = 29.12\, F_{SE}(We_L Fr_L)^{0.15}\left[\frac{S^{0.359}}{Re_L^{0.2}\varepsilon^{0.6}(1-0.93\cos\theta_y)(\sin\alpha)^{0.3}}\right] \tag{2.14}$$

where, F_{SE} = surface enhancement factor (for mellapak, F_{SE} = 0.35).

Later, the expression for interfacial area was developed that could be applied for any kind of packing in counter-current flow (Billet and Schultes, 1999).

$$\frac{a_{eff}}{a_p} = 1.5\left(a_P d_{eq}\right)^{-0.5} Re_L^{-0.2} We_L^{0.75} Fr_L^{-0.45} \tag{2.15}$$

where, Re_L, We_L, Fr_L are the dimensionless Reynolds, Weber and Froude number for the liquid phase and d_{eq} is the equivalent diameter.

Another technique of CO_2-NaOH absorption-chemical reaction technique was used to determine the effective interfacial area for Mellapak structured packings (de Brito et al., 1994). Based on the results, the ratio of effective interfacial area and the total packing area can be related as

$$\frac{a_{eff}}{a_P} = 0.465 \left(\frac{\rho_L u_L}{\mu_L a_P}\right)^{0.3} \tag{2.16}$$

Another simple relationship was given by (Olujic et al., 1999) to determine the effective interfacial area for Montz-pak B1-250 type of packings based on the experimental results of (Stoter et al., 1993).

$$\frac{a_{eff}}{a_P} = \frac{1-\varepsilon}{\left(1+\frac{A}{u_L^B}\right)} \tag{2.17}$$

where, ε is a void fraction of the packing surface i.e., the fraction of surface area occupied by holes (0.1 for Montz-pak BSH, Mellapak). A and B are constants dependent on packing type and size (e.g. $A = 2.143*10^{-6}$ and $B = 1.5$ for Montz-pak BSH).

After analyzing many organic and aqueous systems for reliable HETP or HTU values, an empirical correlation for the effective interfacial area that holds good for all types of Mellapak was derived (Duss et al., 1997).

$$a_{eff} = z_1 \left(\frac{T_L}{a_P}\right)^{z_2} \left(\frac{\sigma}{z_3}\right)^{f_{L,a}\left(\frac{T_L}{a_P}\right)} \mu_L^{z_4} f_F(F)\, a_P^{z_5} \tag{2.18}$$

where, z1, z2, z3, z4 and z5 is dimensionless constants, $f_{L,a}$ (Q_L/a_p) is a dimensionless function of the specific liquid load and the total packing area and $f_F(F)$ is a dimensionless function of the F-factor, F.

The interfacial area was also modelled as a function of liquid superficial velocity and density (Spiegel and Meier, 1988).

$$a_{eff} \propto (\rho_L u_L)^{0.2} \tag{2.19}$$

The proportionality constant for the above relation need to evaluate from the test data.

Another model considering the flow channel similar to the bundle of column with diameter d_e, the inclination angle of α with respect to the horizontal, film thickness based on Nusselt film thickness δ was presented (Brunazzi et al., 1995).

$$\frac{a_{eff}}{a_p} = \frac{d_{eq}}{4}\left(\frac{h_L}{\varepsilon}\right)^{1.5}\left[\frac{\rho_L g \varepsilon\,(\sin\beta)^2}{3\,\mu_L u_L}\right]^{0.5} \tag{2.20}$$

For random packing, (Onda et al., 1968) presented a correlation

$$\left(\frac{a_{eff}}{a_P}\right)_{onda} = 1 - exp\left[-\,1.45\,\left(\frac{0.075}{\sigma}\right)^{0.75}\left(\frac{\rho_L u_L}{a_P \mu_L}\right)^{0.1}\left(\frac{a_P u_L^2}{g}\right)^{-0.05}\left(\frac{\rho_L u_L^2}{\sigma_L a_P}\right)^{0.2}\right] \tag{2.21}$$

Considering the Onda model, (Olujic et al., 2004) presented a correlation for effective interfacial area.

$$\frac{a_{eff}}{a_P} = \left(\frac{a_{eff}}{a_P}\right)_{onda}(1-\Omega)\left(\frac{\sin 45}{\sin\beta_{L,e}}\right)^{n} \tag{2.22}$$

Where,

$$n = \left(1-\frac{a_P}{250}\right)\left(1-\frac{\beta_{L,e}}{45}\right) + \,ln\left(\frac{a_{e,onda}}{250}\right) + \left(0.49-\sqrt{\frac{0.101}{P_{op}}}\right)\left(1.2\,-\frac{\beta_{L,e}}{45}\right) \tag{2.23}$$

$$\beta_{L,e} = arctan\left(\frac{\cos(90-\beta)}{\sin(90-\,\beta)\,cos[arctan(b/2h)]}\right) \tag{2.24}$$

These correlations described in this section will be discussed in detail in section 5.2 to understand the prediction of wetting area.

2.4 Geometrical parameters of the Corrugated Sheet of Packing

Geometrical features of corrugated sheets of packing plays a crucial role in flow behaviour inside the packing. The surface of the corrugated sheets can be grooved, lanced, textured or smooth. The sheets may be perforated or unperforated. The sheets on each element are arranged at a fixed angle to vertical. Adjacent elements are rotated so that the sheets of one element at a fixed angle to layer below (Kister, 1992).

The corrugation size defines the opening between adjacent corrugated layers (see Fig. 2.5). The ratio of B to h, S to h, and the crimp angle (β) define the geometry of the flow channel and of the vapour-liquid contact zone. Packing can be classified based on the specific surface area. Crimp angle varies from 28˚ to 45˚ and base-to-height ratios range from 2:1 to 4:1. Most of the packing are not a strictly triangle as shown below but is the rounded top apex. Corrugation angle (α) also plays important role in deciding the capacity of the packing.

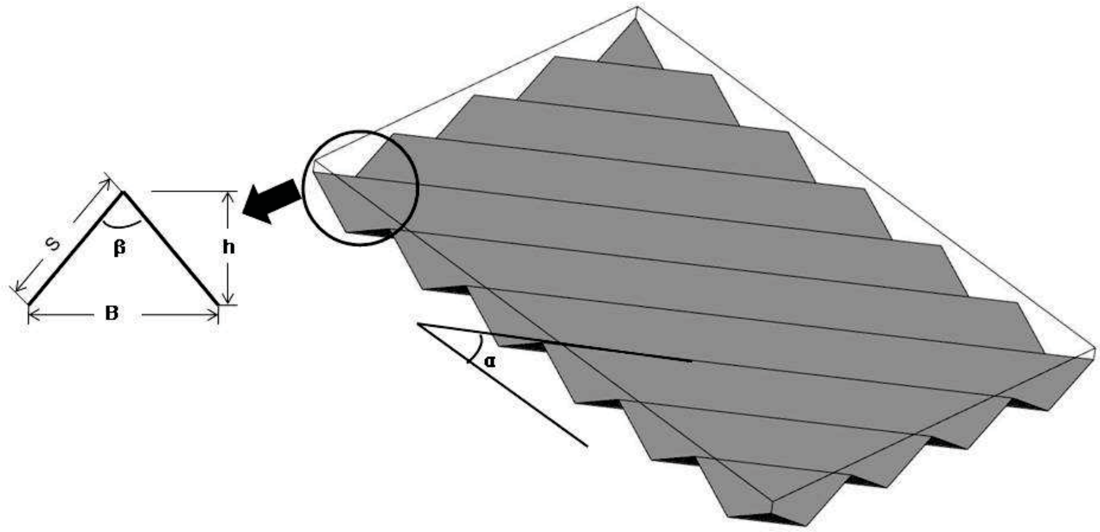

Figure 2.5 Elementary geometry details of the corrugated sheet of packing.

2.4.1 Element Geometry

Due to corrugations, vapour and liquid flow through a single element spreads in a series of parallel planes. To have better spreading, each element is rotated at a certain angle with respect to the element below. The angle of rotation and element height affect the extent of vapour and liquid spread in a structured packing. For this reason, element height is relatively short (typically 20 to 28 cm) and the angle of rotation is around 90˚. As mentioned earlier, corrugation angle of about 45˚ to the vertical, enables good drainage of liquid and avoid stagnant and liquid accumulation, and small enough to prevent gas from bypassing the metal surfaces.

The liquid hold-up of three different structured packing with different crimp angle and specific surface area using gamma ray absorption technique was measured. Also, derived the empirical equation for the hold-up as a function of liquid load, liquid viscosity and specific surface area (Suess and Spiegel, 1992).

The result of two different packing series from Montz GmbH namely, B1 (embossed sheet metal, non-perforated) and BSH (expanded metal, perforated) packing were studied. In total, six different packing with two different corrugation angles of 45° and 60° and two different specific surface areas of 250 and 400 m^2/m^3 was investigated. The outcome showed that increasing the corrugation angle decreases the pressure drop, increases the capacity and decreases the mass transfer. BSH packing showed a slight larger capacity than B1 packing and the reason can be attributed to the presence of holes in the surface. The influence of the corrugation angle on the performance of the packing was presented (Olujic et al., 2000).

An idea of inserting a monolith like structure between the two corrugated sheets of packing has also been studied. In this way, specific surface area was observed to be increased considerably. Although, the increase in surface area led to significant reduction in pressure drop, accompanied by an appreciable capacity increase with respect to that of original packing. However, the closed channel structure proved to be a detrimental effect on mass transfer efficiency (Behrens et al., 2001).

The influence of change in geometry in both capacity and pressure drop was investigated extensively. Various modifications were made in the geometry like height-staggering, packing sheets flattened end of the bottom part, both flattened ends, with only end flattened, packing sheets in which the corrugation on the bottom and top is bent vertically, with only the bottom part is bent vertically (see Fig. 2.6). For the modification with flattened edges of packing sheets, the capacity increase was about 55%. Height staggered sheets and sheets in which the corrugations at the bottom and top side are bent to the vertical showed an increase in capacity of about 38%. While the use of the modifications on the top side only reduced the pressure drop but did not enhance the capacity, these tested modifications at the bottom side resulted in the substantial capacity increase (Bender and Moll, 2003).

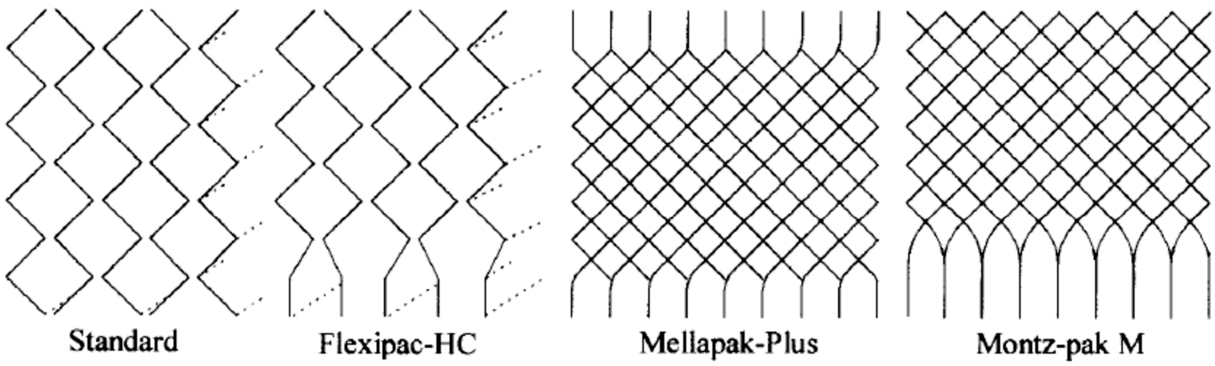

Figure 2.6 Different elementary geometrical modification of corrugated structured packing.

The effect of opening on the performance of the structured packing was studied. Two different opening angles of 90° and 20° were studied both numerically and experimentally. It was also presented that when the opening angle was decreased from 90° to 20°, pressure drop of the packing could reduce by 35% and mass transfer could increase by 13% compared to Mellapak packing having the same specific surface area (Luo et al., 2008).

2.4.2 Surface features

Most of the structured packing surface have roughened, or enhanced surfaces that assists the lateral spread of liquid, promotes film turbulence and enhances the area available for the mass transfer. The measurements performed in the laboratory scale showed that mass transfer efficiency and wetter area are enhanced by textured surfaces. The extent to which mass transfer was improved varies with type of texturing. Texturing is of various types like grooving, lancing, shallow embossing and deep embossing. The different examples of the surface textures are shown in Fig. 2.7. In Fig. 2.7 (a) and (b) represents the corrugated sheet with 2 D textures, Fig. 2.7 (c) represents the corrugated sheets without micro textures, Fig. 2.7 (d) shows the corrugated sheets with 3D microtextures and perforations, whereas Fig. 2.7 (e) shows the corrugated sheets with 3D microtextures without perforations.

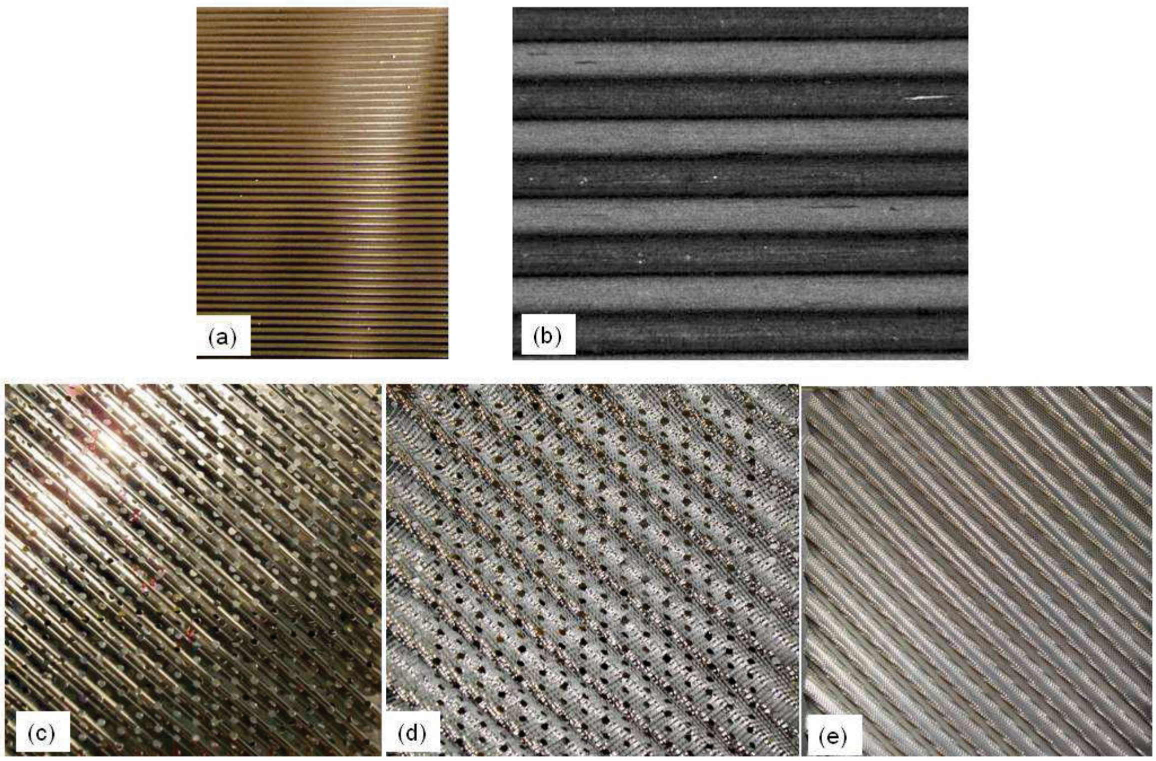

Figure 2.7 Different packing used in industrial applications; (a) & (b) 2D surface textures, (c) Smooth, perforated; unperforated (d) Grooved, perforated; (e) 3D – Embossed, unperforated.

The surface of most of the structured packing contains perforations. The holes serve as communication channels between the upper and lower surface of each sheet. When there are no holes, both sides of a sheet will be wet only at low liquid rates. At high liquid flow rates, the liquid will run down the top surface with little liquid wetting the bottom surface. This may cause a reduction in efficiency as liquid flow rates are raised.

Some major types of packing are tabulated in Table 2.2. Various microstructures such as grooves, lances, embossed surfaces are seen along with the presence of perforations and corrugation of 45° and 60°. Due to complication in meshing, the influence of microstructures was not considered within the scope of this work.

Table 2.2 Different corrugated sheet of packing available in industrial application

Name of packing	Supplier	Surface textures	Crimp apex	Perforations	Corrugation angle
Mellapak	Sulzer Chemtech	Grooved	Sharp	Yes; holes	45˚ or 60˚
Gempak	Glitsch Inc	Lanced	Sharp	Yes; holes	45˚
Montz B1	Julius Montz	Embossed	Sinusoidal	No	45˚
MAX-PAC	Jaeger Products	Smooth	Sharp	Yes ; W-shape	45˚
Montz BSH	Julius Montz	Expanded metal surface	Sharp	No	45˚
Flexeramic	Koch Engineering company	Smooth	Round	No	45˚
Intalox high performance structured packing	Norton Company	Deeply embossed	Flat	Yes; tiny	45˚

Various research studies mainly experimental work have been contributed exclusively to study the influence of surface textures on flow behaviour and their further impact on mass transfer.

The effect of 2 dimensional roughness on the flow behaviour and hence in gas-liquid absorption was reported (Davies and Warner, 1969). They observed that the rate of absorption of CO_2 into water flowing over a plate with large scale roughness can go up to 3.5 times faster than a smooth plate. The results are also compared with theoretical correlations. Two dimensional roughness considered and other factors are shown in Fig. 2.8.

Similarly, various research contributions are presented to know the influence of film flow over complex and periodic surfaces (Zhao and Cerro, 1992;Shetty and Cerro, 1993;Shetty and Cerro, 1998).

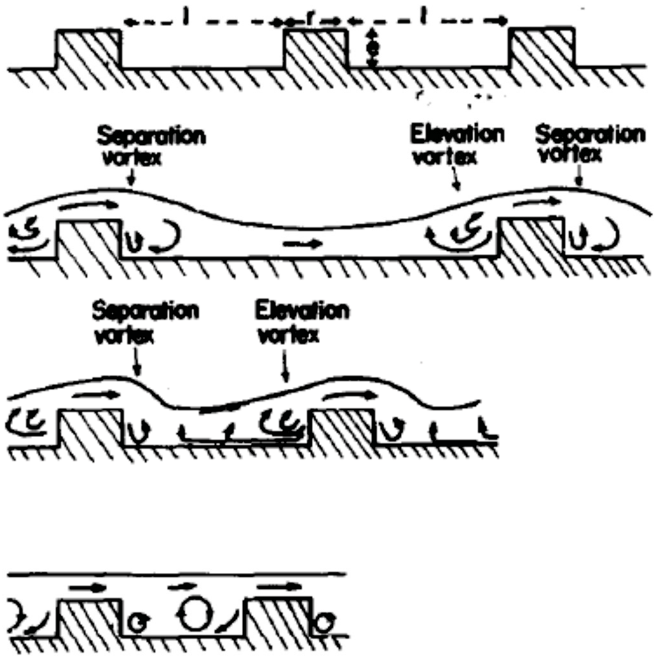

Figure 2.8 Different 2D roughness behaviour studies by (Davies and Warner, 1969).

Different discussion regarding the instability and eddies in viscous flow over inclined wavy planes are reported (Wierschem and Aksel, 2003;Wierschem et al., 2008).

The gravity-driven flow of a liquid film down an inclined wall with oblique two-dimensional, orthogonal three-dimensional, hexagonal three-dimensional corrugation was considered. A perturbation analysis for small-amplitude corrugations was performed where in the wall geometry was expressed as Fourier series consisting of linear superposition. The reduction in surface deformation was reported for three-dimensional geometry than two-dimensional corrugations (Luo and Pozrikidis, 2007;Luo, 2006;Blyth, 2006).

Recently, the influence of two dimensional and three dimensional textures on the structured packing was studied at microscopic level using micro PIV and PTV (Paschke, 2011). Velocity profiles on the three dimensional microstructures in Montz Pak and the change in velocity vectors on a different region of small textures for was analyzed systematically using μPIV. Three dimensional microstructure analyzed is shown in Fig. 2.9.

The impact of liquid-side controlled mass transfer in falling liquid films was quantified experimentally. Micro textures used in industrial applications close to 1mm were analyzed. It was also reported that texture can significantly influence the mass transfer coefficient and it can increase up to 90% comparing the flat smooth surface. More detailed review of various two and three dimensional surface textures on film flows have been presented elsewhere (Kohrt, 2011).

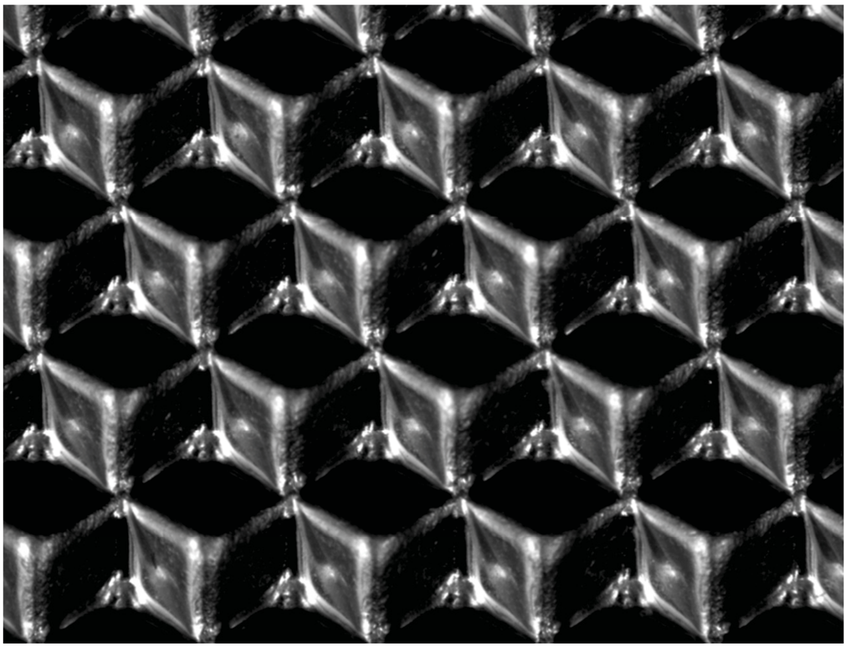

Figure 2.9 Closeup view of tetrahedral microstructure (Paschke, 2011).

In general, it is very clear that the presence of surface textures increases the interfacial area and wetting which in turn increases the mass transfer. Even though lot of experimental studies are available, no empirical correlations or theoretical models are available in-order to describe the wetting on corrugated sheet of packing with micro textures on the surfaces.

2.5 CFD studies and other approaches

2.5.1 Mesoscale - Microscale approach

A new predictive combined mesoscale-microscale methodology was developed to study the fluid dynamics occurring on the macro scale in structured packing in the column. (Petre et al., 2003;Larachi et al., 2003). The entire structured packing is divided into five different Representative Element Units (REU) as shown in Fig. 2.10 and hence the dry pressure drop can be calculated individually and the total pressure drop can be calculated by summing up all the individual pressure drop in different REU's. This requires less computing power. The approach was validated using experimental dry pressure drop for five different packing types.

Later, a two-fluid hydrodynamic model was developed based on volume average mass and momentum balance equations for the counter-current gas-liquid structured packing. The two parameters i.e., the laminar and turbulent Ergun constants were estimated using the above mentioned mesoscale-microscale approach and the results were validated with published literature data related to pressure drop, liquid holdup and wetted area under various conditions (Iliuta et al., 2004;Iliuta and Larachi, 2001).

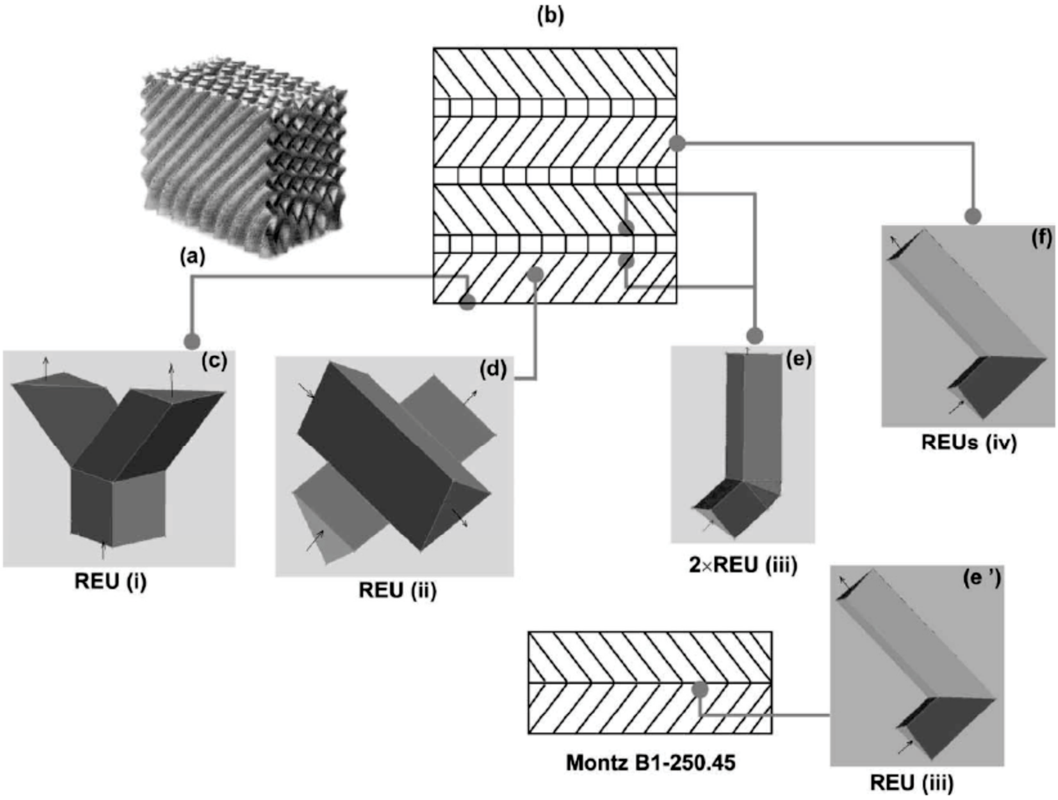

Figure 2.10 Typical REU's (a) Montz pack (b-e) 5 different REU's as proposed by (Petre et al., 2003).

Recently, the same methodology was adopted to study the dry pressure drop for developed Gas flow in structured packing using CFD. Different turbulence models were tested to match with the theoretical correlations and the mean relative error was around 6% (Said et al., 2011).

One of the REU's presented in the above work i.e., the criss cross junctions were further extended to have 4 channels as shown in Fig. 2.11 and the flow behaviour and mass transfer was studied (Chen et al., 2009). Liquid holdup, wetted area and HETP was compared between experiment data, CFD study and the model developed by (Gualito et al., 1997).

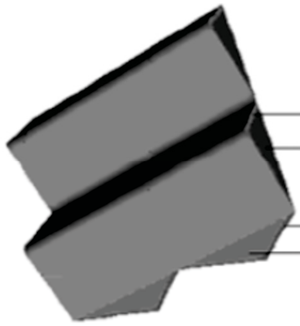

Figure 2.11 Representative element unit studied by (Chen et al., 2009).

2.5.2 Multiscale approach

A multi-scale approach for analyzing the gas-liquid flows in structured packing was presented (Raynal et al., 2004b) as shown in Fig. 2.12. Due to the limitation in the computational resources, two phase flow calculations with a large 3D geometry is presently impossible. Calculations are therefore performed by combining 2D and 3D geometry. At first step, the irrigated packing calculations, i.e. two-phase gas-liquid flow, are carried out in a 2D geometry to determine liquid holdup. In the second step, dry packing calculations i.e., only gas flow is carried out in 3D geometries to determine pressure drop. Finally, combining these two pieces of information in the last step, two-phase flow pressure drop across the packing is calculated. Further, simulations are carried out on a very large scale considering the packed bed as porous media, the latter being characterized by pressure drop coefficients obtained from earlier steps (Raynal et al., 2004b). Pressure drop calculations from simulations are compared with experiments conducted using gamma tomography and all the model values from CFD were within 20% of experimental values.

The same method was further extended to study the influence of texture on corrugated sheets of packing. As described above, the influence of textures was incorporated in the first step of CFD simulations and the rest of the calculations are carried out (Raynal et al, 2004).

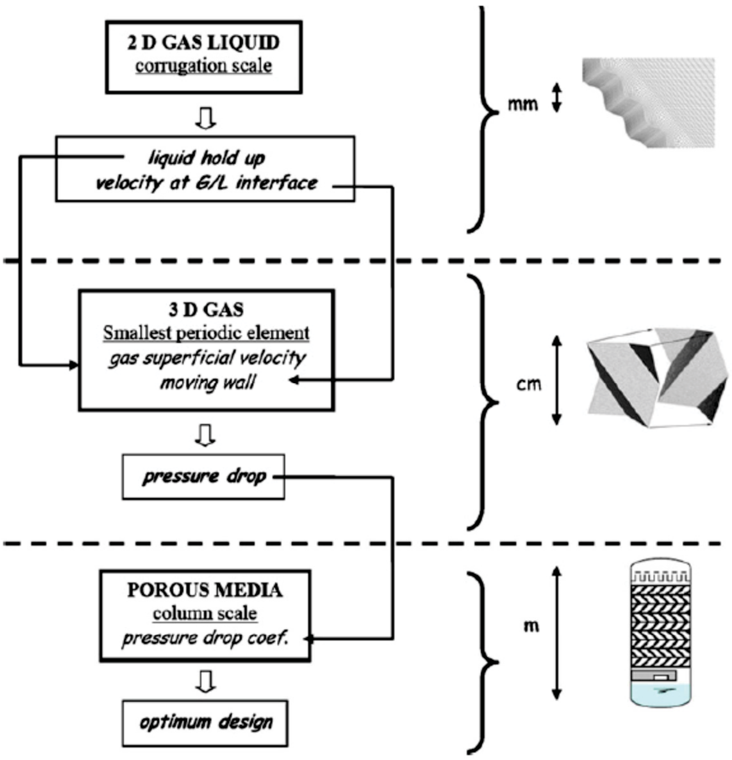

Figure 2.12 Schematic representation of calculation strategy using multiscale approach (Raynal et al., 2007).

2.5.3 Hydrodynamic Analogy approach

The Hydrodynamic Analogy (HA) approach was proposed to describe the hydrodynamics and transport of the process where the exact location of the phase boundaries is not available. The idea of this approach is to replace complex hydrodynamics in column with geometrically simple flow patterns. The idea of this hydrodynamic approach is presented in Fig. 2.13 (Shilkin and Kenig, 2005).

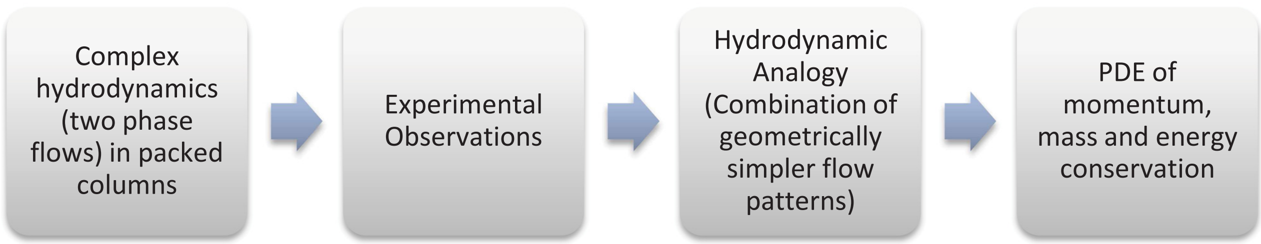

Figure 2.13 Hydrodynamic modelling approach presented by (Shilkin et al., 2006).

The simplified geometric representation of packing was considered in the physical model. It consists of a bundle of channels with identical cross sections as shown in Fig. 2.14. The inner surfaces of these channels are wetted by downward flowing liquid, whereas the rest of the volume is occupied by a countercurrent vapour flow. Both flows are presumed to be laminar and fully developed within intervals of certain length and totally mixed between the channels. The interval lengths for each phase represent the packing specific model parameters and are derived from the packing geometry (Shilkin et al., 2006).

The Hydrodynamic Analogy model is extended to govern a reactive stripping process with heterogeneously catalyzed liquid-phase reactions. It is also compared with experimental investigation and proved that the extension of the Hydrodynamic Analogy model to the reactive column internal is possible (Brinkmann et al., 2010).

Recently, the HA method was also extended to develop an energy efficient packing for vacuum distillation. A two-step procedure was adopted. As the first step, the pressure drop and the local eddy viscosity distribution was calculated using CFD methods. These are used as input for hydrodynamic approach to calculate the packing separation efficiency (Shilkin et al., 2010).

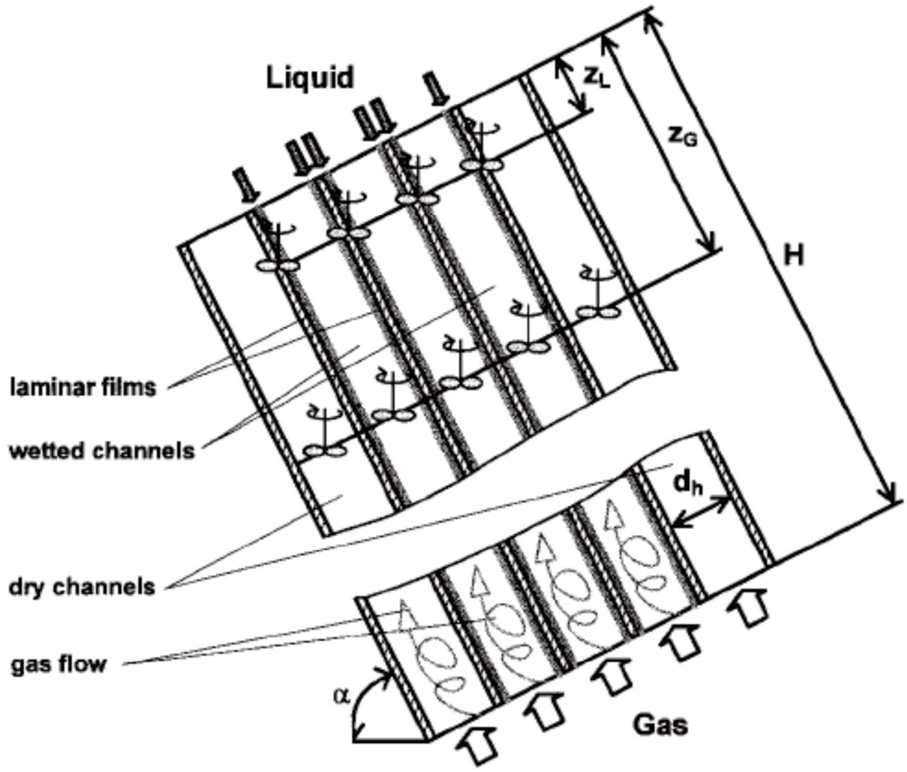

Figure 2.14 Schematic representation of model presented by (Shilkin et al., 2006).

2.6 CFD Studies on Structured packing – a short review

The mathematical model (Arbogast et al., 1990) developed to calculate flow in porous media was extended to study the two-phase flow (Mewes et al., 1999). The model is based on the idea that the entire porous structure can be subdivided into elementary cells. An elementary cell is a representative volume typically comprising several pores. The whole work was dedicated to study the same in random packing (Loser, 2002). As a continuation to that, the same model was extended to study the two-phase flow in structured packing in macroscopic level (Mahr and Mewes, 2007;Mahr and Mewes, 2006a). The geometry representing the column of 960 mm height and 288 mm inner diameter was meshed. Four elements of packing, rotated against each other by 90° with an effective corrugation angle of 19° were used. The model of packing of MELLAPAK 250Y made from polypropylene was considered. Simulations are carried out using CFX 10.0 to study the counter-current two phase flow (Mahr, 2007).

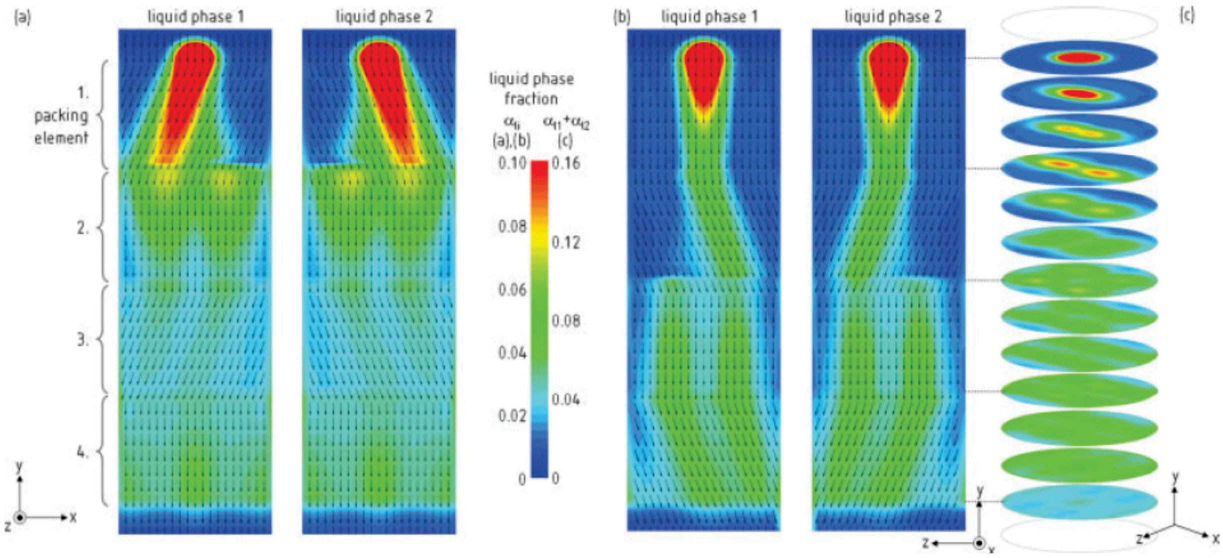

Figure 2.15 Liquid fed from a point source at specific liquid load (Mahr, 2007).

The numerical result of the liquid flow is shown in Fig. 2.15, which shows the flow of liquid through the packing and the redistribution of liquid when it meets the joint of the packing elements. The flow behaviour was also studied experimentally using X-ray tomographic visualization technique using contrast agent tracer (Mahr and Mewes, 2006b).

(Gu et al., 2004) studied the hydrodynamics of falling film flow on inclined and wavy plates corresponding to the surface texture of structured packing using 2D CFD simulation. It was reported that the liquid flow patterns are dependent on the microstructures of plate when there is no gas flow.

(Yuan et al., 2005) proposed a novel internal for packed columns and performed both 2D CFD simulation and experimental analysis of two phase cross/countercurrent flow. The installation of this new internal increase the radial gas velocity and decreases the axial velocity which in turn reduces the pressure drop.

An exclusive study was performed to study the flow behaviour of liquid film and rivulets on inclined planes. A Volume-of-fluid like model in CFX 5.0 was utilized to study the same. The influence of the surface tension was taken into account and the simulation studies were validated with experimental work (Repke et al., 2007;Hoffmann et al., 2005;Hoffmann et al., 2006;Xu et al., 2008).

The three dimensional model to predict the gas flow field in corrugated sheet of packing by dividing the packing into cells and solving mass, momentum and energy balances was presented (Stoter et al., 1993). An extensive study to know the reason for both small and large scale maldistribution in structured packing and to model was performed. Two different types of packing, MONTZ-PAK B1-250 and RALU-PAK 250YC were considered for the study. The first one has an embossed surface without perforations while the second one has jalousie like opening. The predicted distribution was compared with an experimental study. The distributor model was developed to realize the estimate of initial liquid distribution (Stoter, 1993).

(van Baten and Krishna, 2002) analyzed the gas and liquid phase mass transfer in KATAPAK-S structures using CFD simulations. The gas phase mass transfer was in good agreement with the theoretical correlation of (Subawalla et al., 1997), whereas the liquid phase mass transfer was one order of magnitude less than the correlation.

Liquid flow on smooth and structured packing was simulated using 2D CFD simulations and compared with experimental results. The mechanism of droplet formation and liquid-film breakup over flat and corrugated vertical plates with the influence of countercurrent gas-liquid flow was performed (Szulczewska et al., 2003).

The behaviour of complex film flow on the packing surfaces was studied extensively using CFD and compared with experimental results. The sensitivity of the film hydrodynamics to change in fluid and surface properties was tested using the model. The results of the gas-liquid interface were in good agreement with the theory. Various geometries have been developed to resemble the corrugated sheet of packing and hydrodynamics were studied using CFD tool CFX (Valluri et al., 2002;Valluri et al., 2005;Valluri, 2004).

The three dimensional CFD study was performed for one component single phase flow and two-component single-phase flow with species dispersion and the model was developed based on the details of the packing geometry. Experiments were performed on Flexipac 3Y packing and the circular and rectangular column with different structured packing –BX packing with corrugation angles of 30° and 45° and Flexipac 3Y. Simulation predicted good agreement for pressure drop between experiment and models (Wen et al., 2007).

A direct numerical simulation to study physical and reactive absorption in gas-liquid flow on structured packing was recently published. It also showed that the liquid side mass transfer is well predicted by the Higbie theory. The numerical results are compared to approximate solution presented in the literature (Haroun et al., 2010a;Haroun et al., 2010b).

To predict the effective area in structured packing available for transport processes, CFD was utilized and the results are compared with different available empirical equations (Shojaee et al., 2011).

The gap between understanding the wetting behaviour, velocity deviation, holdup due to change in modifications in geometry of corrugated sheets of packing and liquid distributors still exist and there is no universal rule for the same. This work is completely devoted to the better understanding and to develop one model to study the influence of all different parameters which in turn will give better idea for column design.

2.7 Experimental Studies – a short review

Various experimental efforts were carried to study the hydrodynamics of flow in corrugated sheet of packing. Different types of optical measurement methods like Laser Induced Fluorescence (LIF), Particle Image Velocimetry (PIV), Laser Doppler Velocimetry (LDV) and Tomographic methods were used to understand the liquid velocity profile, holdup and film thickness in different corrugated sheet of packing with and without surface textures. These studies gave good insight about the flow behaviour and thus more detail about the key parameters to improve the efficiency of the packing. Here, brief reviews of various experimental studies are summarized. Earlier studies were conducted to formulate a universal model equation to describe nonlinear nonstationary waves on the surface of liquid films for the broad range of Reynolds numbers. Experiments were performed using shadow method (Alekseenko et al., 1985). It was also concluded that full two-wave equations could describe all two-dimensional nonlinear wave regimes observed on the surface of falling liquid films.

The hydrodynamics of the three dimensional waves in laminar flow was studied using Fluorescent imaging technique and PIV method. The formation of waves and their interaction with each other was studied and explained extensively for very broad range of flow rates (Adomeit and Renz, 2000;Adomeit, 1996).

The effect of physical properties of liquids and of surface treatment on wetter area of structured packings was studied experimentally. Several wetting tests were performed on metallic and ceramic plates with flat, smooth or textured surfaces. The experimental results show that the liquid film width, and hence the wetter area, decreased with liquid viscosity contrary to the earlier correlations in the literature. A new statistical correlation for the estimation of the wetter area and for the liquid film thickness was presented (Nicolaiewsky et al., 1999).

The importance of operating and design parameters to mass transfer in the column equipped with four different structured packing namely Gempak 4A, Mellapak 500Y, Mellapak 500X, and Optiflow was compared using pilot plant measurements (Aroonwilas et al., 2001).

The usage of X-ray computed Tomography to determine the Gas-liquid contact area and liquid hold up for structured packing was demonstrated (Green et al., 2007). They compared the liquid holdup of Mellapak 250Y with their experiments.

To measure the liquid film thickness another method using fibre optic sensor was presented (Alekseenko et al., 2003). A detailed experimental investigation was performed using this technique to measure the film thickness inside the column equipped with corrugated structured packing. The results showed that the maximum liquid film thickness is near the contact points of two sheets where the liquid will be redistributed over the surfaces (Alekseenko et al., 2008).

To determine the mass transfer characteristics of structured packing, two different methods, a physical method using high-resolution gamma-ray tomorography and chemical method developed by (Danckwerts, 1970) was utilised. The experimental results are compared with Higbie-Bravo model and a new adapted Higbie model. From these results, it can be seen that the gas side mass transfer is not a rate limiting (Raynal et al., 2004a).

A further detailed work on the measurement of the film velocity of periodically excited two-dimensional-wave films with the Particle Image Velocimetry (PIV) was done. The influence of the wave surface on the heat transfer was examined (Al-Sibai et al., 2003;Al-Sibai, 2005).

Wetting behaviour of structured packing was studied both theoretically using CFD and experimentally using optically assisted mechanical sensor using needle which is perpendicular to the plate surface. Hydrodynamics of flow behaviour in Rombopak 4M was studied both theoretically and experimentally. The liquid hold-up, wetting behaviour and interfacial area was studied and compared with model available in literature (Ataki et al., 2006;Ataki and Bart, 2006;Ataki, 2006).

Single phase flow behaviour of glycerol solution over the structured packing was studied experimentally using Laser Doppler Velocimetry and validated using CFD simulations. Experiments were performed on Plexiglas corrugated sheets and the simulations are also performed in the similar geometry. Author concluded that the velocity distribution along the horizontal plane show good special periodicity (Chen et al., 2007).

Optical measurement methods such as Particle-Tracking-Velocimetry (PTV) and Laser-Induced-Fluorescence methods were further extended to study the multiphase flow behaviour (Ausner, 2006). In addition, the concurrent flow behaviour of immiscible liquids were also studied. Experimental results are also compared with CFD simulations and are validated. (Hoffmann et al., 2005;Hoffmann et al., 2006). A new micro Particle Image Velocimetry was developed which enables to measure the film flow on both smooth and textured surface. The results are compared and validated with CFD simulations. (Repke et al., 2007;Paschke et al., 2007;Paschke, 2011).

A gamma ray tomography measuring method was proposed to measure the liquid holdup and understand the liquid distribution in two different packings such as high capacity Mellapak 252.Y and Koch Glitsch third generation random packing IMTP50 (Alix and Raynal, 2008).

The influence of two-dimensional and three-dimensional micro textures on the surface of the corrugated sheet of packing was studied in relation to liquid holdup and impact on the mass transfer in countercurrent operations. Here, the importance of textures on the surface in increasing the efficiency of the packing has been discussed extensively (Kohrt et al., 2011;Kohrt, 2011).

A novel structured packing using carbon fibers called Sepcarb was patented (Patent, 2005). Detailed analysis of this structured packing including hydrodynamics and mass transfer characteristics was presented (Bessou et al., 2010;Alix et al., 2011).

Recently, a practical methodology was developed to overcome the common problems encountered in X-ray tomography measurements to measure hydrodynamics in catalytic packings (Viva et al., 2011a). Two catalytic packing were analysed and the results were published. The details regarding the liquid holdup and effective interfacial area distribution of catalytic packing were presented as shown in Fig. 2.16 (Aferka et al., 2011;Viva et al., 2011b).

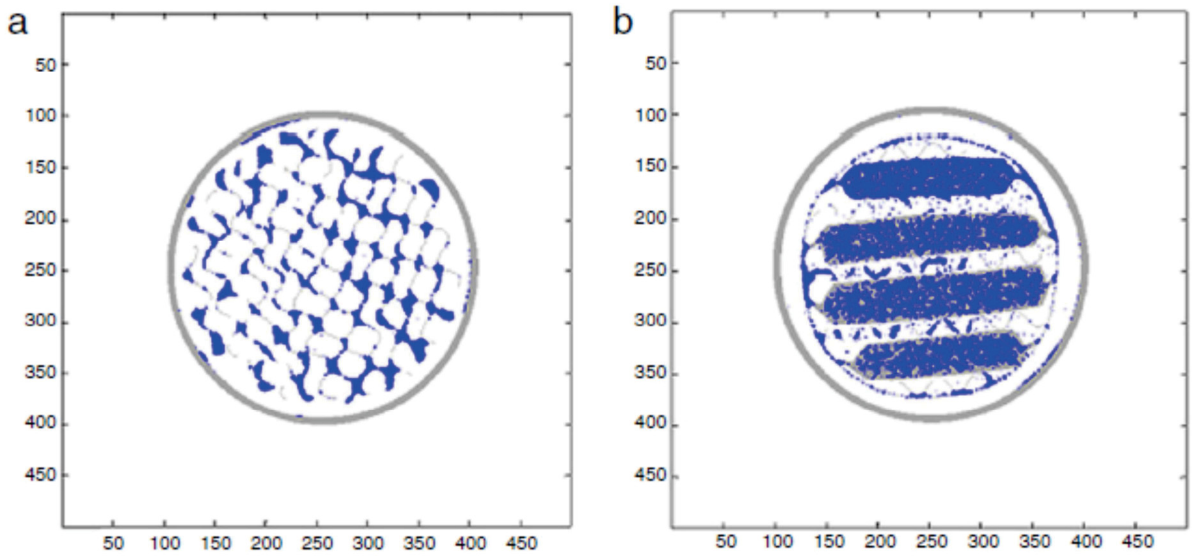

Figure 2.16 Dry and irrigated images for (a) Mellapak 752 Y ; (b) Katapak-SP 11 from X-tomographic studies (Viva et al., 2011).

Even though, various works have been performed to understand the flow behaviour in structured packing, the gap exists in order to understand the local velocity profile. This works enables us to give some deep insight on the flow behaviour especially on wetting and local velocity profiles for different testing systems.

3 NUMERICAL BACKGROUND AND EXPERIMENTAL DETAILS

The aim of the work is to study the local flow behaviour in corrugated sheets of packing computationally. In this chapter, details of the numerical background, geometry details and experimental setup will be described. In section 3.1, two different geometries namely the inclined plate and the corrugated sheets of packing will be presented along with their dimensions and boundary conditions. In section 3.2, details of the Volume of Fluid model and Continuum Surface Force model along with mathematical equations will be explained. Further, in Chapter 3.3, details of the experimental set up used to study the wetting behaviour of different corrugated sheets of packing and μPIV to study velocity profiles will be presented.

3.1 Geometry

As explained in Chapter 2, two major geometries were considered, namely inclined plate and corrugated sheets of packing. Inclined plate geometry was studied in order to validate the model with experimental studies.

3.1.1 Inclined plate

To analyse the fluid flow behaviour, a three dimensional smooth inclined plate was considered. The dimensions of the plate are 0.12 × 0.01× 0.05 m as shown in Fig. 3.1, which resembles the inclined plate used in experimental studies. The details of the dimensions and number of cells are shown in Table 3.1.

The whole geometry is meshed using Gambit 2.3, a meshing tool from Ansys Inc. (ANSYS INC., 2009b). The geometry consists of two different meshing zones. The mesh is very fine i.e., approximately 2.9×10^{-5} m in the liquid region and the interface around the gas and liquid. A coarser mesh was used in the region more than half the height of the plate, which contains only gas phase. The very fine mesh enables to capture the gas-liquid interface. The geometry consists of 516,000 cells and the inclination angle (β) to the base of the plate is 60°. The boundary conditions on the sides of the plate assigned as walls to resemble the experimental set up held by steel supports on the left and on the right side.

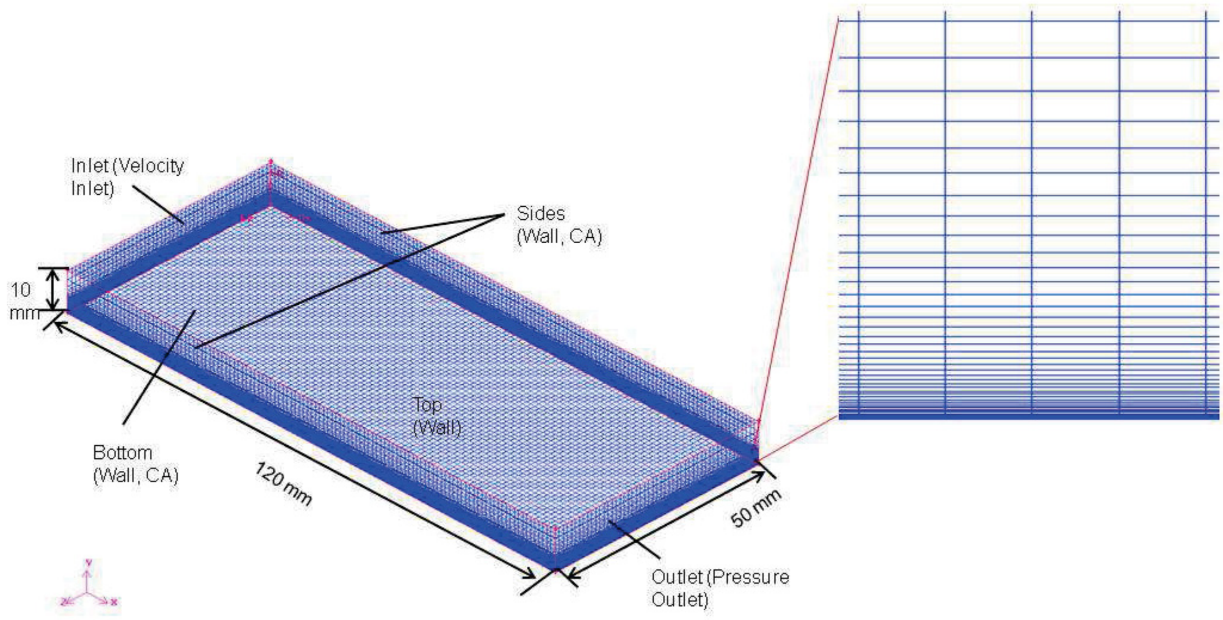

Figure. 3.1 Geometry details of inclined plate. (a) Isometric view, (b) Meshes in the fine zone.

To study the wetting behaviour, geometry similar to the one shown in Fig. 3.1 except for the width of 100 mm was considered. Details of the dimensions of the two different geometries are listed below:

Table 3.1 Dimensions of the two different inclined plate geometry considered in this work.

Geometry	Length (mm)	Width (mm)	Height (mm)	No. of cells
1	120	50	10	516,000
2	120	100	10	600,000

Boundary conditions considered in these simulations are as follows.

Table 3.2 Details of boundary conditions utilised for wetting studies and velocity profiles studies.

	Without countercurrent – wetting studies	Without countercurrent – velocity profile	With countercurrent – velocity profiles
Inlet	Pressure outlet	Velocity inlet	Pressure inlet
Outlet	Pressure outlet	Pressure outlet	Pressure inlet
Top	Velocity inlet	Pressure outlet	Wall
Bottom	Wall (with contact angle)	Wall (with contact angle)	Wall (with contact angle)
Sides	Wall (with contact angle)	Wall (with contact angle)	Wall (with contact angle)

3.1.2 Corrugated sheets of packing

To study the flow behaviour in corrugated sheet of packing, four different modifications are considered. List of geometries used in this work are tabulated in Table 3.3. Four major modifications such as Triangular crimp, Sinusoidal crimp with and without perforations and with two corrugated sheets of packing are taken into consideration. These modifications are chosen to avoid simplification of geometry and to resemble the real corrugated sheets of packing.

Table 3.3 List of different geometrical modifications considered in this work.

S. No.	No. of sheets	Crimp apex	Perforations	Surface textures	Crimp angle
1	One	Triangle	No	Smooth	45°
2	One	Sinusoidal	No	Smooth	45°
3	One	Sinusoidal	Yes	Smooth	45°
4	Two	Sinusoidal	No	Smooth	45°

In most of the computational studies until now, major simplification was in the crimp apex of the corrugated sheet of packing. To reduce the complexity in meshing, crimp apex was considered as strict triangular as shown in Fig.3.2 (black line). However, most of the real industrial packing have smooth crimp surface (red line in Fig. 3.2). To understand the difference in flow behaviour due to this modification, two different geometries with both triangular crimp and smooth surface are developed.

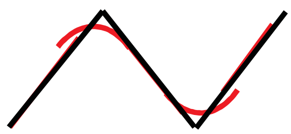

Figure 3.2 Line sketch showing of Triangular (black) and Smooth (red) crimp apex.

Table 3.4 Dimensions of different geometries resembling corrugated sheet of packing studied in this work.

Geometry	Height (mm)	Base (mm)	Crimp angle (°)	Crimp apex diameter (mm)	Perforations diameter (mm)	No. of cells
C1	7	31.11	45°	0	0	129291
C2	7	31.11	45°	0.7	0	1143600
C3	7	31.11	45°	0.7	4	1143600

These modifications are meshed using ICEM CFD 12.0 (ANSYS INC., 2009b).

The geometrical details of the sketch with triangular crimp are shown in Fig. 3.3 and the smooth crimp is shown in Fig. 3.4. Overall dimension of the rectangular geometrical domain is 132 × 88 × 17 mm. Corrugation angle used in all the geometries are 45˚. As shown in Fig. 3.4, gap of 5 mm on the top and bottom of the corrugation facilitates to measure the liquid hold-up and to understand the change in liquid flow pattern. Fig. 3.5 shows the meshing of the geometry and it consists of 1,143,600 cells. Another major geometrical modification considered is the perforation of 4 mm diameter with pitch of 10 mm along the length and width of the geometry which is shown in Fig. 3.6. The geometry shown in Fig. 3.6 is two-in-one geometry in which the influence of the perforations can be included by changing the boundary conditions. In most cases, the film thickness does not exceed 1 mm and hence the width or gap is sufficient. This further helps in giving a closed geometry for corrugated sheet with perforations.

Fig. 3.7 shows the geometry in which two corrugated sheets are arranged. As in practical applications, one corrugated sheet is rotated 90° with respect to another. The details of the crisscross junctions are explained in detail Chapter 5.3.

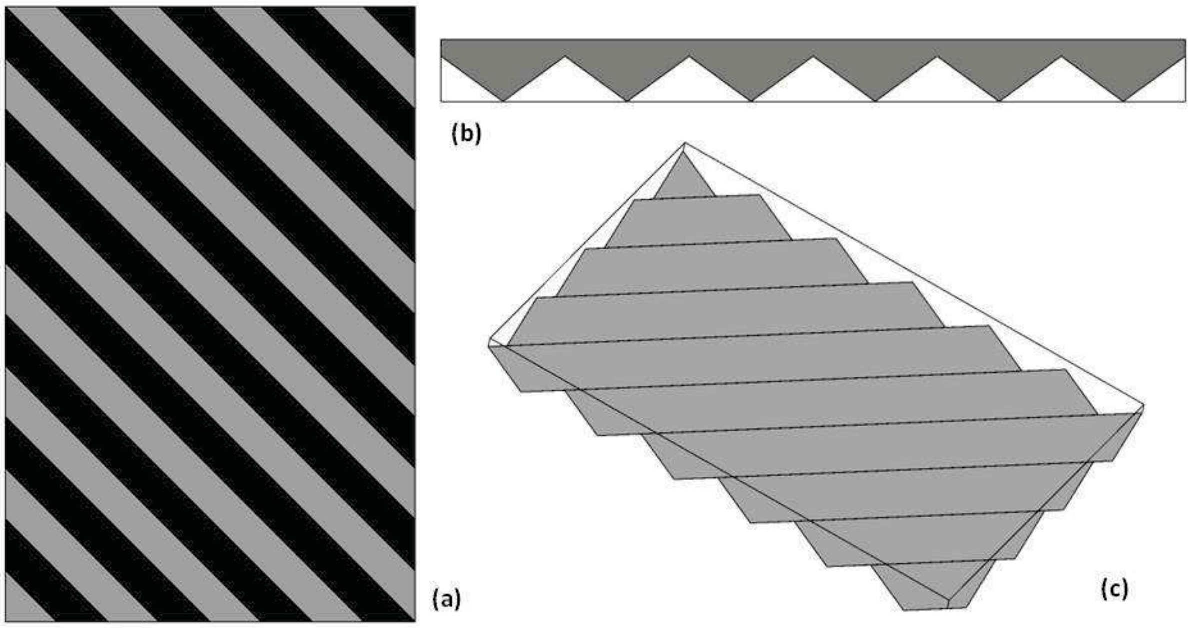

Figure 3.3 Schematic of corrugated sheet of packing with triangular crimp. (a) top view, (b) side view, (c) isometric view. Dimensions are same as shown in Fig 3.4.

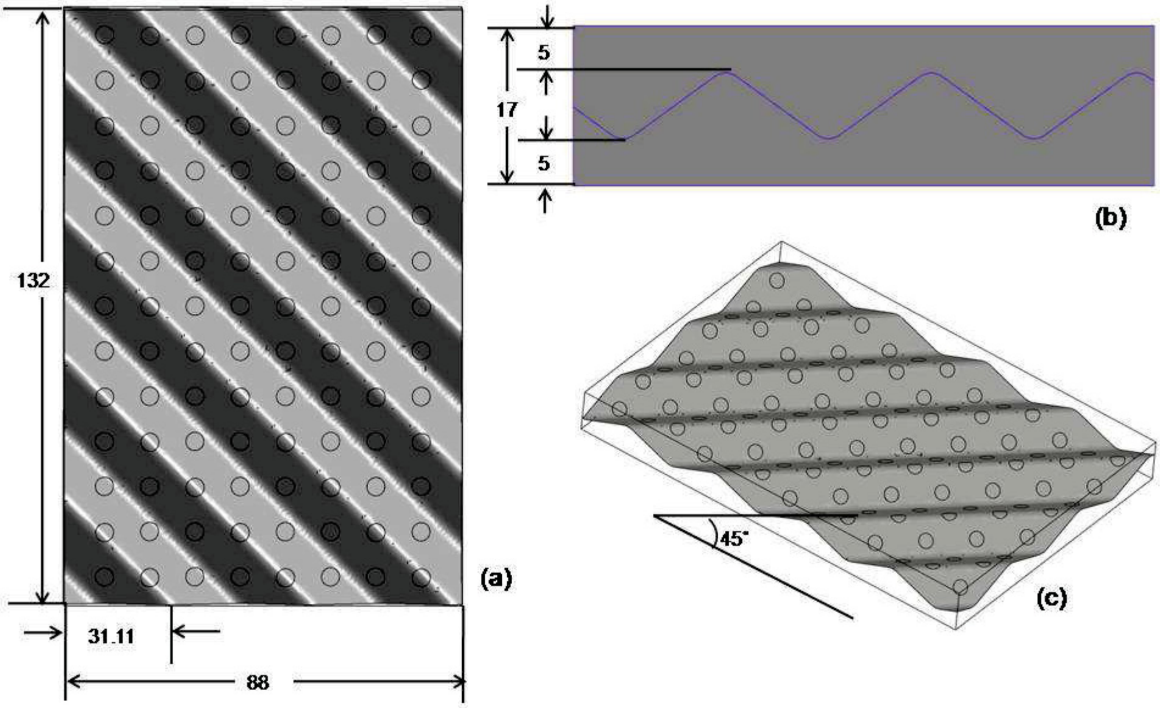

Figure 3.4 Schematic view of corrugated sheet of packing without holes. (a) top view, (b) side view, (c) isometric view.

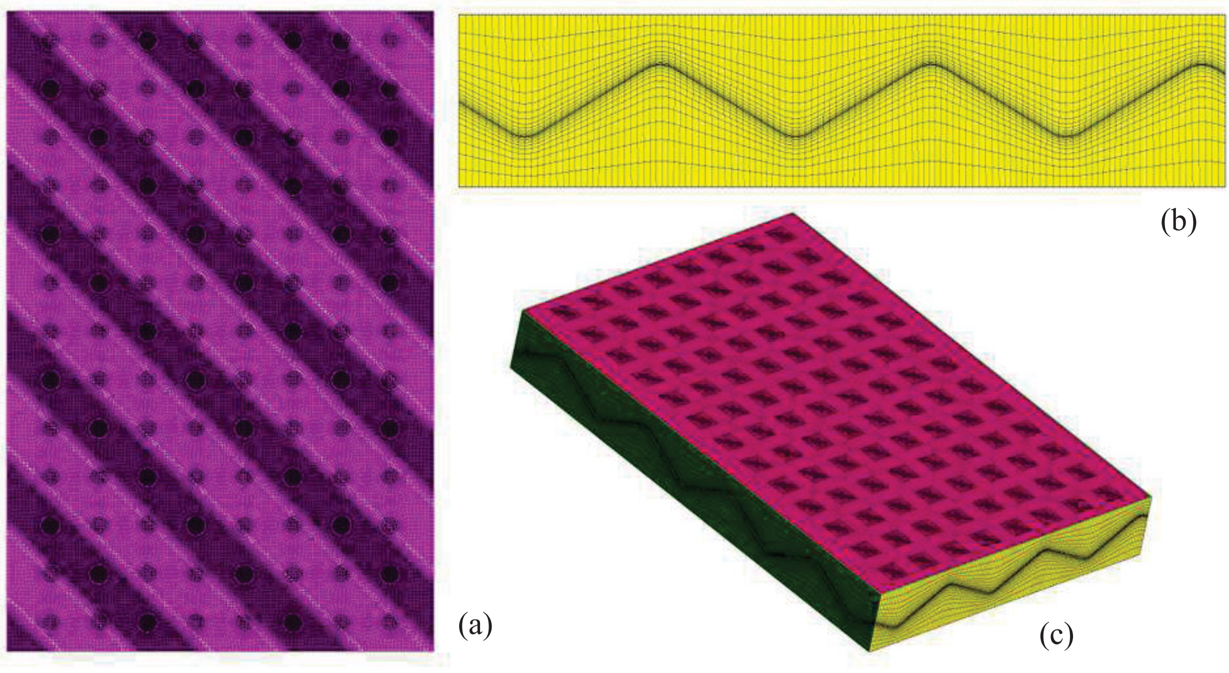

Figure 3.5 Meshes shown in detail for corrugated sheet of packing. (a) top view, (b) side view, (c) isometric view.

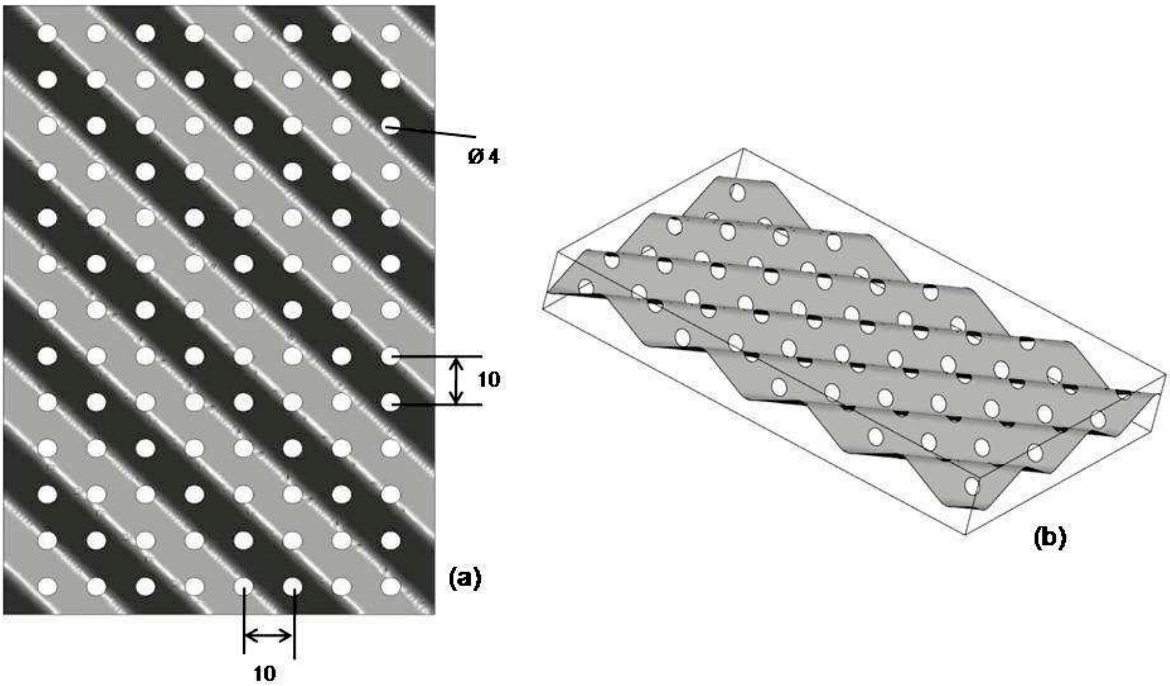

Figure 3.6 Schematic view of corrugated sheet of packing with holes. Dimensions are same as in Fig 3.4. (a) top view, (b) isometric view.

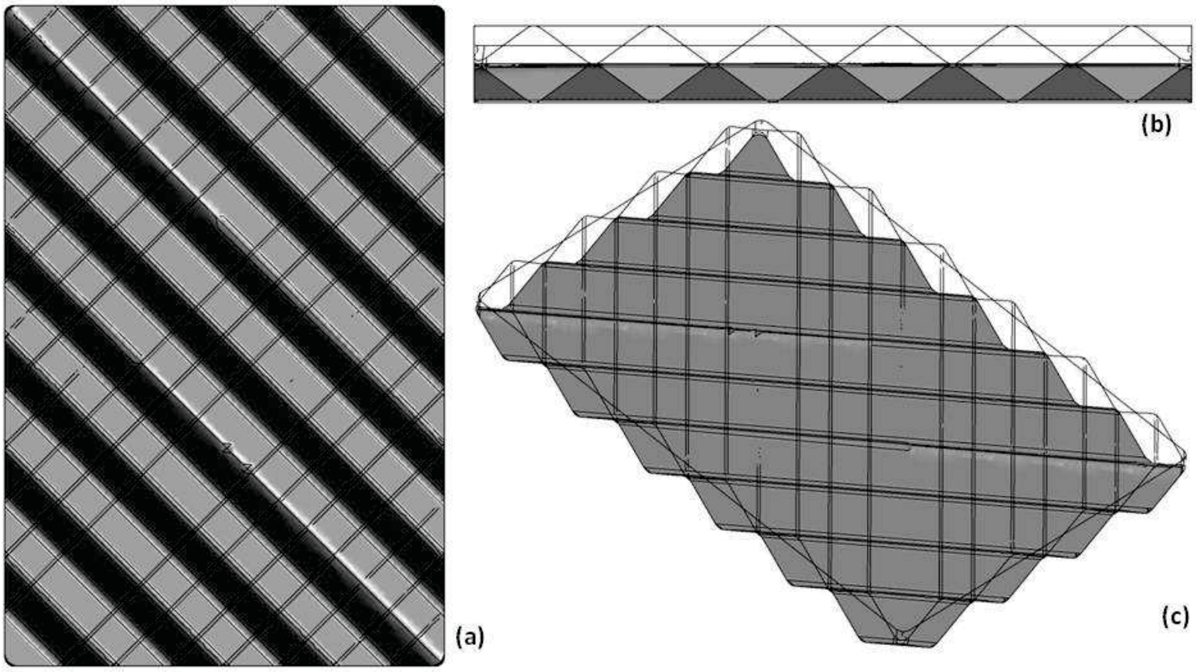

Figure 3.7 Schematic view of two corrugated sheets of packing with smooth crimp. (a) top view, (b) side view, (c) isometric view.

Details of the boundary conditions used in the simulations of corrugated sheet of packings are as listed in Table 3.5. The influence of perforations has been introduced in simulation by changing the boundary conditions of the holes in the geometry. For the simulation with perforations, boundary conditions of the perforations will be considered assigned as interior, otherwise it will be assigned as wall. This method helps in using the same geometry for both the simulations and helps in comparing the influence later.

Table 3.5 Boundary conditions used in simulation of corrugated sheet of packing with and without holes.

	Simulations without perforations	**Simulations with perforations**
Inlet	Velocity inlet	Velocity inlet
Top	Pressure outlet	Pressure outlet
Bottom	Pressure outlet	Pressure outlet
Corrugation – base	Wall (with contact angle)	Wall (with contact angle)
Corrugation – holes	Wall (with contact angle)	Interior
Sides	Symmetry	Symmetry

Details of the boundary conditions used in the simulations of corrugated sheets with triangular crimp and two corrugated sheets are shown in Table 3.6. For the simulation with two corrugated sheets of packing, both the sheets was assumed wall boundary condition with contact angle which enables to include the influence of contact angle in the flow behaviour.

Table 3.6 Boundary conditions for geometry with triangular crimp and two corrugated sheets of packing.

	Triangular crimp geometry	**Two corrugated sheet geometry**
Top	Pressure outlet	Wall
Bottom	Wall (with ontact angle)	Wall (With contact angle)
Inlet	Velocity inlet	Velocity inlet
Outlet	Pressure outlet	Pressure outlet
Sides	Symmetry	Symmetry

3.2 Details of the model

The simulations were carried out with the commercial tool ANSYS Fluent 12.0, ANSYS Inc. The Volume of Fluid (VOF) model (Hirt and Nichols, 1981) with geometric reconstruction scheme was used which is one of the limiting cases of Euler-Euler homogenous model. The VOF model considers that the gas and liquid phase are not interpenetrating.

3.2.1 Volume of Fluid (VOF) model

The VOF model is utilised based on the assumption that two or more fluids are not interpenetrating. For each phase that is added, a new variable is introduced: the volume fraction of the phase in the computational cell. In each control volume, the volume fractions of all phases sum to unity. The fields for all variables and properties are shared by the phases and represent volume-averaged values, as long as the volume fraction of each of the phases is known at each location. Thus, the variables and properties in any given cells are either purely representative of one of the phases, or representative of a mixture of the phases depending upon the volume fraction values. In other words, if the q^{th} fluid volume fraction in the cell is denoted as α_q, then the following three conditions are possible:

- $\alpha_q = 0$; The cell is empty (of the q^{th} fluid).
- $\alpha_q = 1$; The cell is full (of the q^{th} fluid).
- $0 < \alpha_q < 1$; The cell contains the interface between the q^{th} fluid and one or more other fluids.

Volume Fraction Equation

The tracking of the interface(s) between the phases is accomplished by the solution of a continuity equation for the volume fraction of one (or more) of the phases. For the q^{th} phase, this equation has the following form:

$$\frac{1}{\rho_q}\left[\frac{\partial}{\partial t}\left(\alpha_q\rho_q\right) + \nabla.\left(\alpha_q\rho_q\vec{v_q}\right) = S_{\alpha_q} + \sum_{p=1}^{n}\left(m_{pq} - m_{qp}\right)\right] \qquad (3.1)$$

where, m_{qp} is the mass transfer from phase q to phase p and m_{pq} is the mass transfer from phase p to phase q. S_{α_q} is the source term.

The volume fraction equation will not be solved for the primary phase; the primary-phase volume fraction will be computed based on the following constraint.

$$\sum_{q=1}^{n}\alpha_q = 1 \qquad (3.2)$$

The properties appearing in the volume fraction equations are determined by the presence of the component phases in each control volumes. In a two-phase system, for example, with phases represented by subscripts 1 and 2, where the volume fraction of the second of these is being tracked, the density in each cell is given by

$$\rho = \alpha_2 \rho_2 + (1 - \alpha_2)\,\rho_1 \tag{3.3}$$

In general, for an n-phase system, the volume-averaged density can be defined as

$$\rho = \sum \alpha_q \rho_q \tag{3.4}$$

All other properties are computed in this manner.

The volume fraction equation can be solved using explicit time discretization.

Explicit Discretization

In this approach, finite difference interpolation schemes are applied to the volume fraction values that were computed at the previous time step.

$$\frac{\alpha_q^{n+1}\rho_q^{n+1} - \alpha_q^n \rho_q^n}{\Delta t} V + \sum_f \left(\rho_q U_f^n \alpha_{q,f}^n\right) = \left[\sum_{p=1}^{n} \left(m_{pq} - m_{qp}\right) + S_{\alpha_q}\right] V \tag{3.5}$$

where, (n+1) is the index of the new (current) time step, n is the previous time step, $\alpha_{q,f}$ is the face value of the qth fraction, V is the volume of the cell, $U_f$is volume flux through the face, based on normal velocity.

Momentum Equation

A single momentum equation is solved throughout the domain, and the resulting velocity field is shared among the phases. The momentum equation, shown in Eq. 3.6 is dependent on the volume fractions of all the phases through the definition of ρ and μ.

$$\frac{\partial}{\partial t}(\rho \vec{v}) + \nabla \cdot (\rho \vec{v}\vec{v}) = -\nabla p + \nabla \cdot [\mu(\nabla \vec{v} + \nabla \vec{v}^{\mathrm{T}})] + \rho \vec{g} + \vec{F} \tag{3.6}$$

Interpolation near the interface

Geometric reconstruction scheme was utilised in this work. In geometric reconstruction scheme, ANSYS Fluent applies a special interpolation treatment to the cells that lie near the interface between two phases. Fig. 3.8 shows an actual interface shape along with the interfaces assumed during geometric construction scheme. In Fig. 3.8, left represents the real interface and the right shows the interface interpolation due to geometric reconstruction scheme. Both are in very close agreement also in comparison to other interpolation schemes.

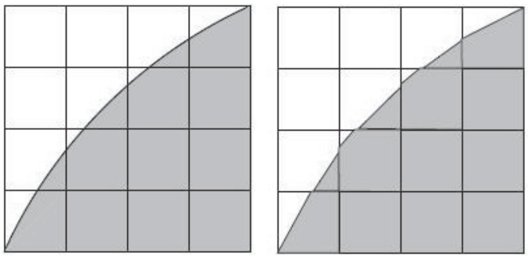

Figure 3.8 Comparison of real surface and geometrical interpolation scheme.

The geometric construction scheme represents the interface between fluids using a piecewise-linear approach. It assumes that the interface between two fluids has a linear slope within each cell and uses the linear shape for calculation of the advection of fluid through the cell faces. The first step in this reconstruction scheme is determining the position of the linear interface relative to the centre of each partially filled cell, based on information about the volume fraction and its derivatives in the cell. The second step is calculating the advecting amount of fluid through each face using the computed linear interface representation and information about the normal and tangential velocity distribution on the face. The third step is calculating the volume fraction in each cell using the balance fluxes determined during the previous step.

ANSYS FLUENT will refine the time step for VOF automatically, based on the input for maximum Courant number allowed near the free surface. The Courant number (*Co*) is a dimensionless number that compares the time step in a calculation to the characteristic time of transit of a fluid element across a control volume.

$$Co = \frac{\Delta t}{\Delta x_{cell}/v_{fluid}} \tag{3.7}$$

In the region near the fluid interface, ANSYS FLUENT divides the volume of each cell by sum of the outgoing fluxes. The resulting time represents the time it would take for the fluid to empty the cell.

3.2.2 Continuum Surface Model

The VOF model can also include the effects of surface tension along the interface between each pair of phases. The model can be augmented by the additional specification of the contact angles between the phases and the walls. The influence of surface tension is taken into account by the Continuum Surface Force Model (CSF) proposed by (Brackbill et al., 1992). With this model, the addition of surface tension to the VOF calculation results in a source term in the momentum equation.

In CSF model, where the surface curvature is computed from local gradients in the surface normal at the interface. Let n be the surface normal, defined as the gradient of $\alpha_{q,}$ the volume fraction of the qth phase.

$$n = \nabla\alpha_q \tag{3.8}$$

The curvature, κ, is defined in terms of the divergence of the unit normal, $\hat{n}$:

$$\kappa = \nabla \cdot \hat{n} \tag{3.9}$$

where,

$$\hat{n} = \frac{n}{|n|} \tag{3.10}$$

The surface tension can be written in terms of the pressure jump across the surface. The force at the surface can be expressed as a volume force using the divergence theorem. It is this volume force that is the source term, which is added to the momentum equation. It can be written as

$$F_{vol} = \sum_{pairs\,ij,i<j} \sigma_{ij} \frac{\alpha_i\rho_i\kappa_j\nabla\alpha_j + \alpha_i\rho_i\kappa_j\nabla\alpha_i}{\frac{1}{2}(\rho_i+\rho_j)} \tag{3.11}$$

This expression allows for a smooth superposition of forces near cells where more than two phases are present. If only two phases are present in a cell, then $\kappa_i = -\kappa_j$ and $\nabla\alpha_i = -\nabla\alpha_j$ and Eq. 3.11 reduces to

$$F_{vol} = \sigma_{ij} \frac{\rho\kappa_i\nabla\alpha_i}{\frac{1}{2}(\rho_i+\rho_j)} \tag{3.12}$$

where, ρ is the volume-averaged density computed using Eq. 3.4. Eq. 3.12 shows that the surface tension source term for a cell is proportional to the average density in the cell.

3.2.3 Drag force source term

Since the aim of this work is to analyse the local flow behaviour of the gas-liquid countercurrent flow, the influence of mass and heat transfer has been neglected. The influence of the drag force cannot be neglected while studying the hydrodynamic behaviour. (Woerlee et al., 2001) developed a model for frictional pressure drop, which can be described as

$$\frac{\partial P_{fi}}{\partial X} = -a_{eff} \times f_i \times \rho_g \times (\bar{u} - u_x)\,|\bar{u} - u_x| \tag{3.13}$$

where, a_{eff} is the effective interfacial area per unit volume and f_i is the interfacial friction factor. (Stephan and Mayinger, 1992) developed a new correlation to describe the interfacial friction in counter-current flow which can be described as

$$f_i = 0.079 \times Re_g^{-0.25} \times (1 + 115 \times \delta^{*N}) \quad (3.14)$$

where, Re_g is the gas phase Reynolds number defined as $Re_g = (\bar{u} \times \rho_g \times D_h)/\mu_g$; $N = 3.95\times(1.8+3.0/Bo)$. D_h is the hydraulic diameter and δ^* is the dimensionless ratio of film thickness and Bo is the Bond number.

These models have been implemented in Fluent by using User Defined Function (UDF). Since the two phases share a common velocity field, the algebraic sign of the drag force source term is opposite to the interfacial velocity to ensure it as resistance. The flow in the simulation was considered as laminar, as the liquid phase Reynolds numbers is always lower than 300 and the velocities of the gas phase are also not very high.

(Nicolaiewsky et al., 1999) illustrated that experiments with decreasing liquid loads were more reproducible than increasing liquid loads. Therefore, the same strategy was adapted in the simulations. The simulation without countercurrent gas flow was continued until it reaches quasi-stable state. To confirm the quasi-stable state, parameters such as mass flow rate and force on the plate were also monitored along with residuals.

3.2.4 Parallel computing

ANSYS Fluent's parallel solver allows computing a solution using multiple processers that are on the same computer or different computers in the network. Parallel processing involves an interaction between ANSYS FLUENT, a host process, and a set of compute-node processes. ANSYS FLUENT interacts with the host process and the collection of compute nodes using a utility called cortex that manages ANSYS FLUENT's user interface and basic graphical functions. Parallel ANSYS FLUENT splits up the mesh and data into multiple partitions, and then assigns each mesh partition to a different compute process (or node). The number of partitions is an integral multiple of the number of compute nodes available (ANSYS Inc., 2009a) .

All the simulations are performed on IBM pSeries 690 super computers with SGI Altix XE 250 and in 32 parallel nodes of the HLRN (High Performance Computing Network of Northern Germany) at Regional computing clusters available at Berlin. It is worth mentioning that simulations performed for inclined plate needs at least 72 hours of computation time and for the geometry of corrugated sheet of packing with 1.1 million cells needs at least 168 hours of computation time. Job i.e., each simulation will be queued in the cluster and simulations are performed batch wise with the availability of licenses and free nodes. An example of the code for batch job is shown in Appendix A.

3.3 Experimental set up

3.3.1 Study of the wetting behaviour

The wetting behaviour of four different corrugated sheets was studied along with inclined smooth plate for reference. In order to study the influence of different geometrical parameters, corrugated sheets from real industrial applications were selected considering the parameters such as microstructures, perforations and specific surface area.

The details of the smooth plate and corrugated sheets are listed below:

Table 3.7 Details of different corrugated sheets of packing studied experimentally. (*) inclination angle.

Packing	Specific surface area (m^2/m^3)	Corrugation angle (°)	Microstructure	Perforations
Smooth plate	-	45(*)	No	No
Mellapak.350.Y-A	350	45	No	Yes
Mellapak.250.Y-B	250	45	Yes	Yes
Mellapak.350.Y	350	45	Yes	Yes
Montz B1-300	300	45	Yes	No

Three different fluids with big difference in viscosity and contact angle were selected for this study. The details of the liquids are listed below in Table 3.8. water-glycerol (45 wt%) has similar contact angle like water but more viscous. Silicon-oil (DC5) has very low contact angle but similar viscosity as water-glycerol (45 wt%). To capture the wetting behaviour, Rhodamine-B was used as colouring pigments in water and water-glycerol solution. As the colour of the testing system is pink, the wetting can be studied without the help of UV-light.

The usage of this colouring pigment has been studied earlier (Paschke, 2011) and it will not influence any of the physical parameters of the testing system. For silicon-oil (DC5), Coumarin was used as a colouring agent, which gave blue reflections when studied with the help of UV-light. However, the corrugated sheet must be coated with black colour to capture the UV light.

Table 3.8 Properties of testing system used in this work.

	Viscosity η [mPa s]	Density ρ [kg/m³]	Surface Tension σ [mN/m]	Contact Angle θ [°]
Water	1	997	72.7	76.6
Water-glycerol (45 Wt%)	4.6	1113	70	69
Silicon-oil (DC5)	4.6	915	18.5	≈ 7

The flow diagram of the experimental setup is shown in Fig. 3.9. Test liquid was pumped from the solution tank (T01) to flow through the testing material. Before flowing through the testing material, it passes through the flow meter (F1) and buffer tank (B01). The buffer tank was used in order to avoid pulsations that arose from the pump. The camera was placed in the stand opposite to the corrugated sheet, which enables to take pictures. The picture of the experimental set up utilised for studying the silicon-oil (DC5) with UV light is shown in Fig. 3.10.

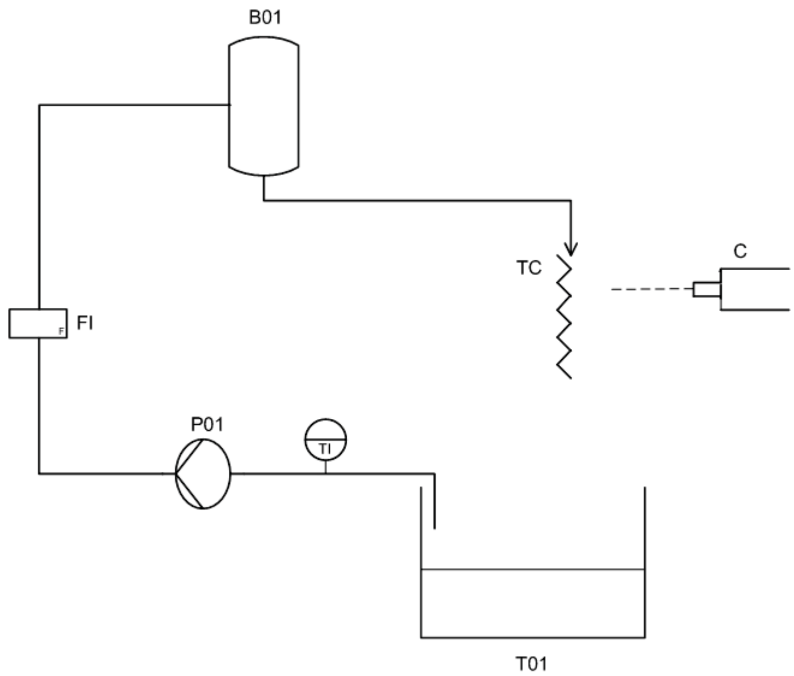

Figure 3.9 Experiment set-up for wetting studies. Sample picture from water-glycerol study. P01 – Pump; T01 – Solution tank ; TC - Testing cell ; FI - Flow meter ; C- Camera ; B01 – Buffer tank.

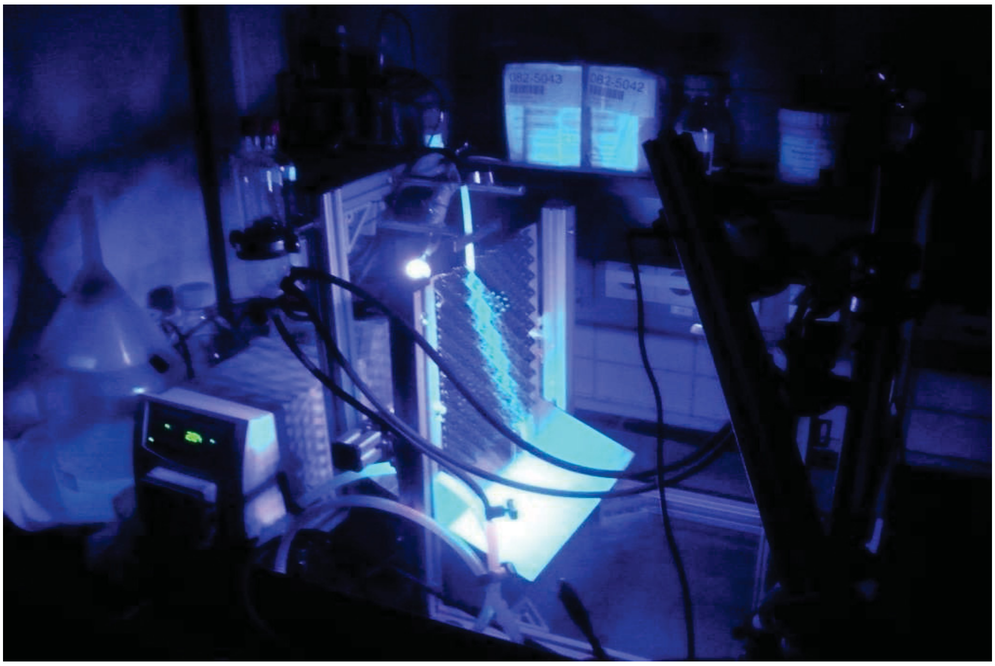

Figure 3.10 Sample picture from silicon-oil DC5 Study with UV light in a dark room.

3.3.2 Velocity Profile measurement

In order to validate the simulation with experimental studies, μPIV experiments were performed separately within our group (Paschke et al., 2007). For the experimental analysis of the countercurrent flow behaviour, a measuring cell was built and the new micro Particle Image Velocimetry (μ-PIV) method was used. The sketch of the experimental setup is shown in Fig. 3.11 and the detailed description can be found in (Paschke et al., 2007).

This method was characterised by the fact that the measurements are carried out through the gas-liquid interface, so that the measurements on non-transparent smooth and structured solid surface materials are enabled. The setup enables the countercurrent flow analysis in a wide working range and for different material systems. With the aid of an overflow weir (G), the liquid is fed on the top of the stainless steel plate and flows down the measurement cell as a closed free liquid film flow. The flow was measured using the Rotameter (F). High speed CCD camera (D) was used to take high resolution pictures which will be processed separately later and reconstructed as velocity profiles. The width and height of the plate is same as mentioned above, but the length is 300mm. The measuring area is approximately 3 x 2.3 mm. The gas inlet is close to the liquid outlet at the end of the plate. To minimize the wall effects and take the entrance area into account the measurement position is in the middle of the plate and 11cm behind the inlet weir. The time–weighted average velocity profile can be calculated after processing the images from optical measurements.

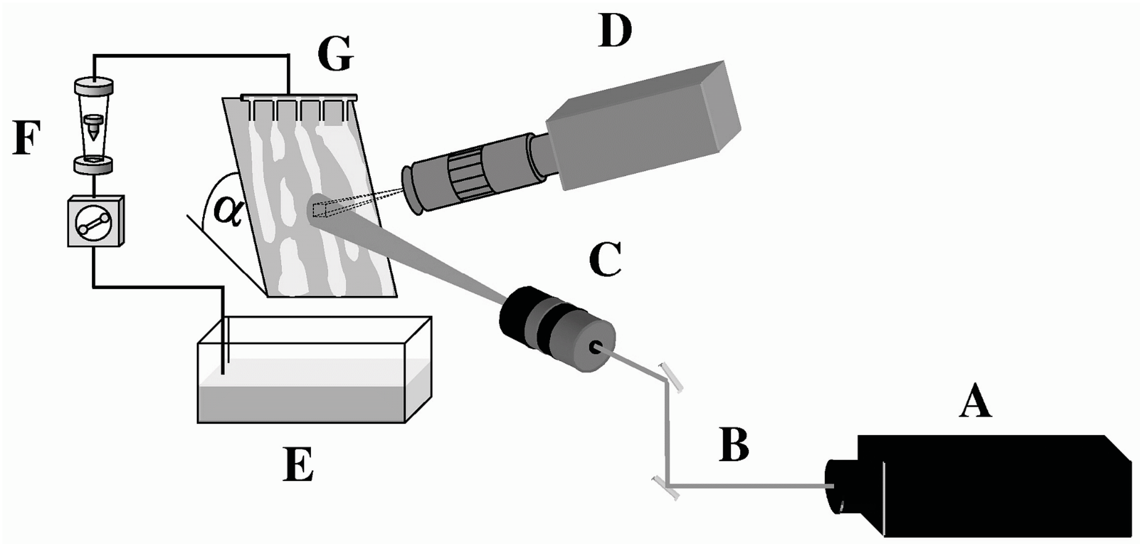

Figure 3.11 Schematic diagram of experiment setup used for velocity measurements. A - Laser (ND:YAG); B - Mirror (Light Arm); C - Laser Light Optic; D - CCD Camera with band-pass Filter and microscopic lens; E - Collecting Water Tanks; F - Peristaltic Pump with Rotameter; G - Feed Tubes; α - Inclination angel (Paschke et al., 2007).

4 HYDRODYNAMICS ON INCLINED PLATE

The hydrodynamic behaviour on an inclined smooth plate as described in the section 3.1.1 is studied for three different testing materials. These materials differ in viscosity and contact angle as shown in table 3.8. The hydrodynamics are characterized in two parts:

1. The wetting characteristics.
2. The velocity profile in the thin liquid film.

In section 4.1, the results of wetting characteristics of the three different test systems from simulation are compared with experimental studies. In section 4.2, velocity profiles obtained from CFD simulations are compared with profiles obtained from μPIV experimental studies given by (Paschke, 2011). In order to understand the differences between the results of experiments and simulations, detailed sensitivity analysis was performed by selecting the most important parameters which influence the velocity profile. Further, a comparison is presented for countercurrent flow. After validating the model, it will be further extended to study more complex geometries resembling corrugated sheets of packing utilized in industry for distillation and absorption. The results for these geometries will be explained in detail in the next chapter.

4.1 Wetting characteristics of different testing system

In this section, the wetting characteristics of water, water-glycerol and silicon oil flowing over a smooth inclined plate will be discussed. Here, the plate is inclined at 45° to the base and the liquids flow through a pipe of 4 mm diameter. Fig. 4.1, 4.2, and. 4.3 shows the pictorial comparison of the experimentally observed wetting characteristics of water, water-glycerol and silicon-oil DC5 respectively with simulation results. Fig. 4.4 shows the rivulet width for all 3 above mentioned test mixtures along the length of the plate in flow direction. For all materials, wetting is studied for at least two different flow rates i.e., one high and another low flow rate. From Fig. 4.1 – Fig 4.5, the difference in wetting behaviour due to a change in flow rate, viscosity and contact angle is clearly visible.

The comparisons of experimental and simulation results for the flow of water in three different flow rates are shown in Fig. 4.1. One observes that first the width of the rivulet increases, then the liquid stream narrows and after a certain distance in flow direction, it forms a lump. This characteristic is common for all different flow rates; however, the width of the rivulet decreases with decreasing flow rate.

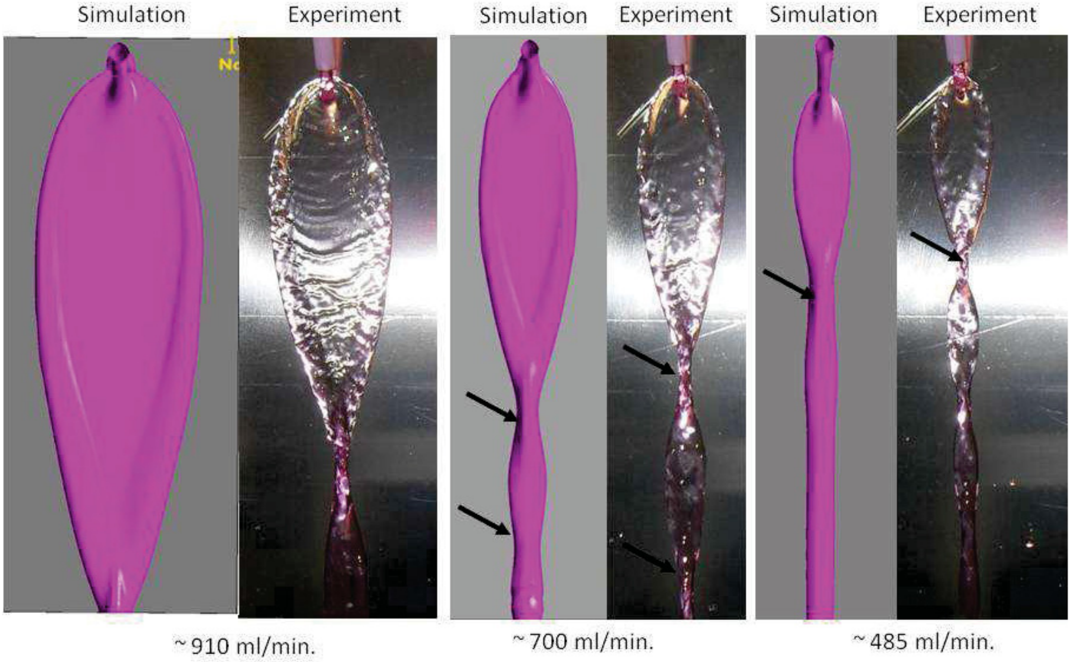

Figure 4.1 Comparison between experiment and simulation of wetting behaviour of water on inclined plate for three different flow rates.

Moreover, the position at which a lump forms is also influenced by the flow rate, i.e., lumps form earlier at lower flow rates and more such lumps are observed periodically. For low rates, more such lumps were observed in experimental studies but the simulation failed to predict those lumps. The simulation findings match very well with the experimental results. Also, this rivulet flow behaviour is in agreement with other works in literature (Hoffmann et al., 2006). Hence, simulations are also performed for other testing mixtures such as water-glycerol (45 wt. %) and silicon-oil to check the model prediction for different liquid properties such as viscosity and contact angle.

The comparisons for the water-glycerol mixture at two different flow rates are presented in Fig. 4.2. The maximum width of the rivulet formed is around 20 mm range at very high flow rates. It should be mentioned that the viscosity of the water-glycerol (45 wt. %) mixture is approximately five times higher than water, whereas, the contact angle remain almost in the same range of around 70°. Compared to the results obtained for water, similar trends like the formation of lumps can also be noticed for water-glycerol as liquid but the rivulet width is found to be much less, as mentioned earlier. At very low flow rates, except for one small lump, the flow is almost straight. Also here the simulation can predict the same behaviour along with the lump in the beginning. But, the later lumps are not predicted accurately as mentioned in the water case.

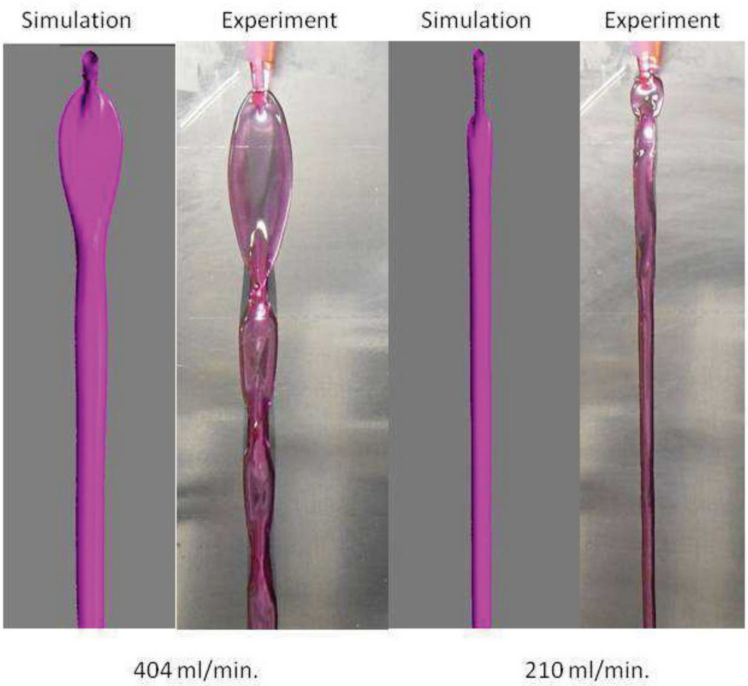

Figure 4.2 Comparison between experiment and simulation of wetting behaviour of water-glycerol on inclined plate for two different flow rates.

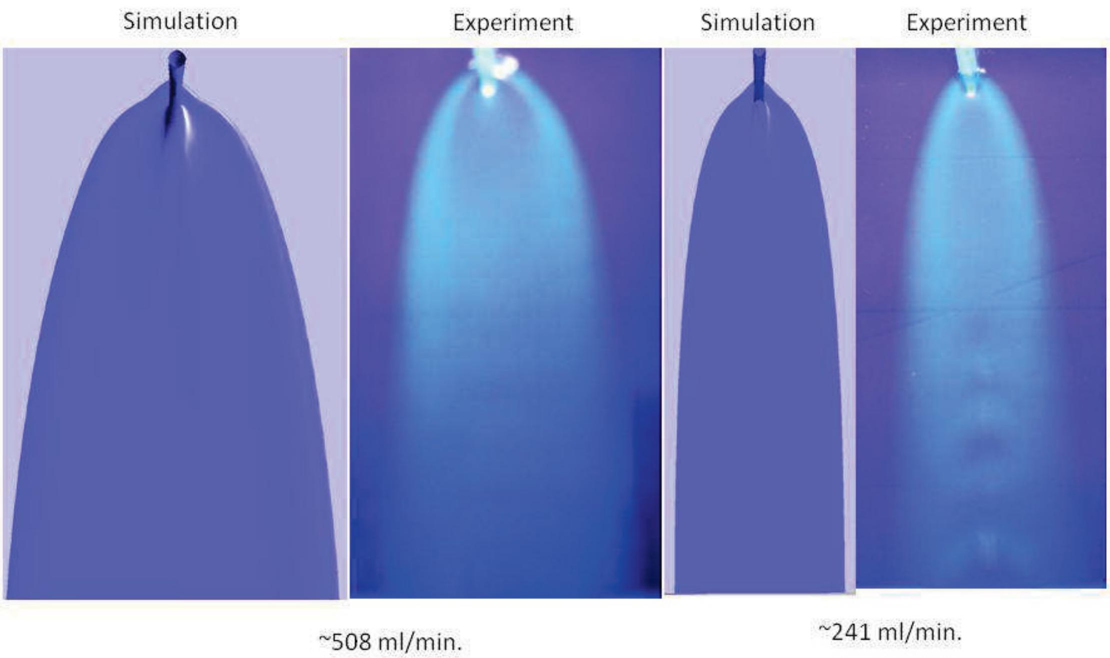

Figure 4.3 Comparison between experiment and simulation of wetting behaviour of silicon-oil on inclined plate for two different flow rates.

The comparison between simulation and experiment for silicon-oil (DC5) for two different flow rates is shown in Fig. 4.3. Compared to water and water-glycerol mixture, silicon-oil (DC5) has a very low contact angle of around 7° and therefore shows a completely different wetting behaviour. The rivulet width increases along the length of the plate for both high and low flow rates. The lump cannot be seen in contrast to the other two fluids. Also, the area of wetting is very high compared to water and water-glycerol.

Pictures taken during the experimental measurement are further analyzed using the freeware called Sigma scan. The analysis was based on the pixel rate present in the area in comparison to the pixel rate from the calibration, and further calculated to find the rivulet width. The error range for this analysis is +/- 1 mm. In the simulation, the rivulet width is calculated based on the volume of fraction of liquid on the bottom of the plate. In Fig. 4.4, the change of the rivulet width along the length of the plate in the flow direction is plotted for water, water-glycerol and silicon-oil (DC5). The simulation results are in good agreement with the experimental studies. In simulations the first lump that is formed is correctly predicted, but the additional lumps that form at low flow rates are not clearly visible. However, the trend of reduction in the rivulet width with increasing distance from the inlet in flow direction can be noticed. In the case of water, the range of error is observed to be around 5% for both the flow rates. At very low flow rates, the water flow is very chaotic without the formation of any rivulet sometimes it even flows as droplets (Not shown here).

The difference between experiment and simulation is around 5% which can be explained very well based on the sensitivity studies performed in the next section for velocity profiles. It is worth mentioning that the wetting characteristics from simulation match very nicely with experiments for a wide range of fluid properties; like low and high viscosity, low and high contact angle.

The comparison of the wetted area for three test mixtures water, water-glycerol and silicon-oil (DC5) is shown in Fig. 4.5. The agreement between the experiment and simulation is very good. The deviation is in the range of 3 – 5% for all three testing mixtures. The reason for this error can be studied while studying the velocity distribution profiles in section 4.2., where a detailed sensitivity analysis has been done for the influential factors.

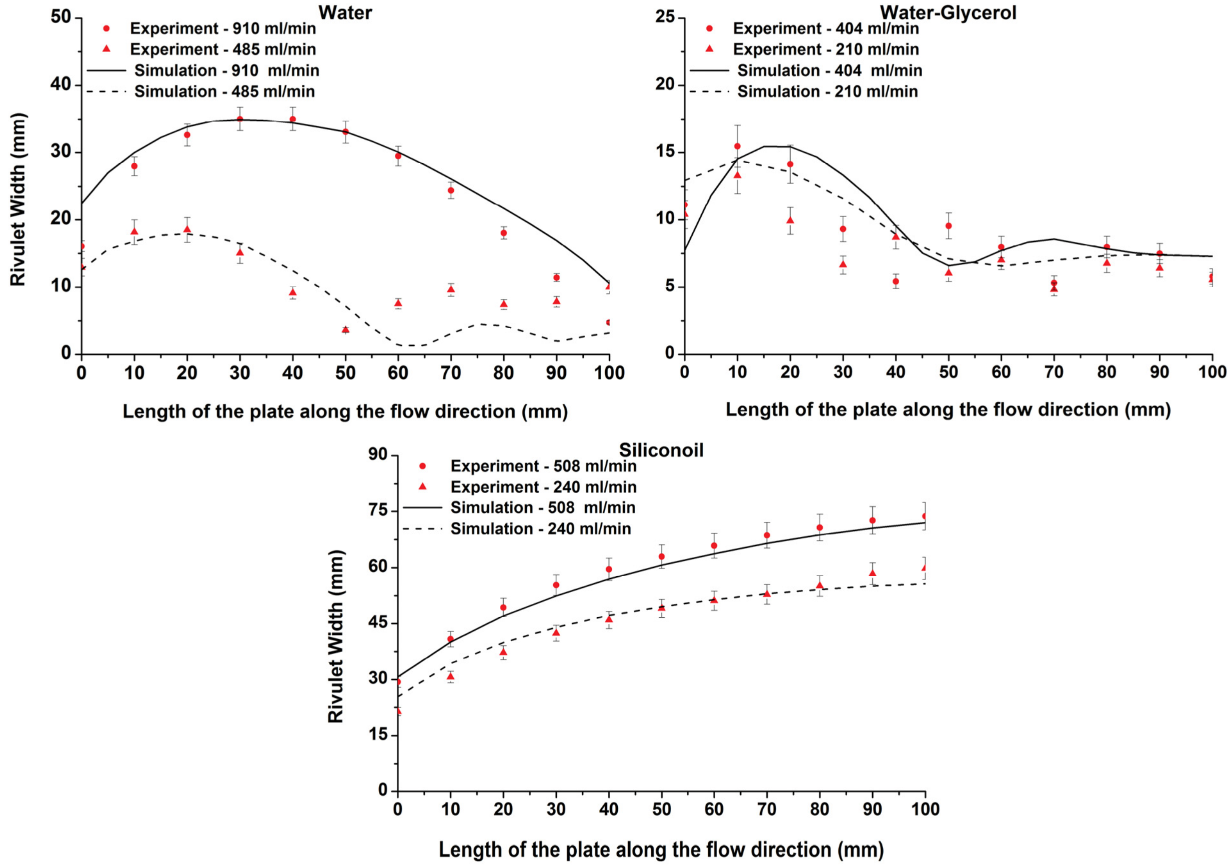

Figure 4.4 Rivulet Width along length of the plate in the flow direction for water, water-glycerol and silicon-oil (DC5).

From Fig. 4.5., the change in wetting due to change in viscosity and surface tension is clearly seen while comparing the percentage of the wetted area for water, water-glycerol and silicon-oil. For the liquid with low contact angle (i.e., silicon-oil here), the wetted area is almost 6 times more than liquid with high contact angle (i.e., water-glycerol (45 wt. %). The percentage of wetting can also be understood by comparing the width of the rivulets shown in Fig. 4.4. The increase of the width of rivulets for silicon-oil (DC5) as shown in Fig. 4.4 can be interpreted to the maximum % of wetting in comparison to other testing liquids (water and water-glycerol).

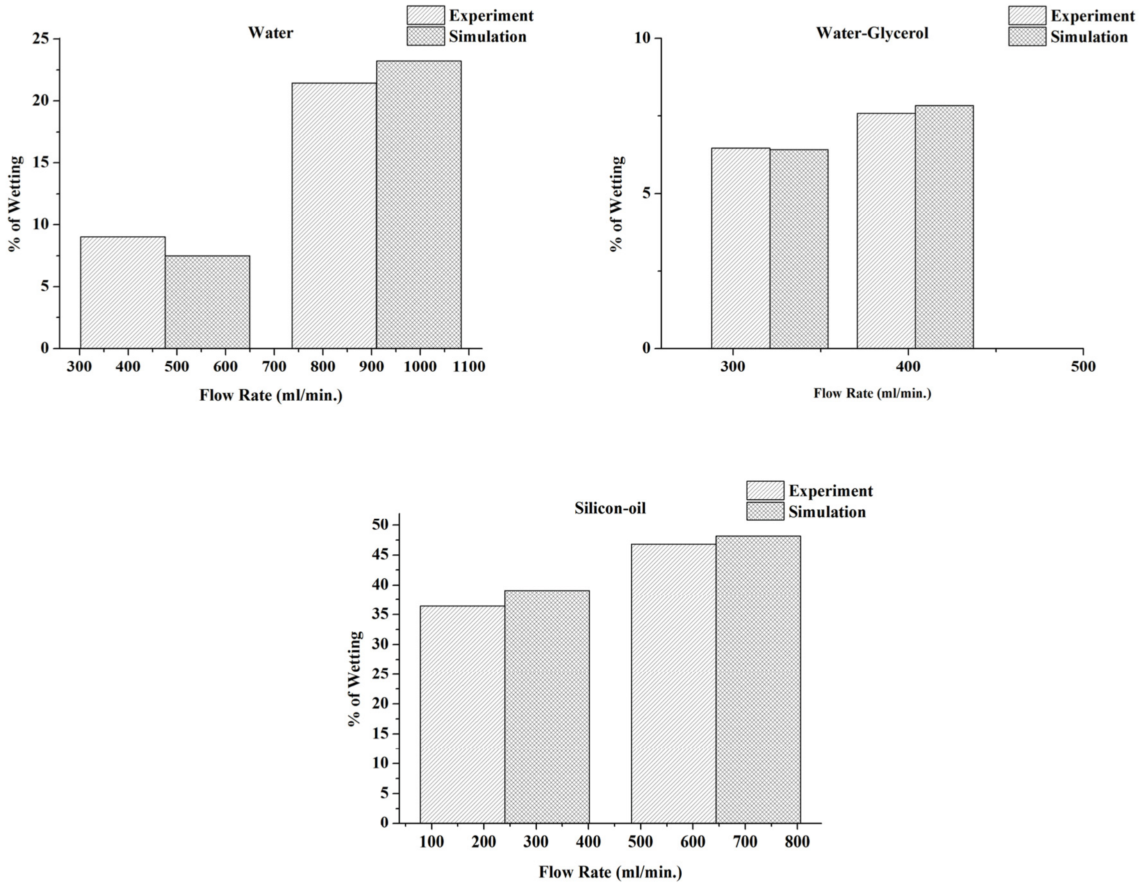

Figure 4.5 Comparison between experiment and simulation for the percentage of wetting of water, water-glycerol and silicon-oil in inclined plate (Note different scales for different fluids).

4.2 Study of velocity profile without countercurrent gas flow

4.2.1 Comparison for different Reynolds number

The velocity profile obtained from simulations with the water-glycerol mixture has been compared with experimental results for three different Reynolds numbers (Re_L = 64, 32 and 20) as shown in Fig. 4.6. The experimental measurements from (Paschke et al., 2007) are considered for comparison. The agreement between experiment and simulation is adequate as both exhibit a similar parabolic profile, but the difference between the profile from experiment and simulation is found to be high near the interface. Some specific fluid parameters might influence the deviation of the velocity profile and film thickness.

In order to explore the reason for this deviation, sensitivity analysis was performed considering the specific parameters. These parameters were selected based on the theoretical background of the flow behaviour which will be explained in next section.

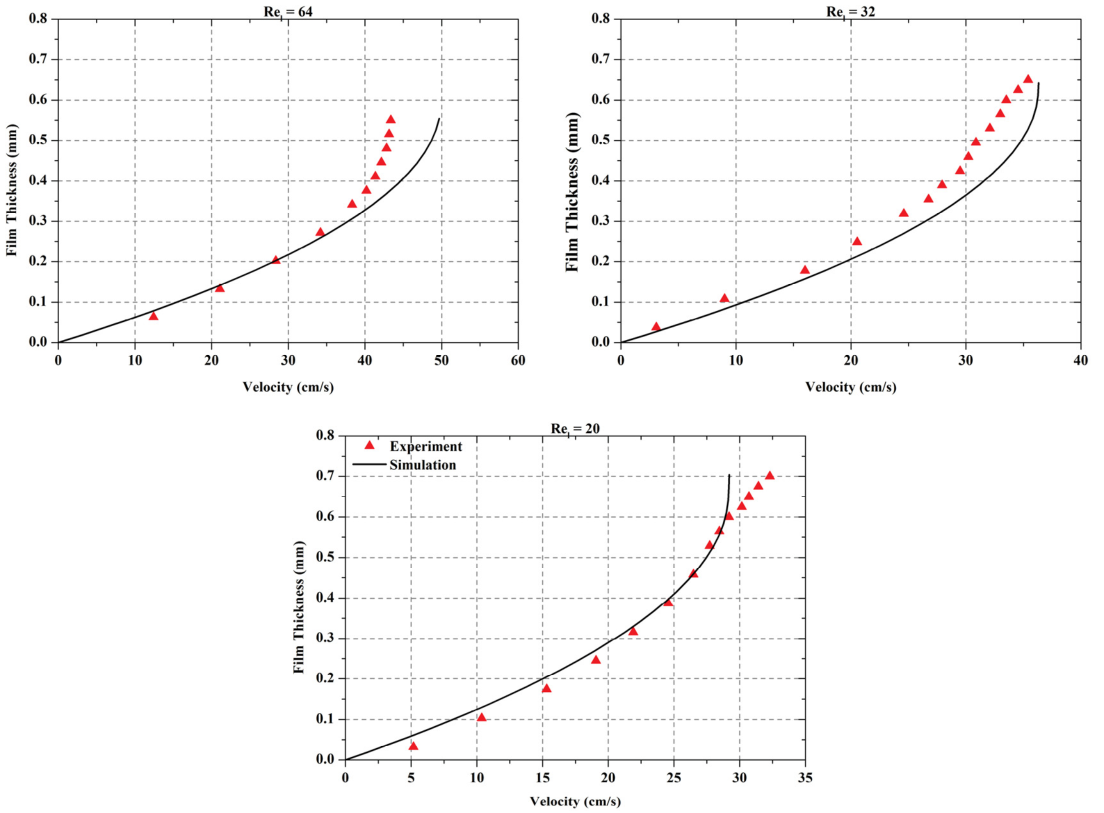

Figure 4.6 Comparison of velocity profile between experiment and simulation for water-glycerol.

4.2.2 Sensitivity Analysis

Parameters selected for sensitivity study are as follows:

a. Volumetric flow rate.
b. Temperature – viscosity.
c. Inclination angle.
d. Tilting angle.
e. Mass fraction.
f. Surface tension.

From the theoretical background, it is clear that the factors (a), (b) and (c) are more influential than (d), (e) and (f). The ranges of error are chosen according to the limitation of the experimental set up and considering possible measurement errors.

Table 4.1 An example of Sensitivity details for Re_L = 32.

	Re_L	Flow rate (mL/min)	Temperature (° C)	Inclination angle (°)
Base case	32	436.54	25	60
Flow rate (5% dec.)	30.40	**414.71**	25	60
Flow rate (5% inc.)	33.60	**458.36**	25	60
Temperature (3 °dec.)	29.50	436.54	**22**	60
Temperature (3 ° inc.)	36.25	436.54	**28**	60
Inclination angle IA (2° inc.)	32	436.54	25	**62**
Inclination angle IA (2° dec.)	32	436.54	25	**58**

The change of the velocity profile due to the 5% increase and decrease of the flow rate from the base case is shown in Fig. 4.7. The whole velocity profile shifts according to the change in flow rate as well as the change in maximum velocity at the interface. For example, the decrease in flow rate leads to the decrease in maximum velocity at the interface.

The influence of the change in temperature of +/- 3° C from the base case on the computed velocity profiles is shown in Fig. 4.8. The change in temperature affects the viscosity, which in turn, influences the whole velocity profile from the bottom of the plate up to the interface. With a high temperature, viscosity reduces slightly and hence velocity increases.

Fig. 4.9 shows the velocity profile for the change in inclination angle (IA) of +/- 2° from the base case. Within this error range, the change in the profile is not predominant.

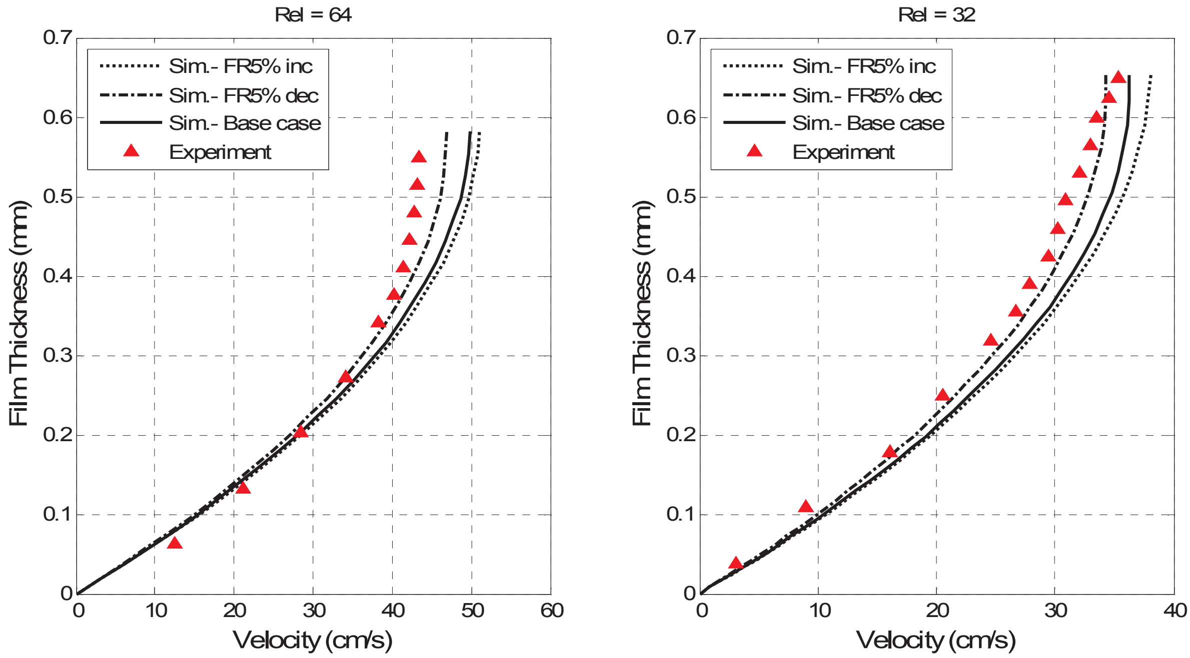

Figure 4.7 Sensitivity study of change in flow rate with 5% error range.

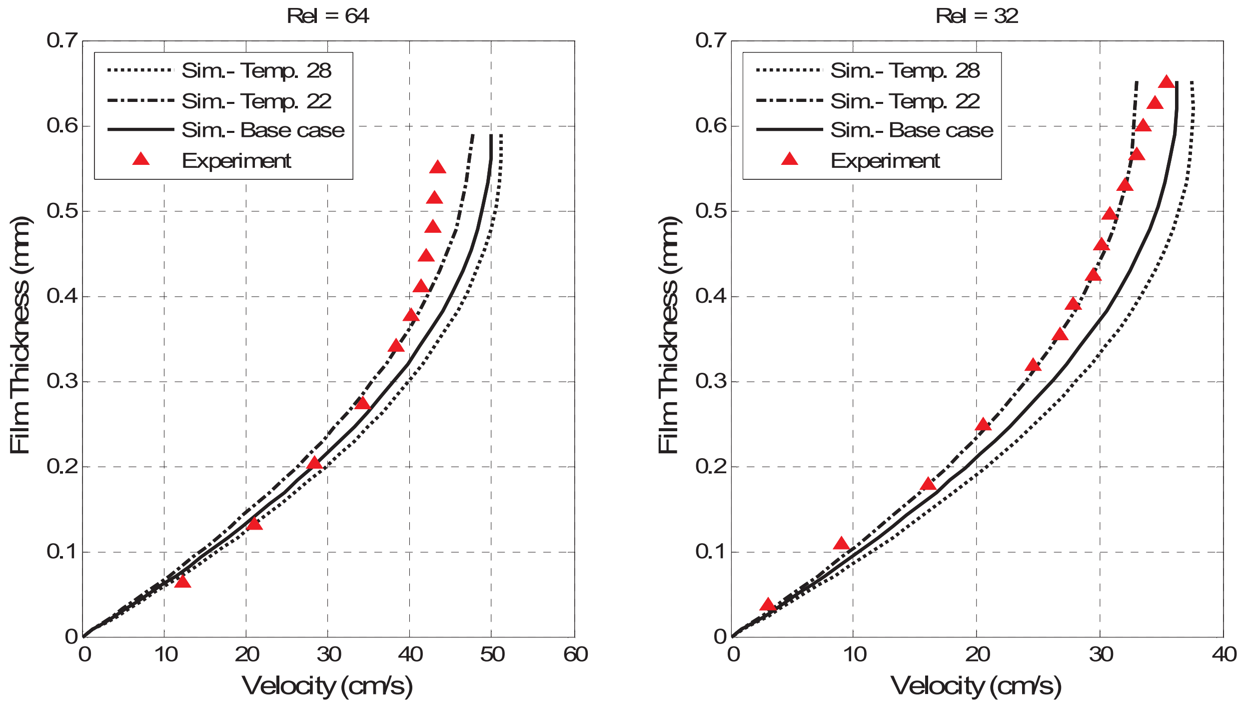

Figure 4.8 Sensitivity study of temperature with +/- 3°C difference.

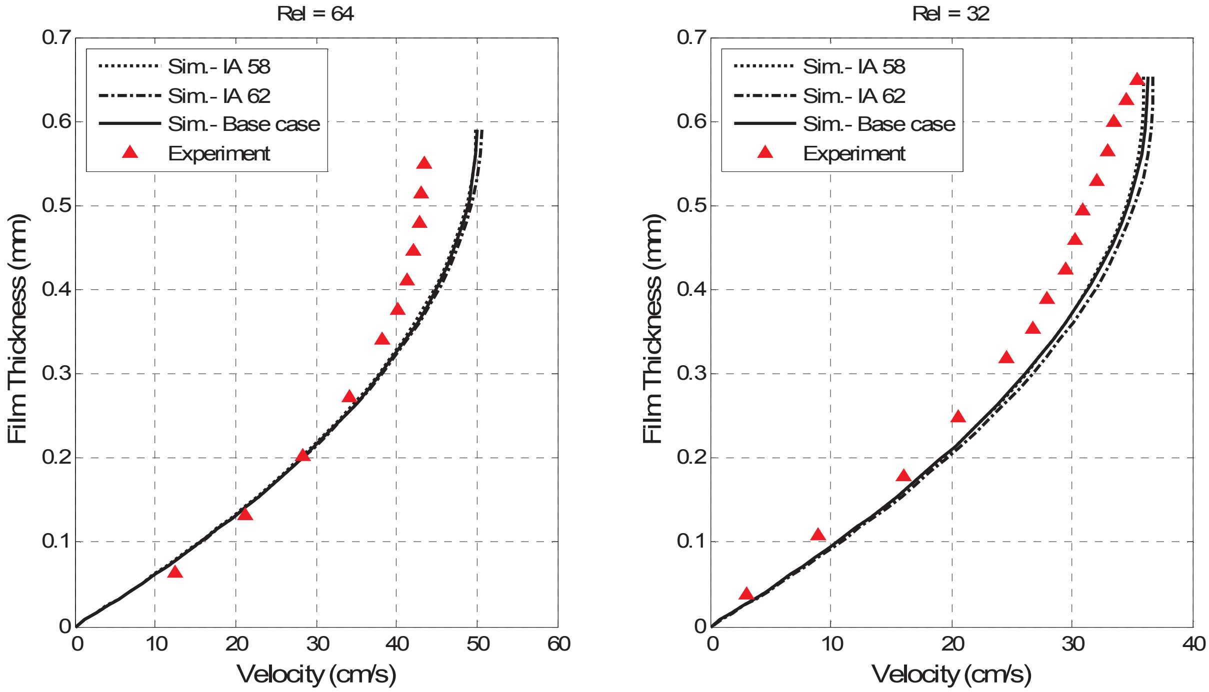

Figure 4.9 Sensitivity study of velocity due to change in inclination angle of +/- 2°.

A sensitivity study on the influence of flow rate, temperature and inclination angle has been performed for two different flow rates (Re_L = 64 and 32) and the trends are similar. This study explains clearly the difference in velocity profile between experiments and simulation. It is shown that a change of the flow rate or the temperature according to the measurement accuracy from the experimental setup has a pronounced effect on the computed velocity profile from the simulations. The difference in the computed profiles due with changed flow rate or temperature to the base case is comparable to the difference between the simulation and experiment for the base case. The change in inclination angle of +/- 2° which is in the measuring range of error doesn't cause much deviation in velocity profile. With this conclusion, further simulations are performed for the cases with countercurrent flow.

4.3 Study of velocity profile with countercurrent flow

The validated geometry and model for the case without countercurrent flow is now extended to study the influence of the countercurrent gas flow. Water-glycerol (45 wt. %) and air is used as testing mixture. For comparison, the profiles with and without countercurrent flow are presented. To analyze the influence of countercurrent gas flow, the study has also been performed for different gas phase velocities. The F-factor which is commonly used to express countercurrent gas velocity in distillation and absorption can be defined as

$$F = u_g \cdot \rho_g^{0.5} \tag{4.1}$$

The liquid flow in the simulation and experiment is laminar, as the liquid phase Reynolds numbers are always lower than 300 and the velocities of the gas phase i.e., F-factor is also in the range of 1.5 and 2.5 $Pa^{0.5}$. This resembles the range used in industrial operating conditions.

The position-weighted average profiles are calculated in simulation by analyzing the local profiles on different positions along the length and width of the plate. The measuring position is around center of the plate along the width and around 110 mm along the length, which is the same as the experimental measuring position.

In Fig. 4.10, the velocity profiles from experiment and simulation for both the cases with and without countercurrent flow is compared. In Fig. 4.10, dots represent the experiment and the line represents the simulation.

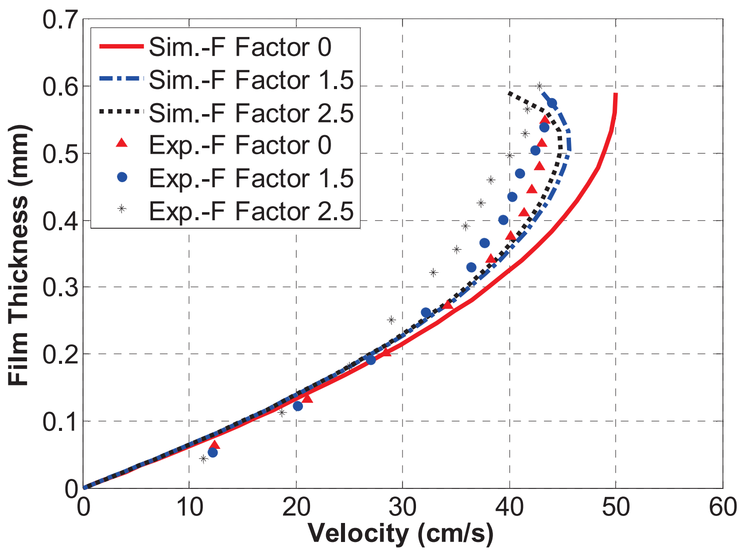

Figure 4.10 Comparison of velocity profile flow with and without countercurrent for water-glycerol (45 wt. %) with Re_L = 64.

The different between the simulation and experiment for the case without countercurrent gas i.e., F-factor 0 (Red line and Red triangles in Fig. 4.10) was discussed in the earlier section. Here, the difference between the experiment and simulation due to countercurrent gas flow i.e., F-factor 1.5 and 2.5 $Pa^{0.5}$ will be discussed. While discussing the influence of countercurrent gas flow, the difference due to other factors such as viscosity and flow rate as shown in section

4.2.2 should be kept in mind. In the simulation, the influence of countercurrent gas flow can be noticed around the interface of the phases. The velocity at the gas-liquid interface reduces due to the influence of countercurrent gas velocity and in turn increases the film thickness. The increase in thickness is not visible here as it is in the range of 0.02 to 0.04 mm. The profile shown in Fig. 4.10 has been cut up to the liquid film height and the gas region is not shown. The standard deviation between the experiment and simulation is around 5 – 8%. This difference is within the acceptable range considering the challenges in the experimental measurement.

The velocity profile obtained from the experiment which starts like parabolic profile at bottom of the plate changes to a linear profile near the gas liquid interface. The linear profile near the interface obtained from the experiments has two main reasons. Firstly, the deceleration due to the countercurrent gas phase. Secondly, due to formation of waves as observed in the experiments. The profile is obtained by averaging images, from all the wave and film regions. Hence, the possibility of the averaging error plays a major role. Simulations are performed for shorter duration than experiments due to the restriction in computational power and time constraints. To confirm the formation of waves using simulation, simulations should be performed for a considerably longer time and the profiles must be compared.

The experimental film thickness is slightly higher than in the simulation. Experimental measurements have an error in the y direction that is the same as the depth of focus which is almost equal to +/- 0.04 mm. This error depends on the properties of the testing system such as refractive index.

Overall, the VOF model gives good agreement between experiments and simulations for both the case with and without countercurrent flow. The detailed sensitivity analysis also confirmed the influences of various fluid properties and flow parameters on the liquid velocity and liquid film thickness. This model should be extended for studying the flow behaviour in the complex geometry which resembles the industrial packing such as corrugated sheets of packing.

5 HYDRODYNAMICS ON CORRUGATED SHEET OF PACKING

The hydrodynamic behaviour on corrugated sheets of packing with different geometrical modifications (see section 3.1.2) was analysed for three different testing systems (see section 3.3.1.). Different modifications in corrugated sheet considered in this study are

- Triangular crimp surface.
- Curve crimp surface.
- Influence of perforations.
- Influence of second corrugated sheet.

In section 5.1, the results from the CFD simulations on corrugated sheets of packing with triangular crimp surface will be described. In section 5.2, different parameters such as film thickness, holdup and velocity profiles from simulations are compared with experimental studies for both corrugated sheets of packing with and without perforations. The influence of perforation on wetting behaviour will be discussed in detail. In section 5.3, the influence of second corrugated sheet on liquid hold up and wetting will be explained.

5.1 Flow on corrugated sheet with Triangular Crimp surface

As explained in section 3.1.2 and shown in Fig. 3.3, simulations are performed for geometry with triangular crimp surface. Here simulation results are presented for two different testing systems i.e., water and silicon oil. Fig. 5.1 and Fig. 5.2, shows the velocity vectors for the flow of water and silicon oil, respectively. Here, simulations are performed considering the corrugation sheet of packing is at 90° and the flow is from top of the sheet flowing parallel to the sheet. Liquid flows through two circular inlets of 4 mm diameter, which resembles the distributors utilized in industrial applications.

From Fig 5.1 and Fig 5.2, it was that in triangular crimp the liquid deflects outside the corrugation and does not flow in the direction of corrugation. It is also true that the triangular edge has more influence on deflecting the liquid flowing over it. Further, the velocity of the liquid also increases drastically after meeting the triangular crimp. In addition, the difference of flow due to smooth crimp surface can be clearly visualized from the next section. The same behaviour was noticed in another lesser flow rate for both the liquids (Not shown here).

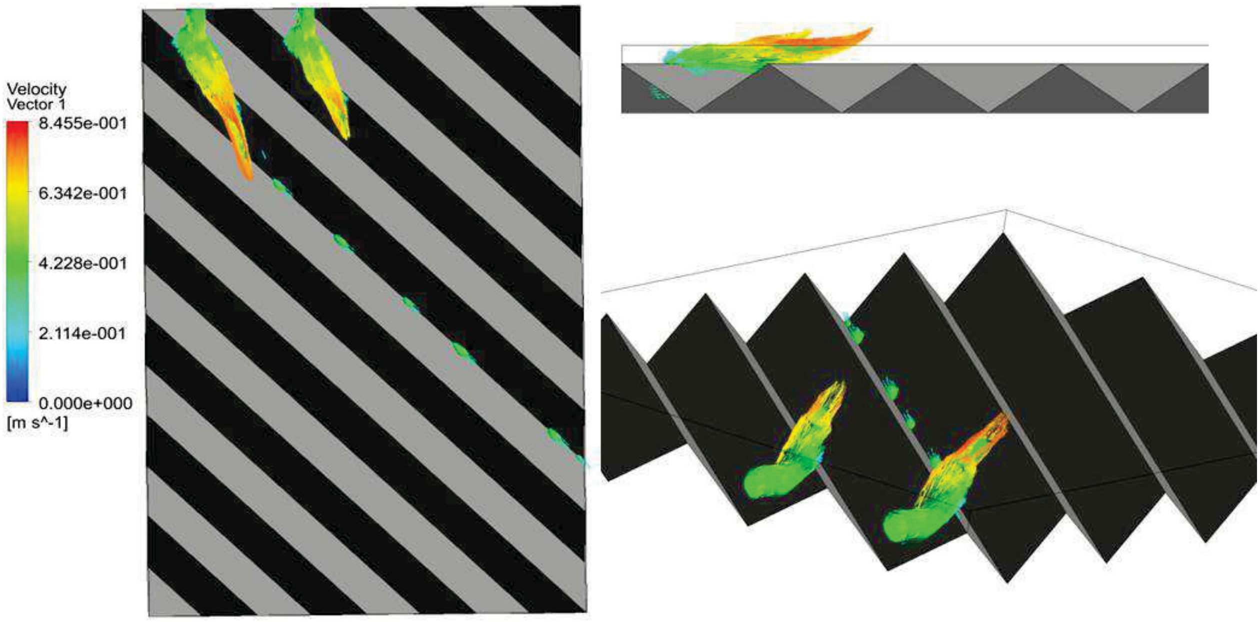

Figure 5.1 Velocity vector of water on geometry resembling corrugated sheet of packing with triangular crimp surface (Flow rate - 386 mL/min, Re_L - 2033).

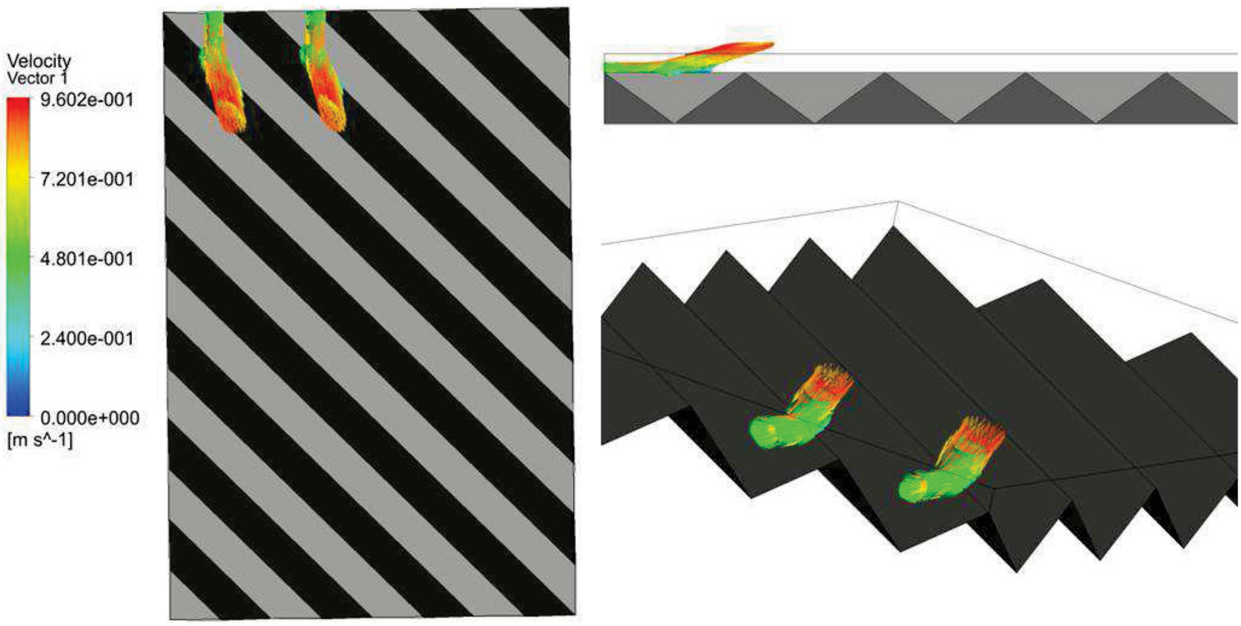

Figure 5.2 Velocity vector of silicon-oil (DC5) on geometry resembling corrugated sheet of packing with triangular crimp surface (Flow rate - 241 mL/min, Re_L - 230).

In general, the industries uses corrugated sheet with smooth crimp surface and most of the real corrugated sheet are made of stainless steel. Only very few packings are made of ceramics which has strict triangular crimp surface. Overall, the general simplifications of corrugated sheet of packing with smooth crimp surface to triangular crimp surface for meshing purpose needs to be reconsidered.

5.2 Flow on Corrugated sheet with smooth crimp surface with and without perforations

The flow behaviour on corrugated sheets of packing was analyzed to understand four different parameters such as flow direction, wetting, film thickness and velocity distribution.

5.2.1 Flow direction

The change in flow direction for the corrugated sheets of packing without perforation is shown in Fig. 5.3. It is clear that the liquid mainly follows the corrugation and sometimes drips from one crest to another.

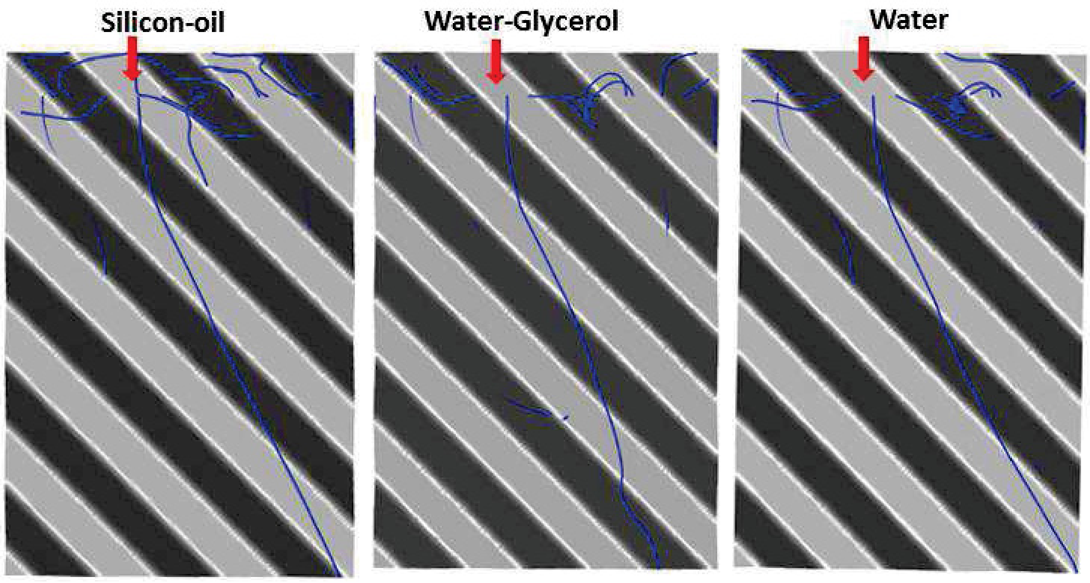

Figure 5.3 Flow direction for silicon-oil (Re_L - 241), water-glycerol (Re_L - 386) and water (Re_L - 386) in corrugated sheets of packing without perforations.

The liquid flow direction did not change much with the change in physical properties of the liquid, especially viscosity and contact angle. For the liquid with low contact angle, liquid flows over the crest than just following the direction of corrugation. This is also in relevance with the finding of (Shetty and Cerro, 1997) where they presented the flow direction to calculate the exposure time of liquid film and compared it with empirical correlation for effective flow angle developed by (Spekuljak, 1986).

In Fig. 5.4., the change in liquid flow direction for the corrugated sheet of packing with perforations is shown. It can be noticed that the liquid flow follow the corrugation both in front and back side of the corrugated sheet. The phenomenon is similar to corrugated sheet without perforations.

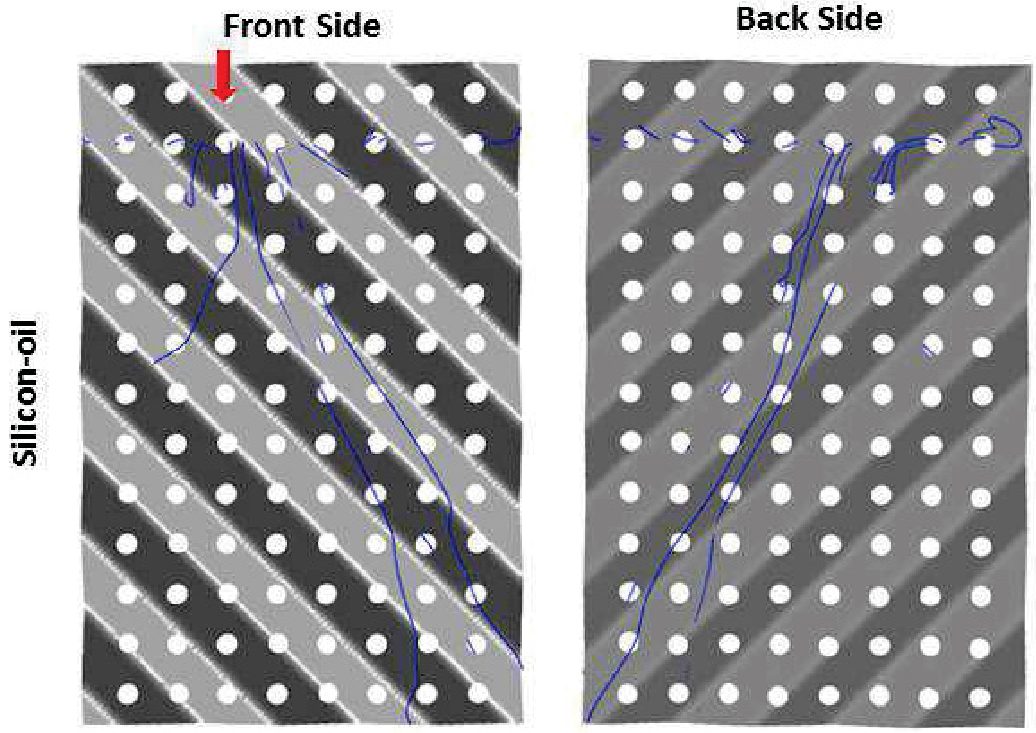

Figure 5.4 Flow direction for silicon-oil (Re_L - 241) in corrugated sheets of packing with perforations.

The phenomenon of wetting was studied (Battista and Böhm, 2003) experimentally and compared with the empirical correlation developed earlier in the literature (Shetty and Cerro, 1997). In the next section, the phenomenon of wetting is described in detail.

5.2.2 Wetting

In this section, the change in wetting behaviour of three different liquids due to change in flow rate and contact angle without the influence of gas flow is shown for corrugated sheets of packing with and without perforations. The comparisons of interfacial area predicted by various empirical equations are also shown.

Geometry utilized in the simulation is similar as shown in Fig. 3.4. As explained in the section 5.1, liquid flows through 4 mm circular inlet which flows over the corrugated sheet at 90° parallel to the sheet. The influence of liquid inlet is taken into consideration via velocity boundary condition rather than using the geometry. The details of the flow rate and Re_L used in this work are shown in Table 5.1. Two flow rates are used for each testing liquid. Experiments are performed on Montz B1-300 packing. These packing are without perforation, but contain microstructure on the surface. However, the geometry used in the simulation is built without microstructure on the surface of the packing. Hence, these differences should be considered while comparing the results of simulation with experiment. In simulations, three dimensional microstructures are not considered for now because it is very complicated to mesh the geometry and in turn increases the computational time extensively. The liquid flow requires only less energy to flow over and through the corrugation and it does not deflect highly as it can be seen in triangular crimp. This is also in accordance with experimental studies performed. The flow of the silicon-oil over corrugated sheets of packing with smooth crimp for two different flow rate is presented in Fig. 5.5.

Table 5.1 Details of the flow rate and Reynolds number used in this work.

	Flow rate (mL/min)	Re_L
Water	386	2033
	623	3291
Water-glycerol (45%)	386	486
	590	743
Silicon-oil (DC5)	241	230
	508	486

Fig. 5.6 and 5.7 shows the comparison between experiment and simulation for flow of water, water glycerol and silicon-oil over real corrugated sheet of packing with smooth crimp and without perforation. Rectangular box shown in red colour is the geometry considered in simulation studies.

Fig. 5.8, 5.9 and 5.10 shows the comparison between experiment and simulation for flow of water, water-glycerol and silicon-oil over a corrugated sheet of packing with smooth crimp and perforation.

Simulations are performed for all three testing liquids with two different flow rates. Fig. 5.11 summarizes the percentage of wetting for all three liquids for corrugated sheet of packing with and without perforations.

Influence of Flow rate

The change in wetting behaviour due to change in flow rate for silicon-oil (DC5) is shown in Fig. 5.5. As seen in chapter 4 for inclined plate, the percentage of wetting increases with increase in flow rate. This phenomenon was also noticed in experimental studies and in other literature (Battista and Böhm, 2003). The change in the wetting for all three liquids due to flow rate is summarized in Fig. 5.11. For low viscous liquid like water, influence of flow rate is more predominant than for high viscous liquid like water-glycerol and silicon-oil, i.e., increasing the flow rate by two times from 386 mL/min to 623 mL/min increases the wetting by almost 2.5 times from 4.23 to 11.33 % for water, but on other hand, for high viscous liquids like silicon-oil, it is only around 1.5 times. For high viscous liquid with high contact angle like water-glycerol, the change in wetting area changes only around 0.5% even with change in flow rate of almost twice. For water, in the case of the corrugated sheets with perforations, the percentage of wetting increases from 6.67 to 12.83 due to increase in flow rate by almost 2 times from 386 to 623 mL/min. The same trend of wetting was noticed for corrugated sheet of packing with and without perforations.

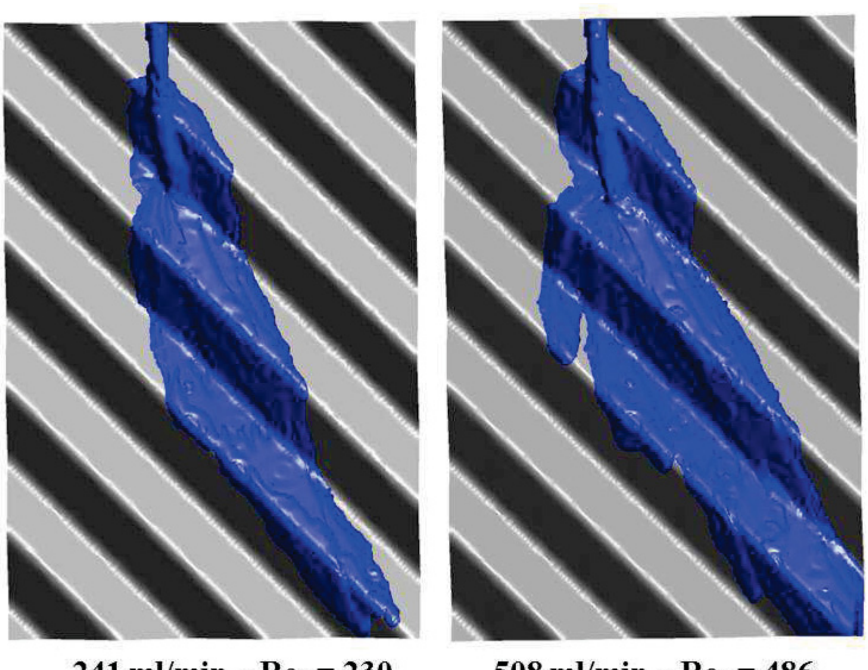

241 ml/min. - $Re_L = 230$ 508 ml/min. - $Re_L = 486$

Figure 5.5 Comparison of wetting for silicon-oil (DC5) for two different flow rates from CFD simulations.

Influence of viscosity

The influence of viscosity on wetting can be noticed by comparing the wetting behaviour of water and water-glycerol shown in Fig. 5.6. The change in the wetting for all the three liquids due to flow rate is summarized in Fig. 5.11. For the low flow rate, the change in percentage of wetting is significant for high viscous liquid. For the same flow rate, the percentage of wetting is 4.75 and 10.0 for water and water-glycerol respectively (see Fig. 5.11). On the other hand, for higher flow rate, the percentage of wetting is 11.5 and 10.5 for water and water-glycerol respectively. The trend looks similar for corrugated sheets of packing with and without perforations.

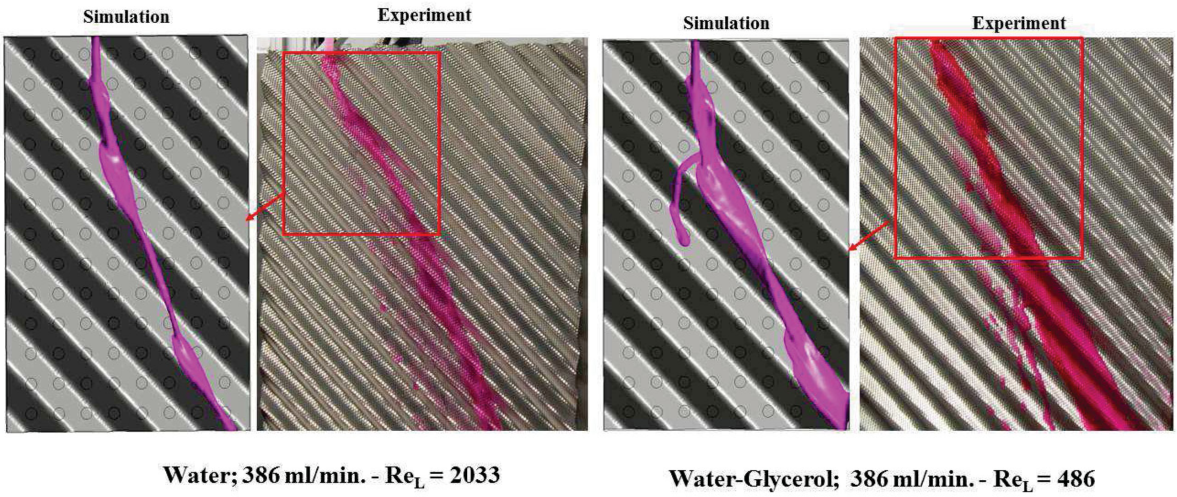

Figure 5.6 Comparison between simulation and experiment for flow of water on corrugated sheet of packing without holes.

Influence of Contact Angle

The fluid with low contact angle i.e., silicon-oil (DC5) has high wetting in comparison to water and water-glycerol (45 wt. %), which has very high contact angle and is visible while comparing Fig. 5.6 and 5.7. The influence of contact angle is very clear when water-glycerol and silicon-oil is compared as they are in the same viscosity range. For the same flow rate, percentage of wetting for silicon-oil is almost twice than water-glycerol (see Fig. 5.11)

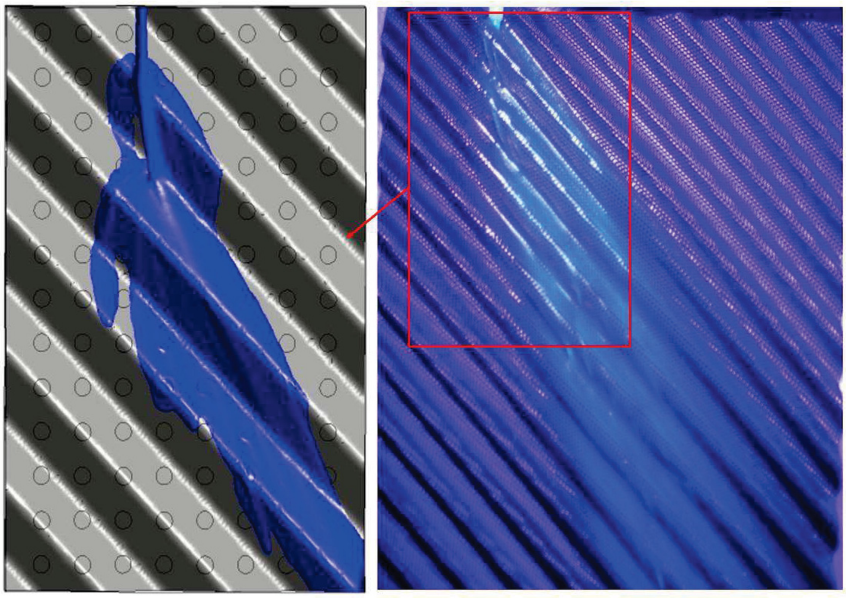

Figure 5.7 Comparison between simulation and experiment for flow of silicon-oil (DC5) on corrugated sheet of packing without holes.

Influence of perforation

In this section, the influence of the perforations in wetting is discussed in detail. The comparison between experiment and simulation for flow of water, water-glycerol (45 wt. %) and silicon-oil (DC5) on corrugated sheet of packing with perforations is shown in Fig. 5.8 to 5.10 respectively. The change in flow and in wetting can be seen while comparing with the Fig. 5.8 and 5.10. It is rather tedious and difficult to capture the flow on back side of the corrugated sheet experimentally. Hence, only qualitative experiments were performed as a part of this work. Using CFD simulations, wetting on both the sides of corrugated sheets of packing can be studied. The flow on front side of the sheet is shown in comparison with experiment and simulation. Simulation area is similar to the one mentioned in earlier section. (Red box in Fig. 5.6 and Fig. 5.7). To capture the flow behaviour on the back side of the packing and to study the influence of perforations on velocity, wetting and holdup, CFD gives good opportunity.

Fig. 5.11 shows the wetting on both front and back side of corrugated sheet with perforations in comparison with wetting of corrugated sheet without perforations. Due to perforations, both sides of the corrugated sheets are wetted. Even though, the percentage of wetting for corrugated sheets without perforations in the front side is higher than the percentage of wetting for corrugated sheets with perforations, the total percentage of wetting (i.e., sum of both front and back) for corrugated sheets of packing with perforations is higher than total percentage of wetting (here only front side) for corrugated sheets without perforations. There is an increase of about 2 – 5% (see Fig. 5.11) in the wetting area for the corrugated sheet with perforation in comparison to the one without perforations.

As mentioned earlier, the liquid with low contact angle (silicon-oil) utilizes both the sides of corrugated sheets than the liquid with high contact angle (water and water-glycerol).

The wetting is higher for high flow rates both on the front and back side of the packing. Hence the wetting of liquid on the back side of the packing is high for high flow rate. For the high viscous liquid like water-glycerol, the difference in wetting on the back side of the packing is not very high even with increase in flow rate. For testing system with low contact angle i.e., silicon-oil, the increase in flow rate also increases the wetting area on the back side of the corrugated sheet.

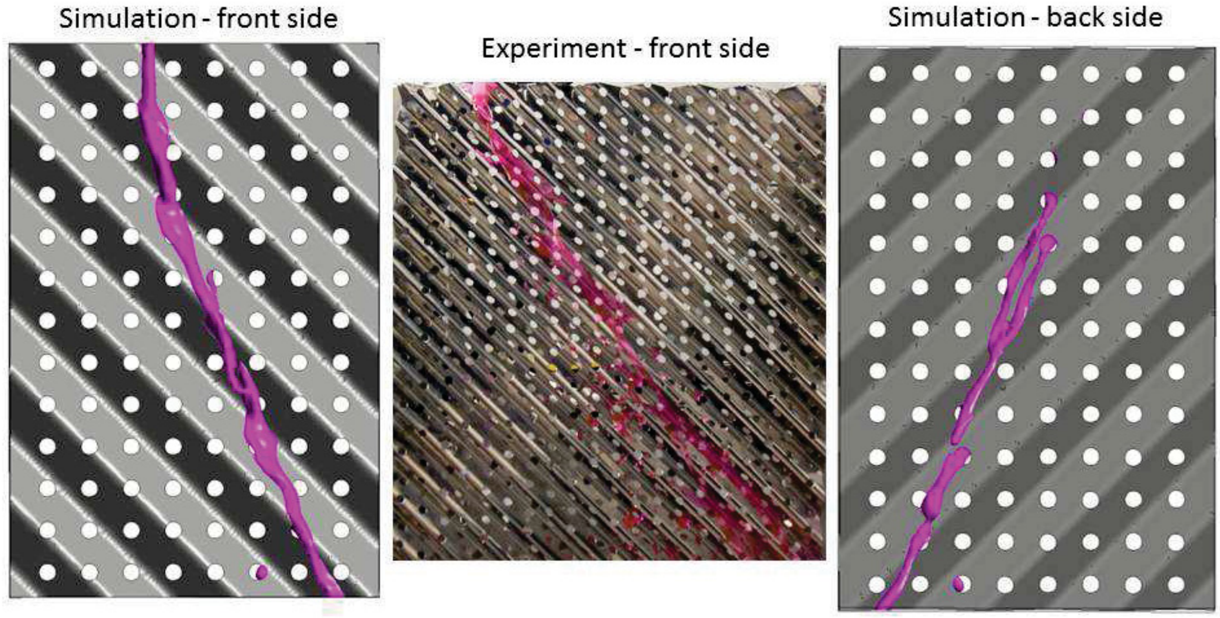

Figure 5.8 Comparison between simulation and experiment for flow of water on corrugated sheet of packing with perforations. Flow rate - 386 mL/min ; Re_L - 2033.

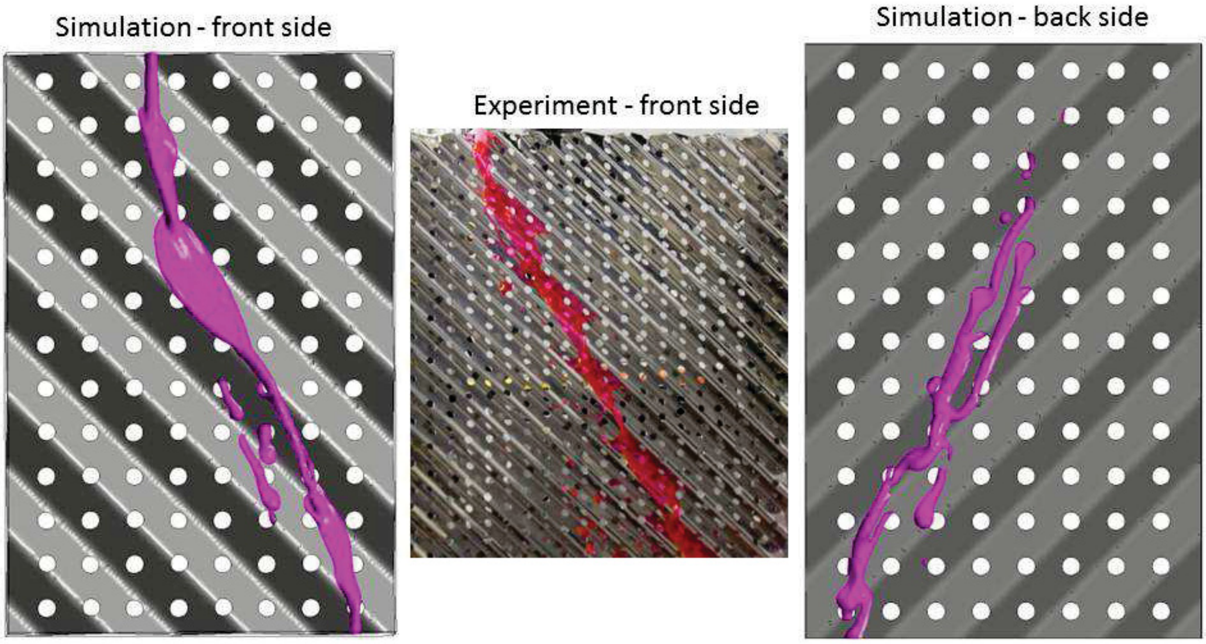

Figure 5.9 Comparison between simulation and experiment for flow of water-glycerol on corrugated sheet of packing with perforations. Flow rate - 386 mL/min ; Re_L - 486.

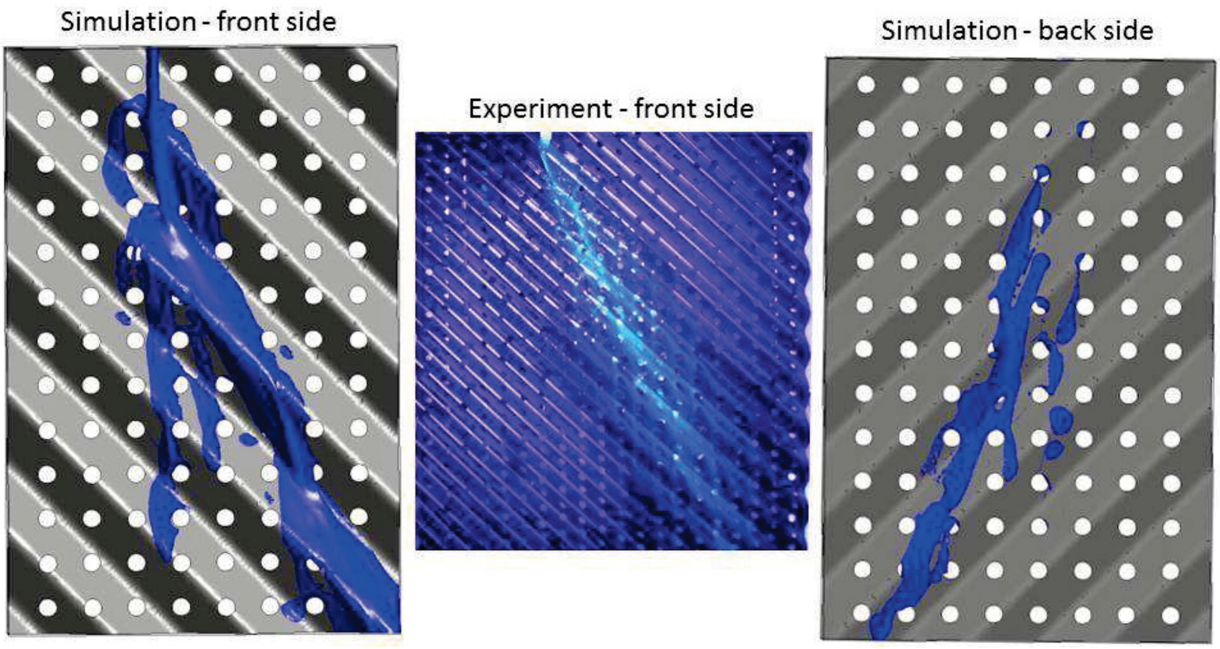

Figure 5.10 Comparison between simulation and experiment for flow of silicon-oil on corrugated sheet of packing with perforations. Flow rate - 241 mL/min; Re_L - 256

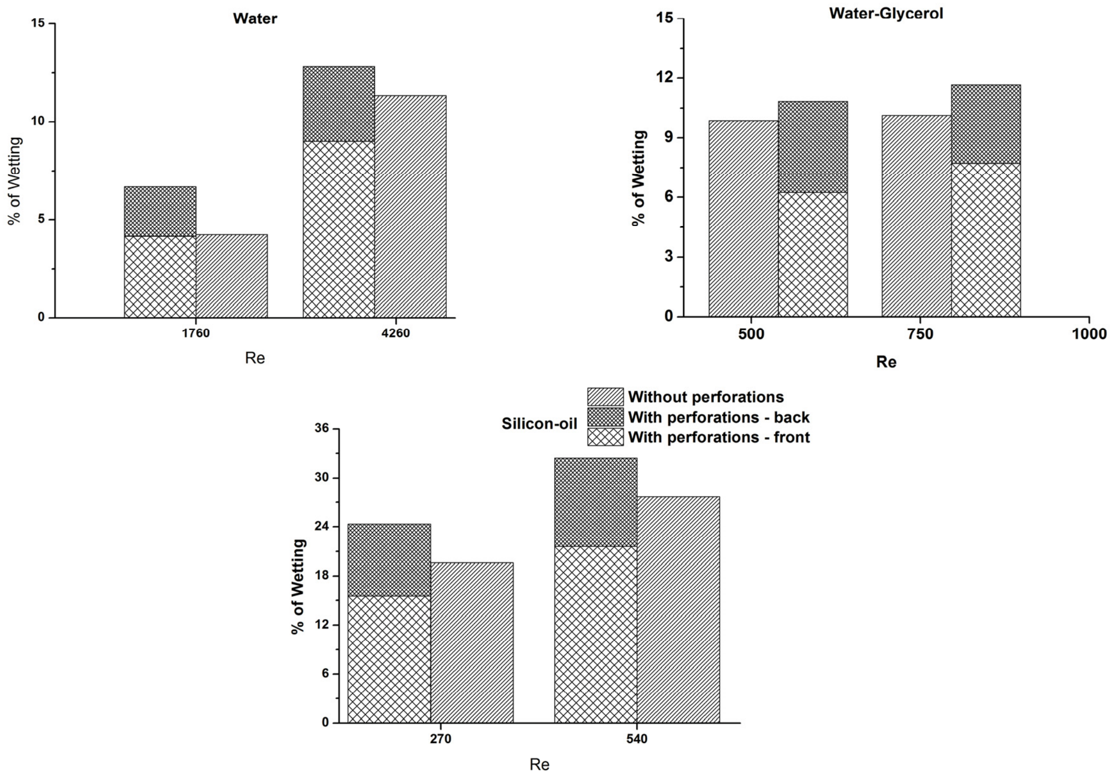

Figure 5.11 Comparison of percentage of wetting for corrugated sheet of packing with and without perforations for water, water-glycerol and silicon-oil using CFD.

Comparison of different empirical correlations

The comparison of five different empirical correlations available in the literature for the ratio of interfacial area to total packing area as a function of different flow rate for all three testing liquids water, water-glycerol and silicon-oil is shown in Fig. 5.12. Here, five different empirical correlations explained in section 2.3.2 have been compared. It is clear that all the correlations predict the increase in interfacial area with increase in flow rate. In Fig. 5.11, when (a_e/a_p) is greater than 1, it indicates that the packing is completely wetted. (de Brito et al., 1994) correlation predicts the complete wetting for almost all flow rates. In experiments and in simulation, it is not the case. This behaviour of complete wetting is shown for all three testing liquids. The correlation shown in Eq. 2.16, considers only the liquid density and viscosity but the other important wetting parameter such as surface tension and contact angle was not considered. The wetting of water-glycerol and silicon-oil looks the same. These results are in accordance with earlier findings from the literature (Pangarkar et al., 2008).

The correlation proposed by (Rocha et al., 1996) as given in Eq. 2.14 is an extension of the one proposed by (Shi and Mersmann, 1985). In his correlation, (Rocha et al., 1993) considered influence of liquid properties like density, viscosity along with surface tension and contact angle. The geometry of the packing was also taken into consideration by including the length of the corrugation side and corrugation angle. The influence of the microstructure was included by using surface enhancement factor (F_{SE}) but the perforations were not considered while calculating the interfacial area. In this correlation, the influence of contact angle is strong that it predicts complete wetting even for low rates.

(Billet and Schultes, 1999) developed a theoretical model that can be applied to random and structured packing and the correlation is shown in Eq. 2.15. The influence of the surface tension was taken into consideration by Weber number but the contact angle was neglected. The influence of the surface tension was very strong, that it predicted the complete wetting even for low flow rates. In high flow rates, the results from (Billet and Schultes, 1999) correlation were in accordance with (Rocha et al., 1993) correlation as described earlier. For the liquids with high surface tension, it did not match with the (Rocha et al., 1993) correlation.

The correlation proposed by (Olujic et al., 2004) for structured packing is an extension of correlation proposed by (Onda et al., 1968) for random packing as shown in Eq. 2.22. Here, none of the packing specific parameter was required to define the interfacial area. Also, influence of the perforation was taken into consideration by Ω which considered almost 10% of the surface area of wetting. Usually the perforation size in the packing is 4 mm. This equation suggests 10% of less wetting for the corrugated sheet of packing with perforations. From our earlier simulation, it is clear that even though the wetting in the front side is less for the sheets with perforations, the total wetting including the back side of the packing is more.

(Brunazzi et al., 1995) proposed a correlation for interfacial area from film thickness and liquid holdup values which is shown in Eq. 2.20. They utilized the correlation of holdup from the (Suess and Spiegel, 1992) and included other parameters such as density, viscosity, corrugation angle. This analogy missed the influence of contact angle and surface tension. This can be noticed in Fig. 5.11 as it predicts almost the similar wetting for water and silicon-oil.

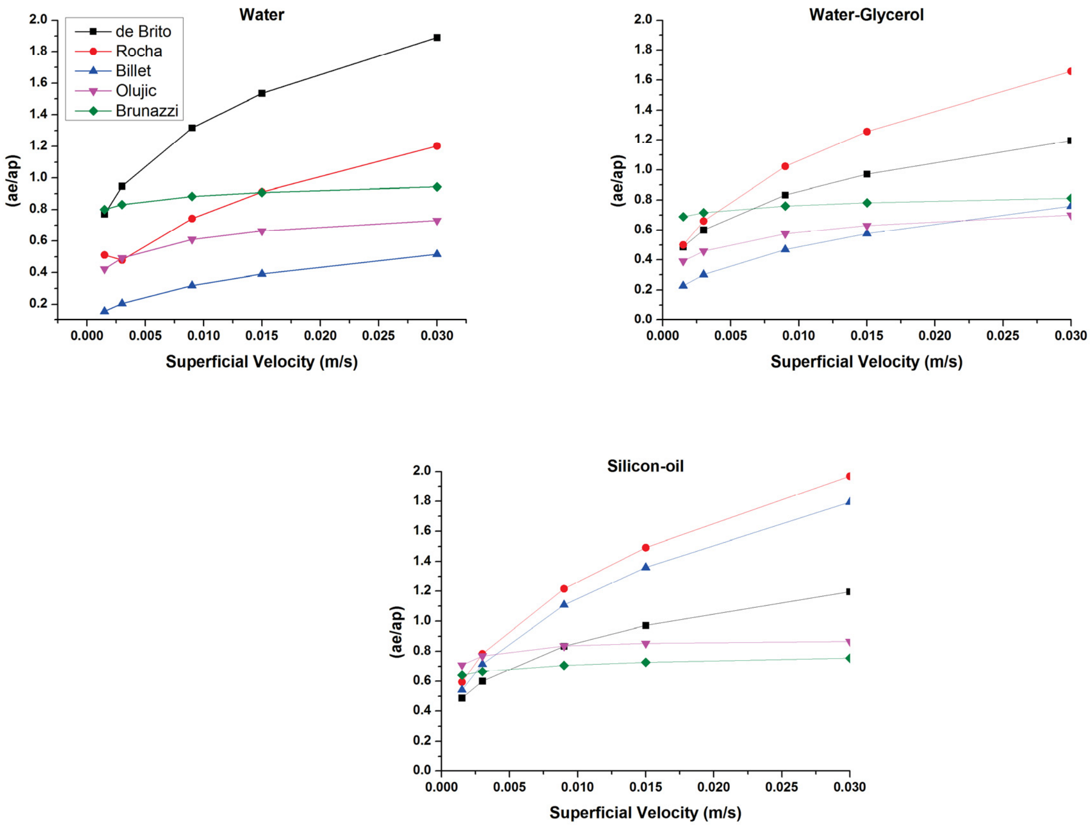

Figure 5.12 Comparison of different empirical correlations for the ratio of effective interfacial area to packing area vs. flow rate for different testing liquids.

Even though, there are many empirical and semi empirical correlations available in literature but none of them are universally acceptable for the different corrugated sheet of structured packing. Especially, these correlations does not consider all the liquid properties like density, viscosity, surface tension, contact angle and packing specific parameters like microstructures and perforations. Hence, still a long gap exists in order to determine the effective interfacial area available for mass transfer in structured packing.

The influence of microstructure in the packing is not considered in the simulation part of this work. However, in general, microstructure on the surface of the packing enhances homogeneity of surface wetting and hence the wetting area. Due to the complexity in meshing the geometry in CFD tools, the influence of microstructure is not considered in this work. But the influence of microstructure on wetting is briefly tested experimentally and is explained in the next sections. Qualitative agreement is found between CFD simulations and experimental findings.

5.2.3 Film Thickness

In this section, the change in film thickness for three testing liquids and corrugated sheets with and without perforations is discussed. The film thickness is shown for different positions in the geometry. Liquid flows in the direction of Z-axis. Results are shown for both ZY and XY plane. As shown in Fig. 5.13, four planes are chosen in XY direction at Z equals to 44, 69, 80 and 90 mm and three planes are chosen in YZ direction at X equals to 44, 55 and 66 mm. XY planes shows the pictures of liquid hold up at different heights along the flow direction and this can be interpreted as liquid holdup at different heights. Fig. 5.14, 5.15 and 5.16 shows the film thickness for water, water-glycerol and silicon-oil respectively in the corrugated sheet of packing without perforations. Fig. 5.17, 5.18 and 5.19 shows the film thickness of water, water-glycerol and silicon-oil respectively in the corrugated sheet of packing with perforations. The results are shown for two flow rates. In all the figures, blue line corresponds to the high flow rate and the red line to the low flow rate.

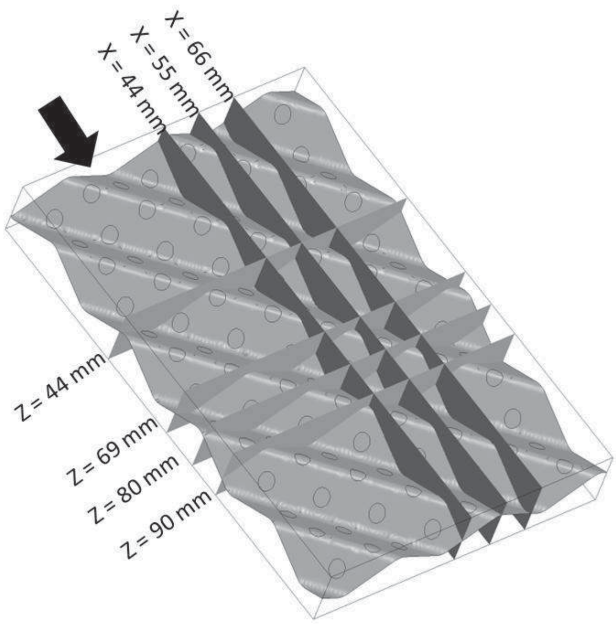

Figure 5.13 Representation of planes used to analyse film thickness in this section.

The comparison between Fig. 5.14 and 5.15 to Fig. 5.16 clearly shows the difference in film thickness which arises due to the change in contact angle. For the liquid with high contact angle (i.e., water and water-glycerol in Fig. 5.14 and 5.15), smooth film flow was not seen like in liquid with low contact angle (silicon-oil in Fig. 5.16). The film thickness and hold up was completely different for these two sets of liquid. For silicon-oil, film thickness was almost same both in the crest and in the well of the corrugated sheet of packing. On other hand, for water and water-glycerol, film thickness was not uniform but tends to hold-up more inside the corrugation of the sheet.

In most of the numerical models and empirical correlations, film thickness was calculated based on the Nusselt theory which is based on flow over smooth plane. From the simulations, it is clear that the final film thickness do not match the prediction based on Nusselt theory. Hence, it should be seriously discussed whether the extrapolation of Nusselt film thickness to the calculation of film thickness in corrugated sheets of packing is still valid or more extra terms need to be included for the calculation.

Fig. 5.17 to 5.19 shows the film thickness for the corrugated sheets of packing with perforations. It should be noted that the perforations did not change the trend of film thickness for water and water-glycerol to a major extent, but for silicon-oil the presence of hole in the corrugation side increases the film thickness and hold up near the corrugation and also in the back side of the corrugated sheet. For water and water-glycerol, as noticed earlier in the case of corrugated sheet without perforations, liquid hold up is high near inside the corrugation. Again, Nusselt theory does not hold valid for this case as well.

In the Delft model developed by (Olujic et al., 2004), hold up is calculated as the product of the film thickness and the area of corrugated sheets of packing. This model holds the assumption that the packing is completely wetted and the film thickness is calculated based on the extension of Nusselt film thickness. From simulations, it is clear that the packing is not completely wetted and the extension of Nusselt film thickness also needs to be reanalyzed.

(Brunazzi et al., 1995) extended the correlation developed by (Suess and Spiegel, 1992) for random packing to calculate the hold up for structured packing. In this model, (Suess and Spiegel, 1992) calculated the holdup considering the ratio of the viscosity of testing liquid to water at 20°C as reference but the influence of surface tension was completely neglected.

As discussed earlier, in the case of wetting, huge differences exist between different empirical correlations available in literature for holdup values. This trend of liquid film thickness and hold-up needs to validated with detailed experimental studies using X-ray tomography.

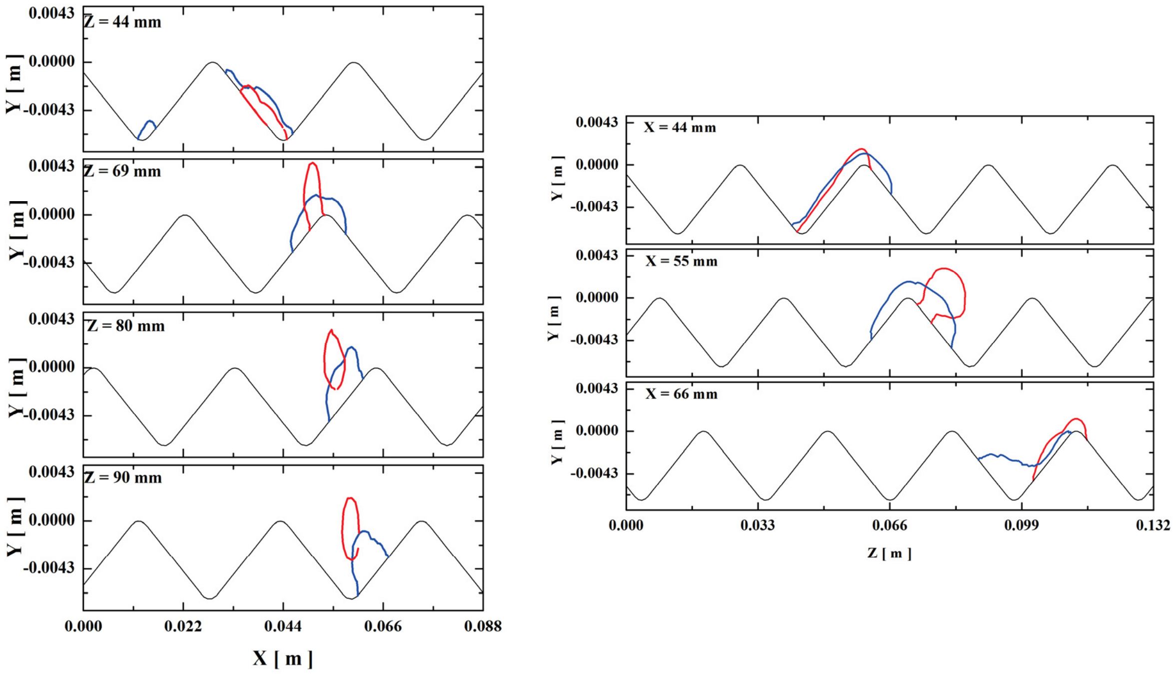

Figure 5.14 Film thickness for water along XY and ZY plane for corrugated sheet of packing without perforations (Blue - Re_L = 3291; Red - Re_L = 2033).

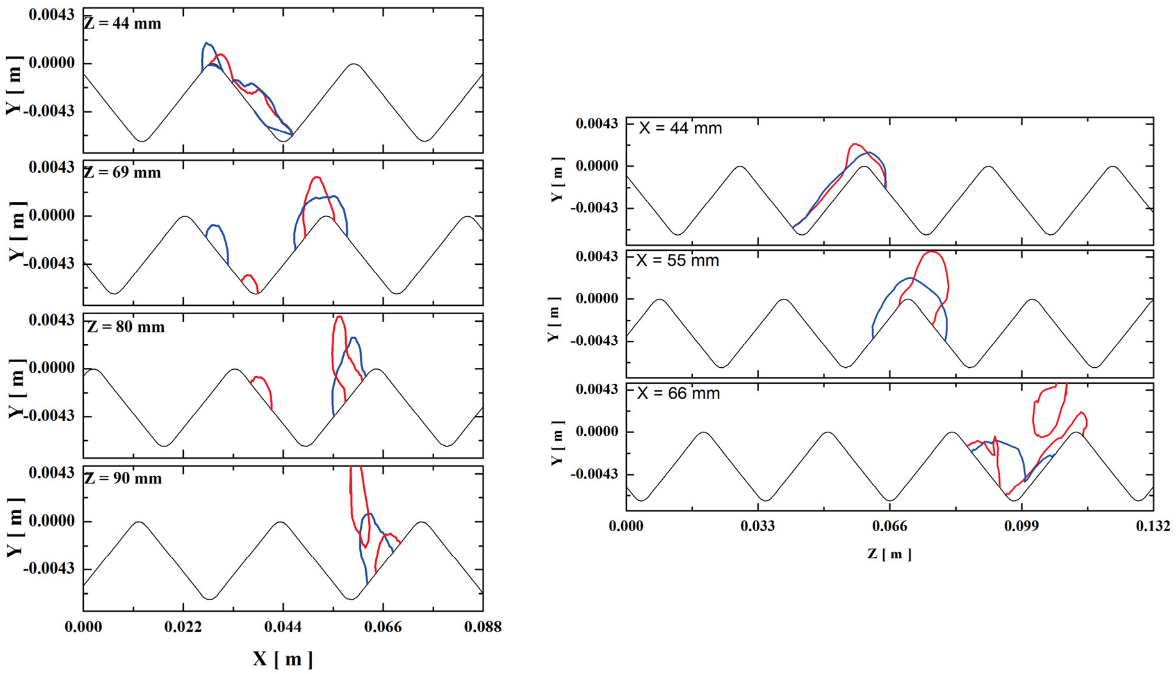

Figure 5.15 Film thickness for water-glycerol along XY and ZY plane for corrugated sheet of packing without perforations (Blue - Re_L = 743; Red - Re_L = 486).

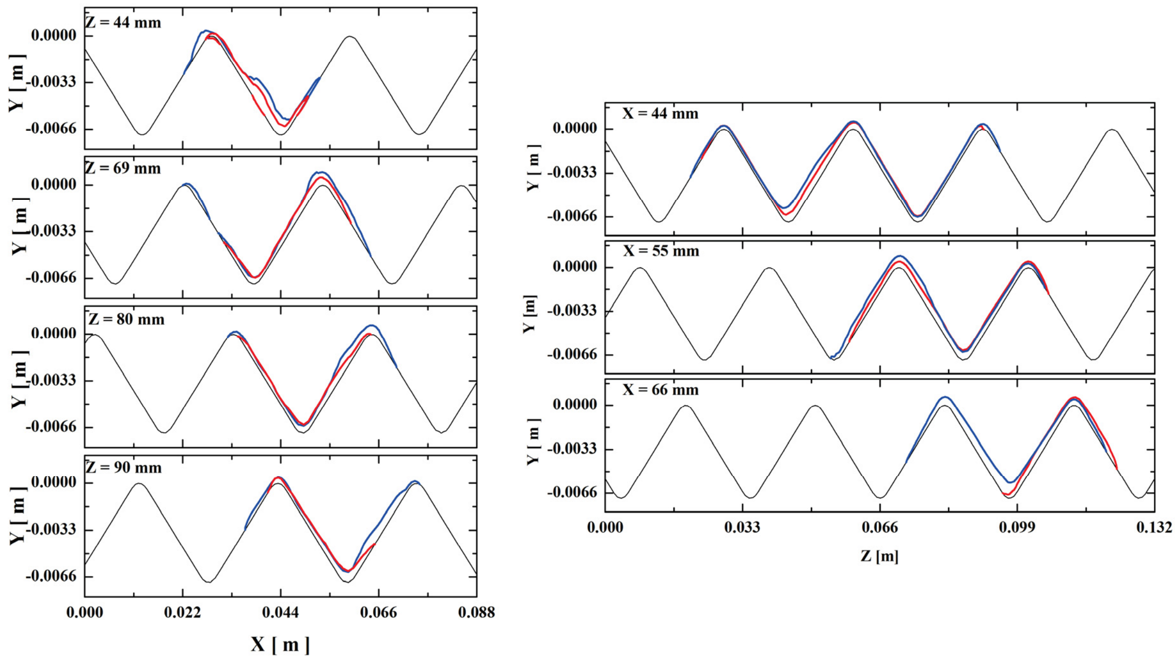

Figure 5.16 Film thickness for silicon-oil along XY and ZY plane for corrugated sheet of packing without perforations (Blue - Re_L = 486; Red - Re_L = 256).

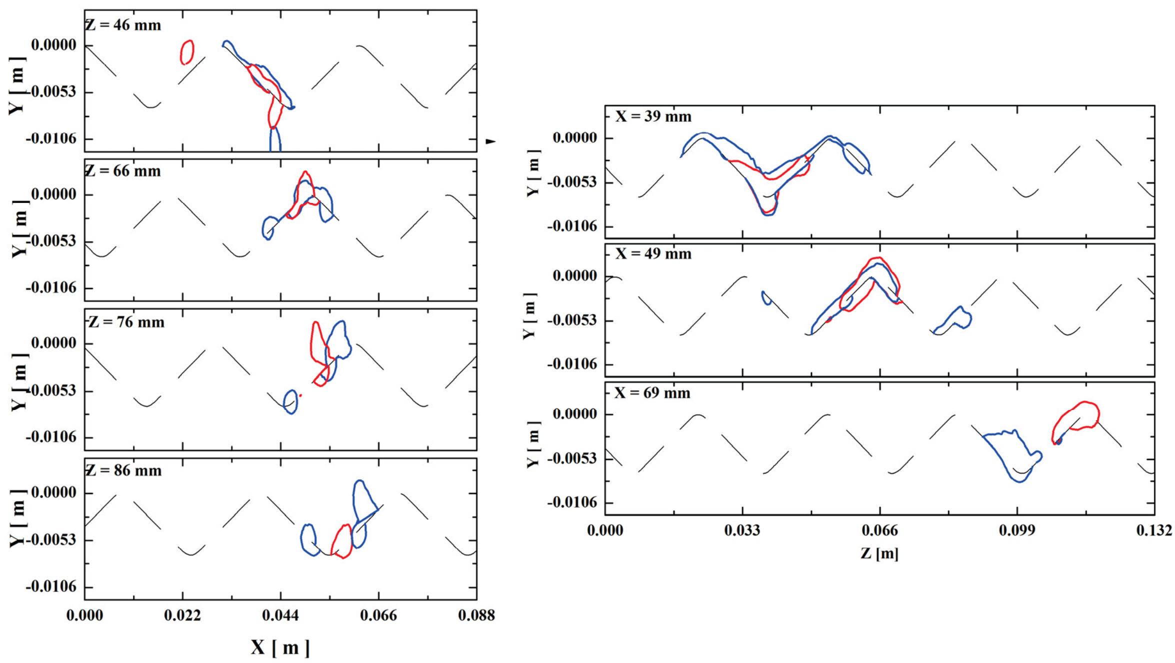

Figure 5.17 Film thickness for water along XY and ZY plane for corrugated sheet of packing with perforations (Blue - Re_L = 3291; Red - Re_L = 2033).

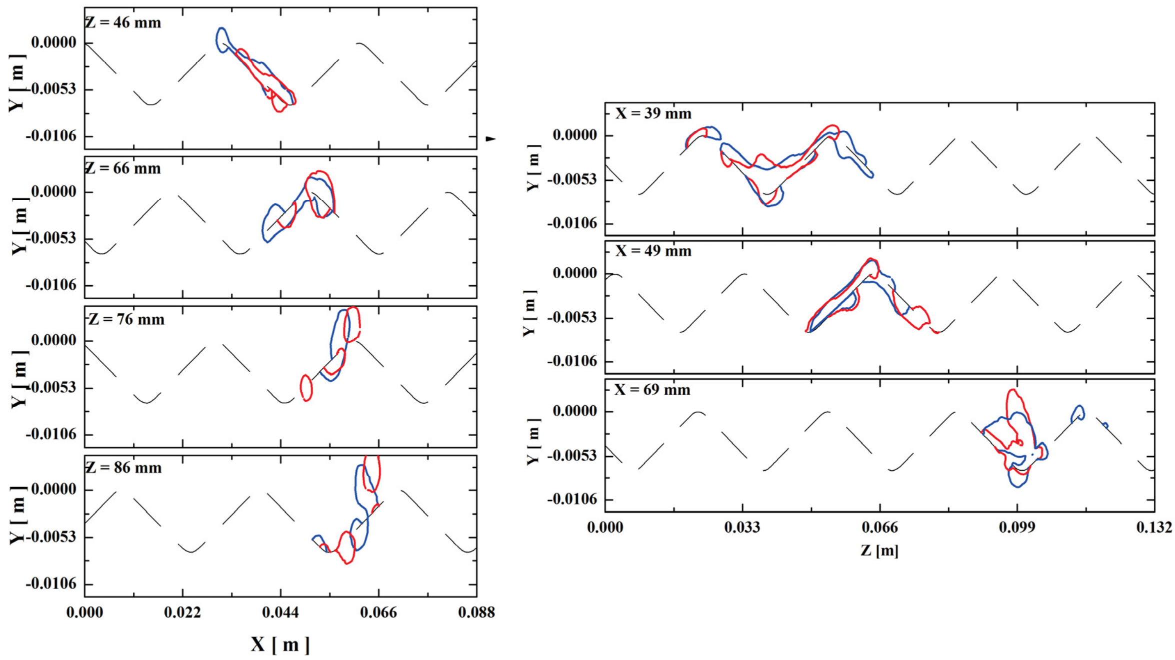

Figure 5.18 Film thickness for water-glycerol along XY and ZY plane for corrugated sheet of packing with perforations (Blue - Re_L = 743; Red - Re_L = 486).

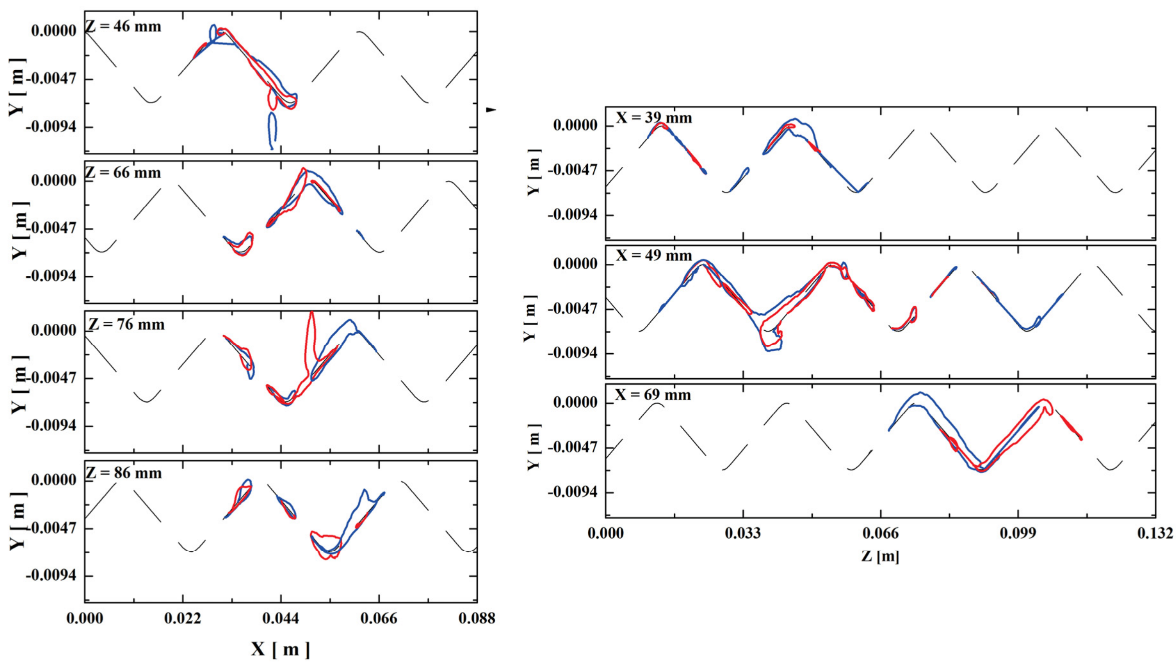

Figure 5.19 Film thickness for silicon-oil along XY and ZY plane for corrugated sheet of packing with perforations (Blue - Re_L = 486; Red - Re_L = 256).

5.2.4 Velocity

The local velocity profile for water, water-glycerol (45 wt. %) and silicon-oil on corrugated sheet of packing without perforations is shown in Fig. 5.20. The film thickness is plotted against velocity of the liquid in the flow direction and it has been normalised to understand the film thickness. The profile shown here is from middle of the geometry i.e., Z = 66 mm; X = 44 mm and only up to the height of liquid film which is decided based on the volume fraction of the liquid from the simulation. The local velocity profile clearly resembles the parabolic profile similar to results from the simulation on the inclined smooth plate in the last chapter (see section 4.2.1). The comparison of the velocity profiles with the experiment is not available.

The difference between the two flow rates is huge for water in comparison to water-glycerol (45 wt. %) and silicon-oil (DC5). The film thickness is very low for silicon-oil in comparison to other two test mixtures. As described earlier, all the empirical correlations available in the literature predicts the film thickness to be around 1 mm, which is valid for water in our case.

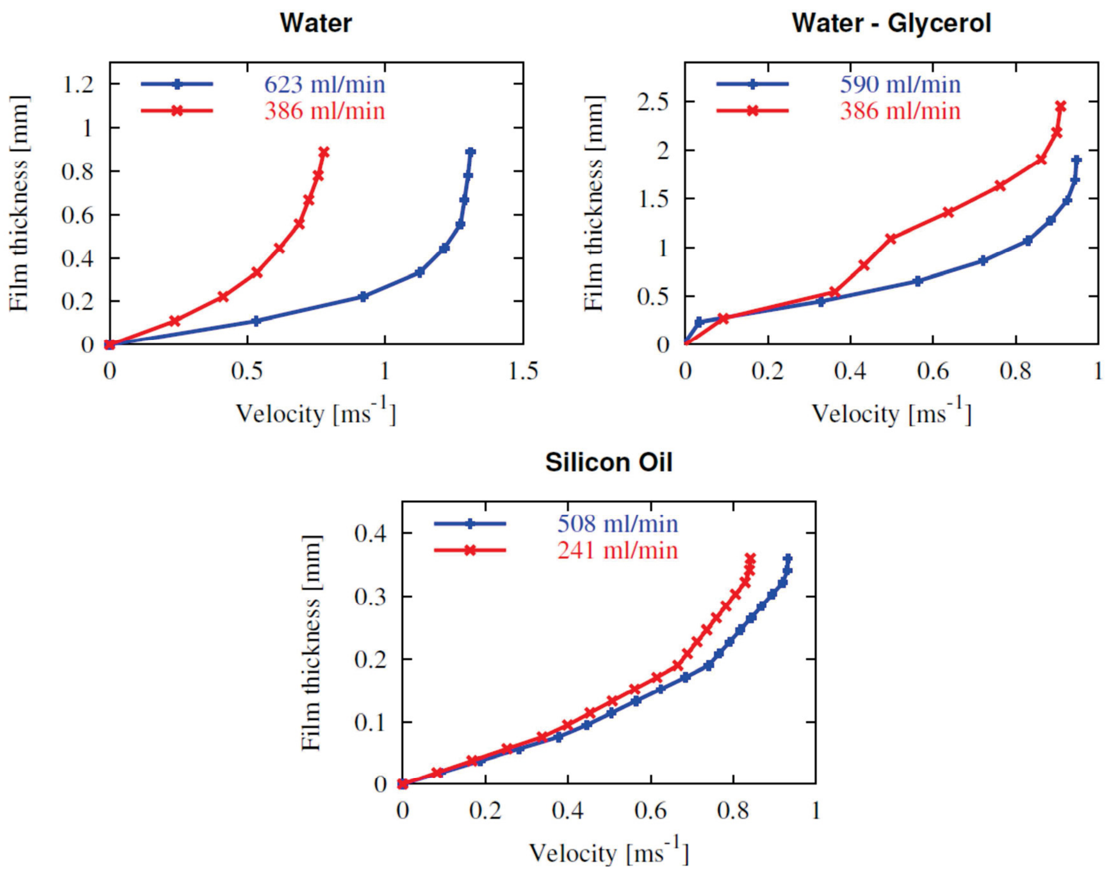

Figure 5.20 Local velocity profile for water, water-glycerol (45 wt. %), silicon-oil (DC5) on corrugated sheet of packing without perforations at Z = 66 mm and X = 44 mm.

On the other hand, simulation predicts low film thickness of around 0.4 mm for silicon-oil (DC5) on corrugated sheet of packing. The influence of the contact angle can be taken into consideration while calculating the film thickness. These local velocity profiles need to validate with experimental studies.

The local velocity profile for silicon-oil (DC5) on corrugated sheet of packing with perforations is shown in Fig. 5.21. The profile shown here is from middle of the geometry i.e., Z = 66 mm; X = 44 mm. Gray line in the Fig. 5.21 indicates the surface of the corrugated sheet of packing. Positive value of the film thickness indicates the liquid film above the sheet and the negative value indicates the liquid film below the sheet. While comparing Fig. 5.20 and 5.21 for silicon-oil (DC5), it is clear that the velocity at the surface of the film decreased due to the presence of the perforation. The velocity on the surface of the film both on above and below the sheet remains in the same range.

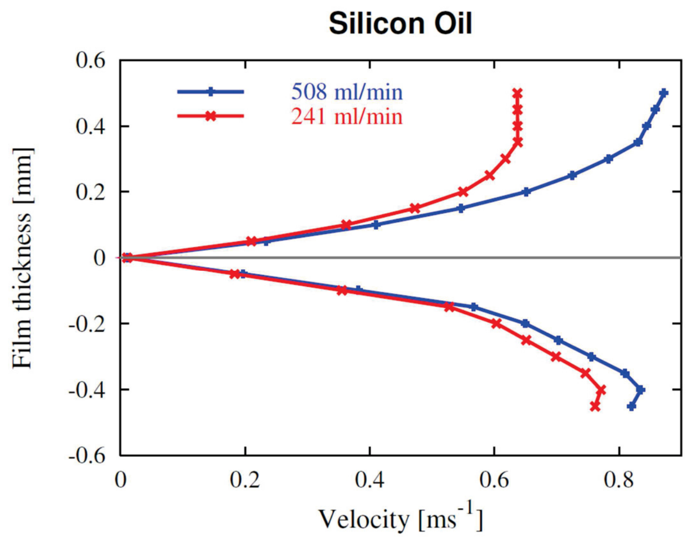

Figure 5.21 Local velocity profile for silicon-oil (DC5) on corrugated sheet of packing with perforations at Z = 66mm and X = 44 mm.

It is very clear that simulation gives very good opportunity to get good insight to understand the local velocity in detail. Precise experimental study is needed to validate the model and hence to understand the necessary improvements.

5.3 Influence of Second Corrugated Sheet

The major aim of this section is to study the extent of wetting on two corrugated sheets of packing. In reality, corrugated sheets of packing are arranged in such a way that one sheet is placed 90° opposite to the other one i.e., corrugation lies in the opposite direction helping the fluids to change its direction. Fig. 5.22 shows the geometry used in simulation in comparison with real packing segment. As shown, only part of the packing segment is considered for simulation in order to understand the influence of second sheet in the liquid-holdup and in the wetting pattern. The main region to be considered is the points where two corrugated sheet meet each other which is explained in Fig. 5.23.

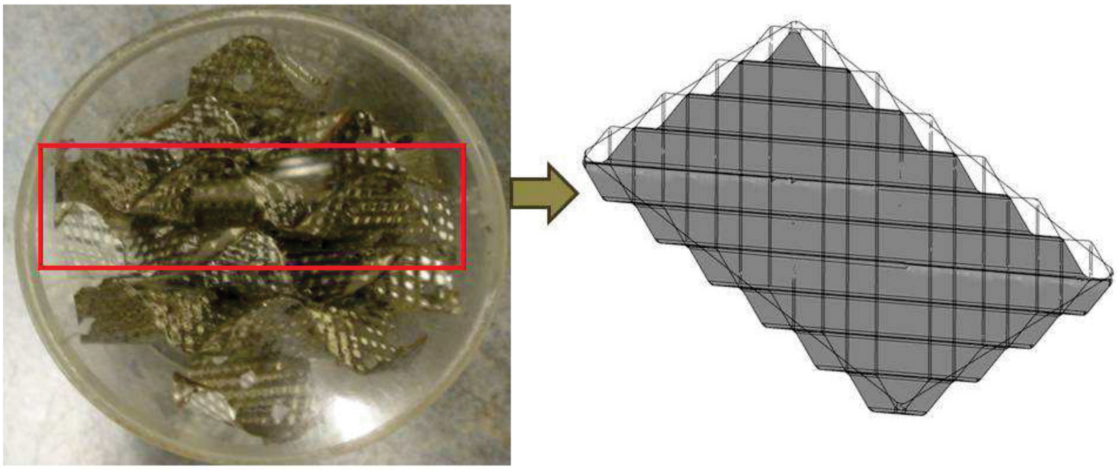

Figure 5.22 Comparison of domain used in simulation from real packing geometry.

To resemble the real industrial condition, Inlet conditions are considered as follows:

a. 4 mm diameter liquid distributors on the top of the packing sheets and the liquid flow through the corrugation.

b. Four inlet distributors are considered in order to understand the maximum wetting possible for two corrugated sheets of packing.

c. Two different inlet positions are explained in Fig. 5.24. Two inlet positions are chosen in such a way that one position is inside the corrugation of the bottom sheet (Position 1) and the other position is outside the corrugation of bottom sheet (Position 2). By this, the influence of meeting point due to second corrugated sheet on the flow of liquid can be clearly seen.

d. Silicon-oil with volumetric flow rate of 811 mL/min showed the maximum wetting in our earlier studies.

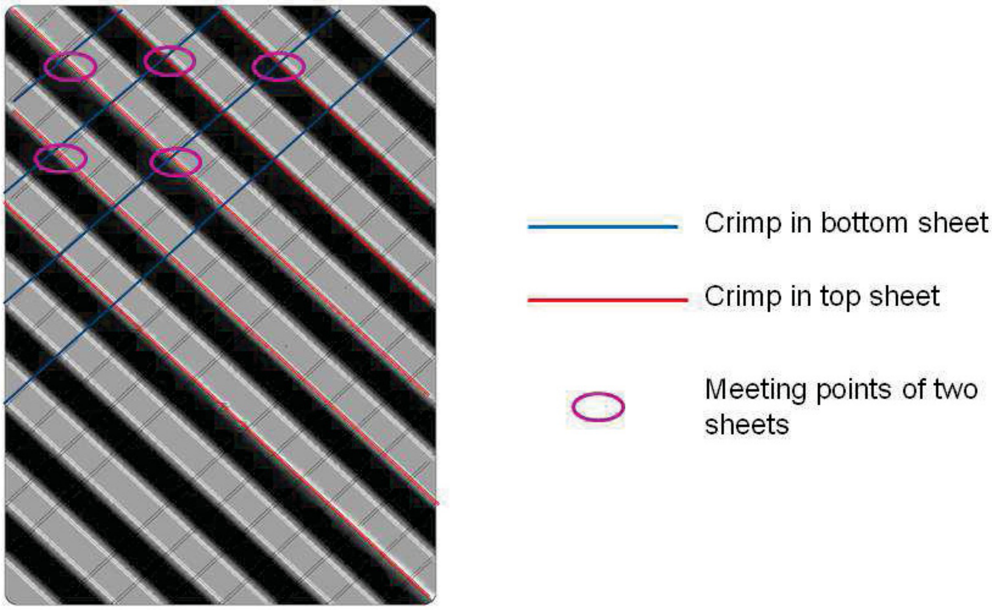

Figure 5.23 Explanation of meeting points from two corrugated sheet of packing and interest of our study.

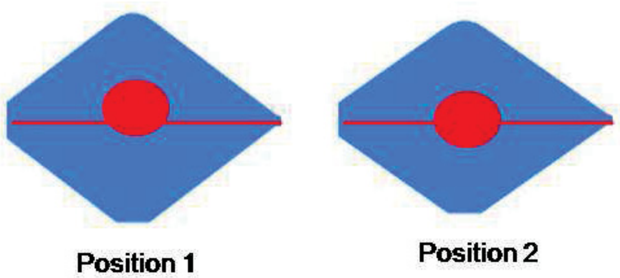

Figure 5.24 Two inlet positions used in the simulation.

5.3.1 Wetting

Fig. 5.25 and 5.26 shows the wetting of bottom and top sheet for simulation with two corrugated sheet of packing and for two different inlet positions mentioned earlier for the same flow rate. It is interesting to note that along with the liquid hold up, small change in inlet positions make a huge impact on wetting of the corrugated sheet. For position 1, i.e., most portion of the inlet inside the corrugation of the top sheet only wets the top packing sheet and the bottom sheets remains mostly dry. For position 2, i.e., the portion of the inlet was equally on both the corrugated sheets, both the packing on the top and bottom got wetted. The comparison of total wetting in percentage between the two inlet positions is shown in Fig. 5.27.

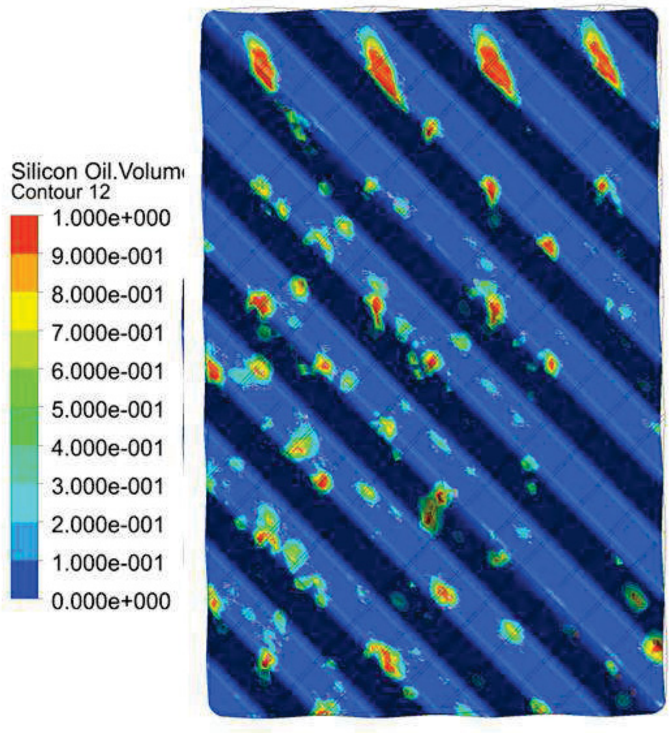

Figure 5.25 Wetted area on the bottom packing for two inlet positions. Left - position 1; Right - position 2; Vol. flow rate = 811mL/min.

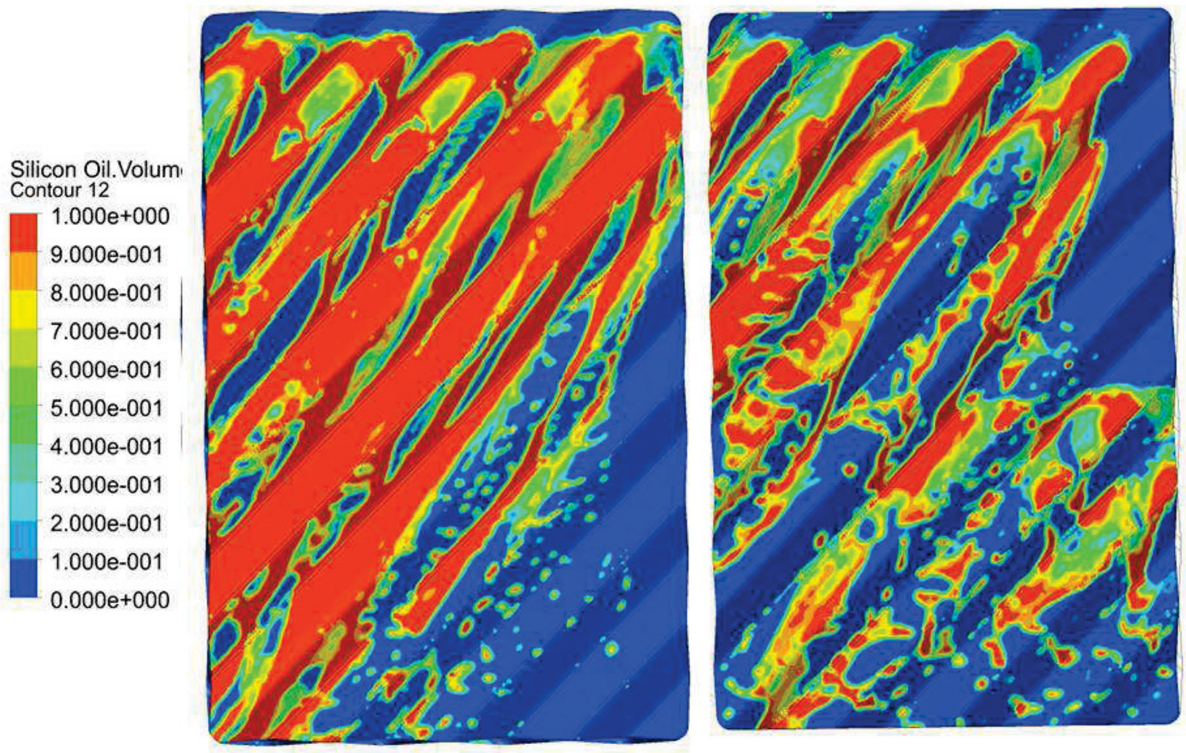

Figure 5.26 Wetted area on the top packing for two inlet positions. Left - position 1; Right - position 2; Vol. flow rate = 811mL/min.

It is clear that from position 1, only 54% of the top sheet and 5.07% of the bottom sheet is wetted. Moreover, from position 2, 15.36 % and 39.06% for bottom and top sheet is wetted respectively. Overall, only 55 to 60% of the packing area is utilised.

As shown, maximum of 60% of the packing area is utilised for wetting of testing system with low contact angle (which usually wets easily), for maximum inlet possible i.e., four inlets through four corrugations and relatively high flow rate of around 811 mL/min

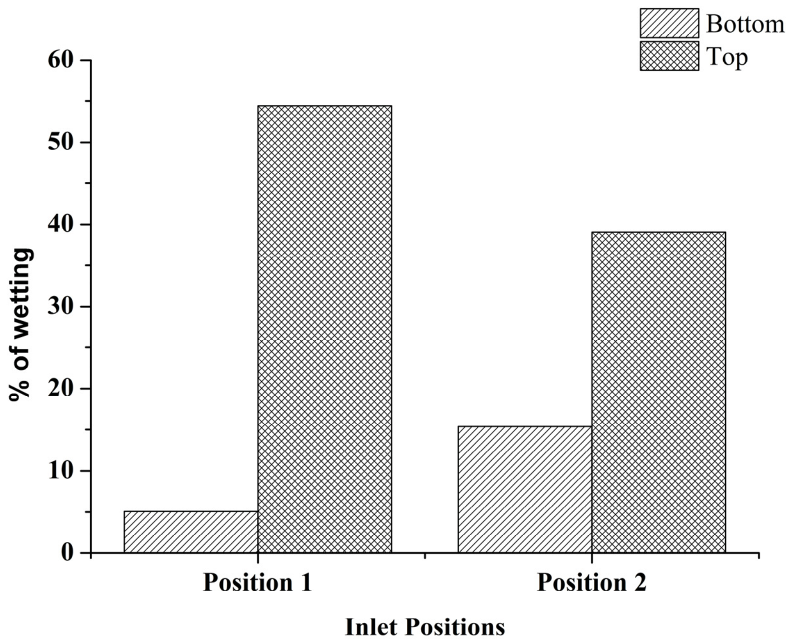

Figure 5.27 Comparison of percentage of wetting for two inlet positions in two corrugated sheet of packing.

It is clear that around 40% of the area can be utilised and hence efficiency of the packing can be further improved. The influence of the surface textures is not considered in the simulation, which can be considered further in the simulation study to understand the wetting behaviour better.

5.3.2 Film Thickness

Fig. 5.28 and 5.29, shows the volume fraction of silicon oil at different XY and ZY planes of the corrugated sheet of packing along the flow direction and the direction perpendicular to the flow direction. As discussed in earlier sections, the planes are chosen in such a way to study the influence of corrugation, meeting point of two crimps and the change in liquid hold-up due to inlet positions. It can be seen that the liquid holds up in corrugation and at the criss-cross junction i.e., around the meeting point of the two sheets. Moreover, the holdup is more near the inlet than in the outlet.

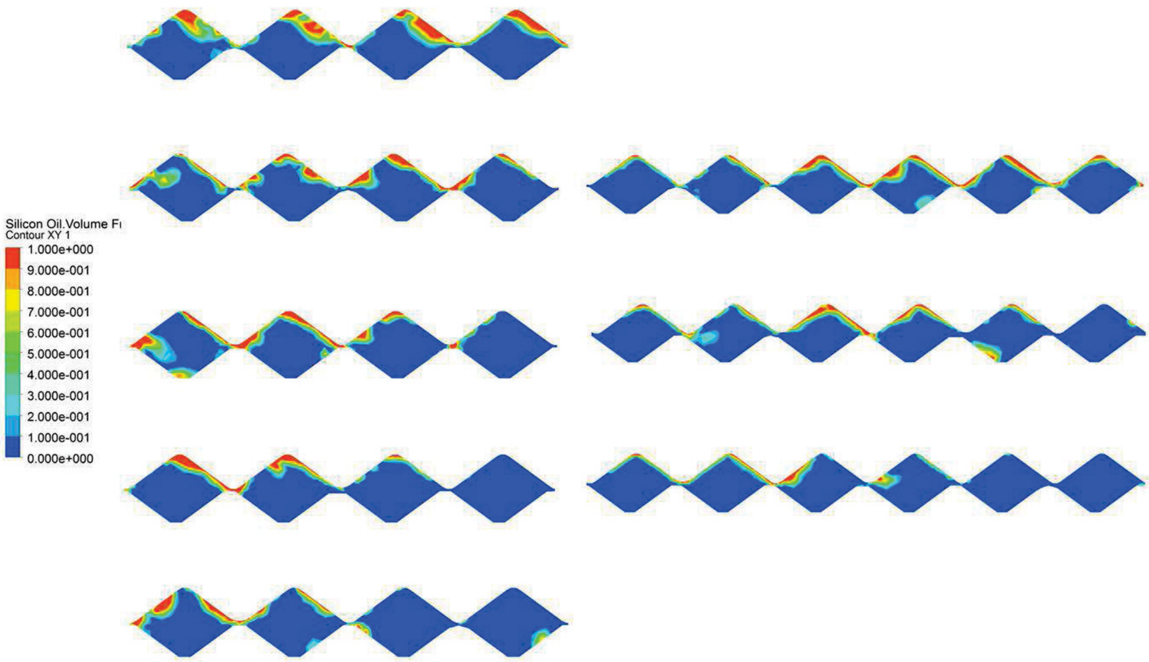

Figure 5.28 Volume fraction of silicon oil fraction at different heights of corrugated sheet of packing along the flow direction for inlet position 1. Vol. flow rate = 811mL/min.

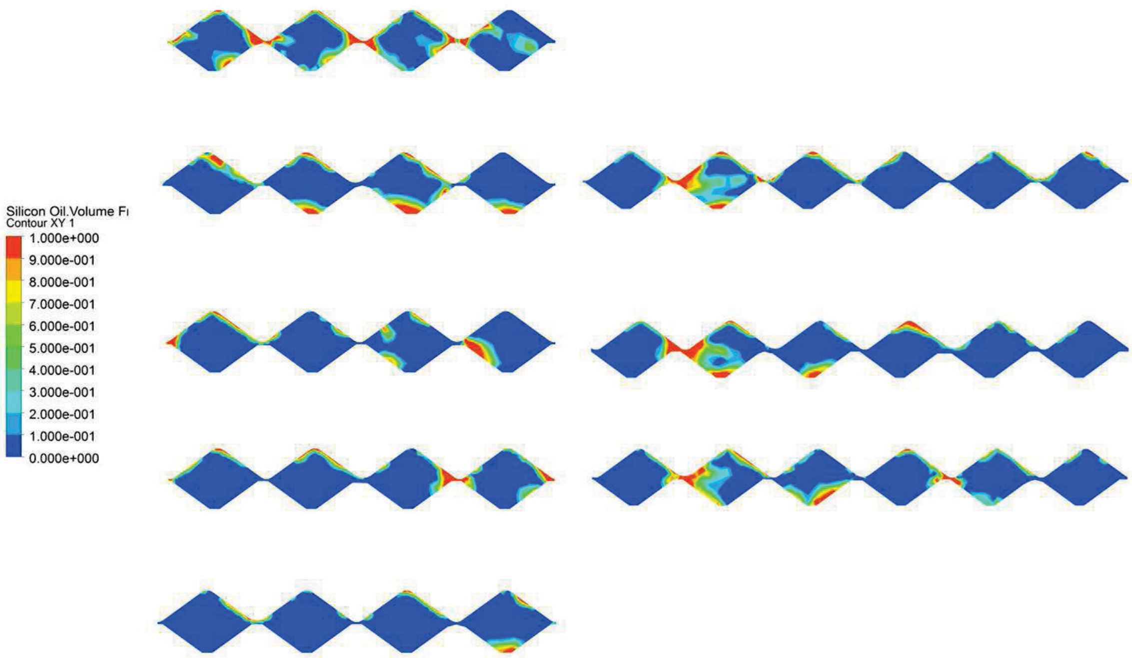

Figure 5.29 Volume fraction of silicon oil at different heights of corrugated sheet of packing along the flow direction for inlet position 2. Vol. flow rate = 811mL/min.

The liquid holdup on the different level of the corrugated sheets of packing along the flow direction is shown in Fig. 5.30. The level at Z = 22 mm is the one which is closer to the inlet and Z = 113 mm to the outlet. Hold up is calculated as the sum of the liquid fraction available at that particular plane. It is clear that the liquid holdup is high near the inlet and it reduces at the outlet.

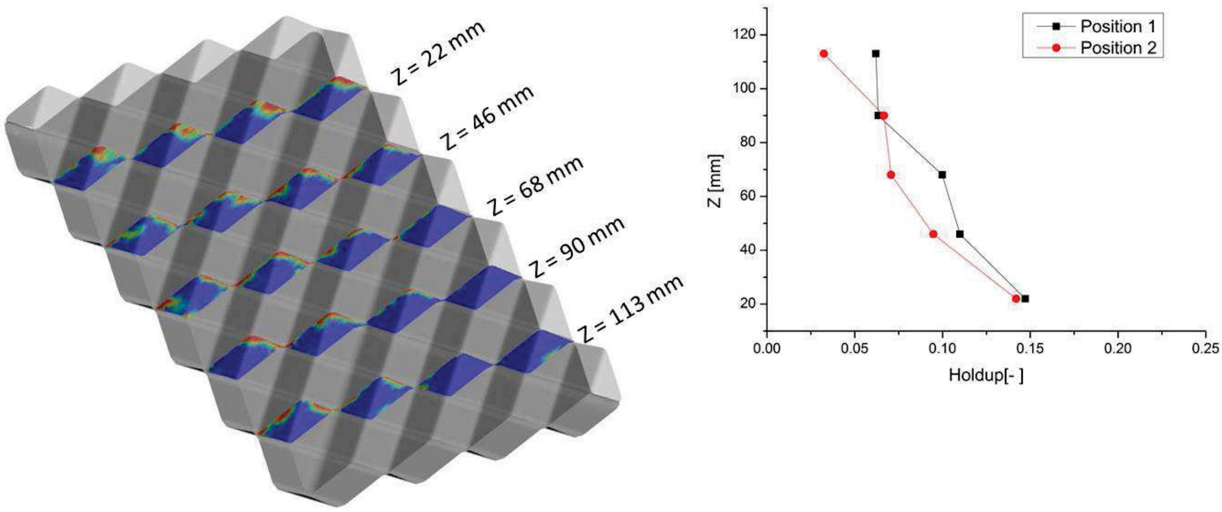

Figure 5.30 Liquid holdup along the flow direction at different heights for Position 1 and Position 2.

The holdup of liquid near the junction of two sheets was observed in the experimental studies as well. This phenomenon of liquid holding up near this junction was elaborated in experimental study (Viva et al., 2011b) performed using X-ray tomography for Mellapak 752.Y.

6 CONCLUSION AND OUTLOOK

The main objective of this work was to develop a three-dimensional CFD model to study the hydrodynamics on the corrugated sheet of structured packing. In-order to understand the same, two steps procedure was adopted. It is very challenging to validate the model with corrugated sheet of packing directly. As a first step to develop a validated model, a simplified geometry of smooth inclined plate was considered. Three testing fluids water, water-glycerol (45 wt. %) and silicon-oil (DC5) were studied with different flow rates. The wetting characteristics of liquids with different viscosity range (1 – 5mPas) and contact angle (70° and 7°) were considered. Initially, the rivulet width of experiments and simulations were compared and an agreement within an error of 5% maximum was determined. The percentage of wetting from simulation was also compared with experimental results. From the wetting, the role of contact angle and surface tension can be clearly understood. The percentage of wetting was around 30% of the total area for liquid with low contact angle i.e., silicon-oil (DC5) compared to 9% for liquid with high contact angle i.e., water and water-glycerol for the same flow rate. These results were also in accordance to earlier observations in literature (Raynal et al., 2004a). The comparison showed that VOF model predicts close to the reality for all three different testing system.

After a qualitative comparison, simulations were extended to compare the velocity profiles obtained from simulation with experimental profiles obtained from μPIV measurements (Paschke, 2011). There were few differences in velocity profiles which were also explained by performing detailed sensitivity analysis. From the experimental experience, few parameters which significantly influence the velocity profile was chosen and simulated for the possible error range. Based on the sensitivity study, it was understood that even the small modification in flow rate and temperature influences the velocity profile considerably. The change in flow rate influences only the interface region but the change in temperature influences also the velocity inside the film region. It was also shown that very small changes in inclination angle did not show much influence in the velocity profile. Now, this validated model was extended to study the flow behaviour in corrugated sheet of packing.

To study the fluid dynamics of the flow in the corrugated sheets of packing, the geometry resembling real industrial packing was developed in Gambit and in ICEM CFD. In initial studies, corrugated sheet of packing with strict triangular crimp was utilized to simplify the meshing. The geometry with strict triangular crimp showed completely different flow pattern than the real packing. Hence, the geometry with smooth crimp surface was developed and utilized for further studies. A single geometry and mesh which enables to perform simulation in corrugated sheets of packing with and without perforation was built. As mentioned in the earlier section, three different liquids were studied. The simulations were performed for two different flow rates to understand the influence of flow rate on wetting and in film thickness. The major flow direction was in the direction of corrugation and also in accordance to empirical correlation available in the literature which was developed after experimental studies (Spekuljak, 1986).

The comparison of wetting showed good agreement with experiments. The change in wetting showed the same trend as seen in inclined plate i.e., the liquid with low contact angle had more wetting than liquid with high contact angle. The significant change in percentage of wetting was noticed for low viscous liquid due to change in flow rate but the change was considerably smaller for high viscous liquid.

The influence of the perforations on the wetting of the corrugated sheet was also studied. The presence of the perforations enables the liquid to wet both the sides. The wetting area on the front side of the corrugated sheet was less for the sheet with perforations but on the other hand, the total wetting i.e., the sum of front and back side was more compared to the sheet without perforations.

Five different empirical correlations available in literature to predict the effect interfacial area was selected and compared. All the five correlations predicted different interfacial area. It is recommended to include the influence of the contact angle and surface tension on the empirical correlations to predict the wetting area. With the CFD simulations as basis, the correlation for interfacial area can be developed which helps to predict the mass transfer studies.

The influence of the micro textures and pre wetting was studied experimentally and their benefits are listed. It is shown clearly that the pre wetting increases the wetting area and hence the interfacial area available for transport processes as well. It was also recommended from the industrial experience to start up the process with maximum liquid load possible to pre wet the packing and to run the process at normal working conditions. This gives the opportunity to maximize the utilization of the packing area (Raynal et al., 2004b).

As a final step, the second corrugated sheet was introduced to the simulation domain to understand the influence of crisscross junctions when both the sheets touch each other as seen in real processes. It is also shown that the minor change in position of the inlet distributors affects the wetting and the direction of flow liquid. It is very important to notice that the complete area of the packing was not wetted. This clearly shows the chance to improve the efficiency by utilizing more area of the packing. Liquid hold-up near the junctions of the two sheets were high as also noticed in some experimental studies performed using X-ray tomography (Viva et al., 2011b).

CFD studies gives better understanding to the flow behaviour and even small things which is not seen in experiments can also be noticed with more precision. With the computation power available till now, it is highly impossible to simulate the whole packed column. But the simulations can be performed in macro scale to understand the flow behaviour better. The results observed from the macro scale can be extended to large scale studies.

Outlook

It is highly recommended to study the influence of the microstructures using the CFD simulations. There are various micro textures both 2D and 3D textures are available in the market. Recently, many experimental works are completely devoted to study the influence of micro textures on spreading of liquid and in wetting of the packing (Kohrt et al., 2011). The validated model will help to understand the influence of micro textures in micro and macro scale. This will help to develop new surface textures and complement the experimental studies. With validated model, experiment efforts can be reduced considerably. More qualitative experiments to measure the flow in micro scale need to be developed.

In the simulations, only the static contact angle is taken into consideration. Usually, the contact angle is measured on the smooth surface. The presence of micro textures less than micro meters will influence the contact angle measured. In future, the influence of dynamic contact angle should be taken into consideration.

This can also be further extended to study the transport processes in distillation and absorption. To help the packing and column designers, a complete flow map considering the influence of liquid parameters such as density, viscosity, surface tension, contact angle and geometry parameters such as corrugation side, height, base width, specific surface area, perforations, micro textures can be developed.

APPENDIX.A. CODE FOR BATCH JOBS IN SUPER COMPUTER AT HLRN

```
#!/bin/bash

#PBS -S /bin/bash
#PBS -o name_by_user.out
#PBS -j oe
#PBS -l nodes=4:ppn=8
#PBS -l walltime=24:00:00
#PBS -l feature=xe

# provide FLUENT through modules call:
. $MODULESHOME/init/bash
module load fluent/12.0
# change to work dir (on the global file system):
cd $WORK/Name_working_directory/

# start solver for 3Ddp, no gui, parallel;
# read commands from here document until "EOFluentInput",
# write log output to file "name_by_user.log":
fluent 3ddp -g -t32 -pib.dapl -mpi=hp -ssh -
cnf=$PBS_NODEFILE<<EOFluentInput>name_by_user.log
/define/user-defined/compiled-functions/compile libudf1 yes
udf.c


/file/read-case-data "name_cas_dat_file.cas"
/define/user-defined/compiled-functions/load libudf1


/parallel/partition/method/cartesian-axes 32
/file/auto-save/data-frequency 100
/file/confirm-overwrite n
/file/autosave/append-file-name-with flow-time 6
/solve/set/time-step 5e-05
/solve/dual-time-iterate 100000 40
exit
y
EOFluentInput
```

APPENDIX.B.

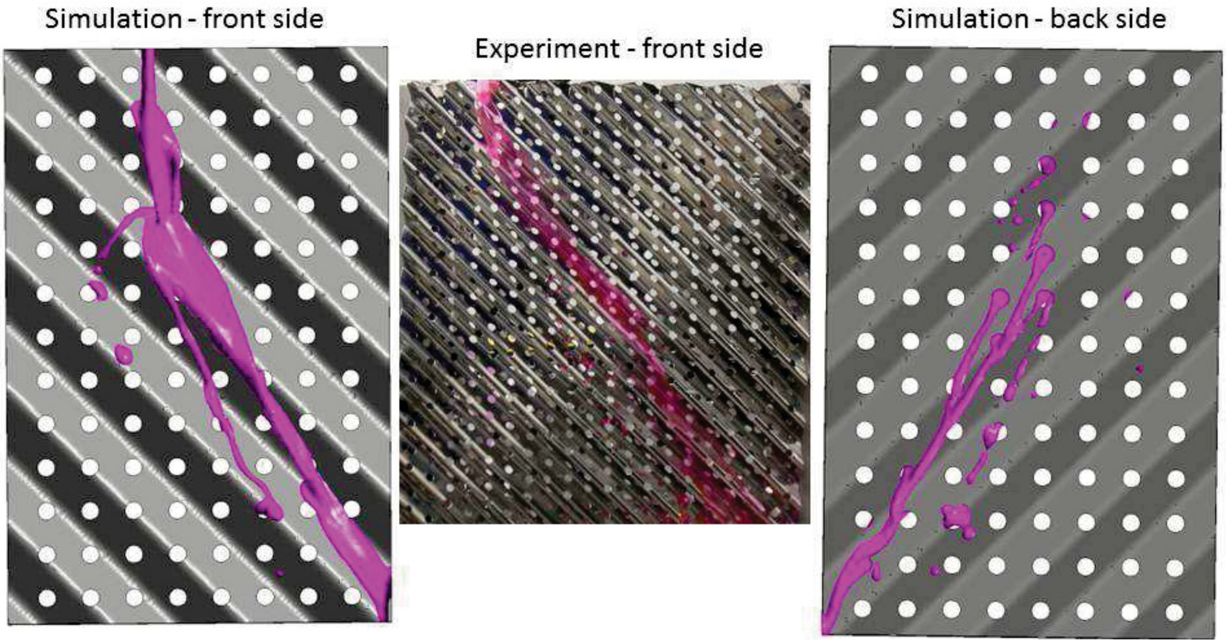

Figure B.1 Comparison between simulation and experiment for flow of water on corrugated sheet of packing with perforations. Flow rate - 623mL/min.; ReL – 3291.

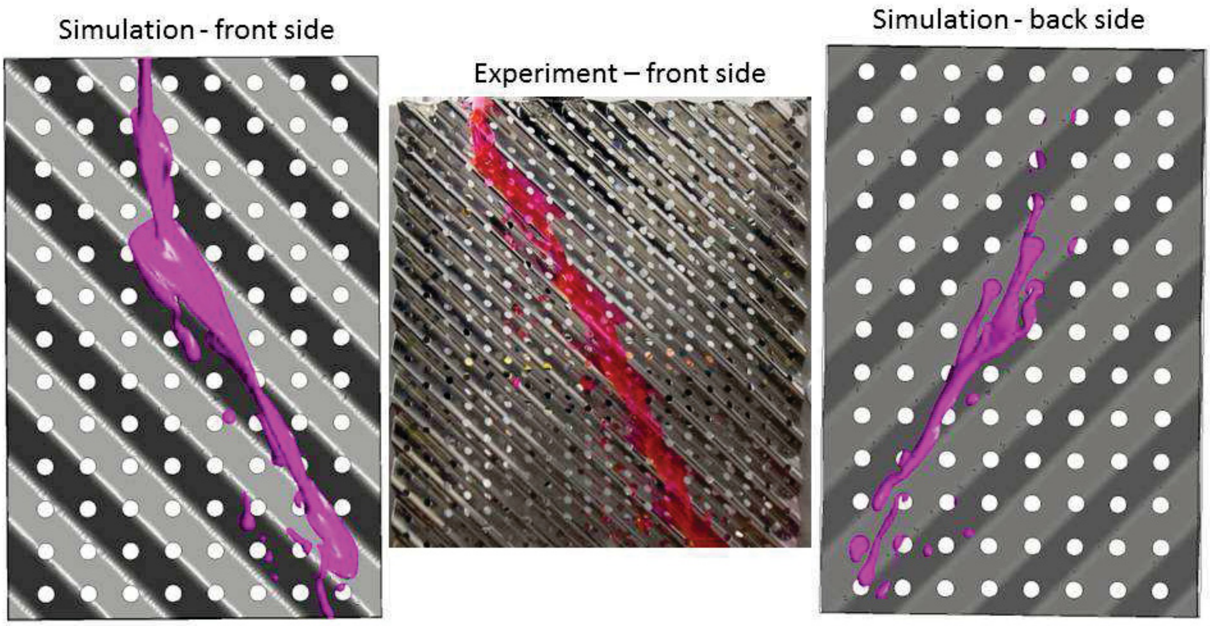

Figure B.2 Comparison between simulation and experiment for flow of water-glycerol on corrugated sheet of packing with perforations. Flow rate – 590 mL/min.; ReL – 743.

APPENDIX.C.

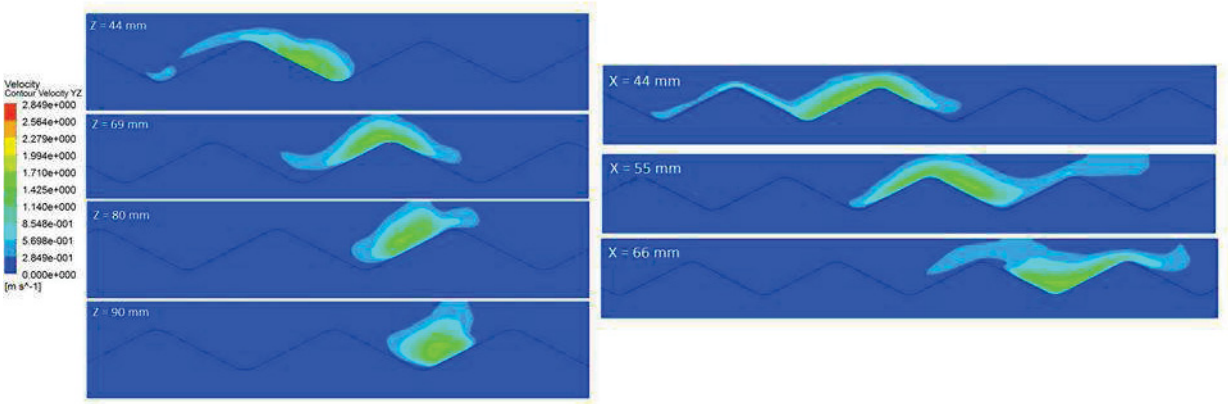

Figure C.1 Velocity contours for water along XY and ZY plane for corrugated sheet of packing without perforations.

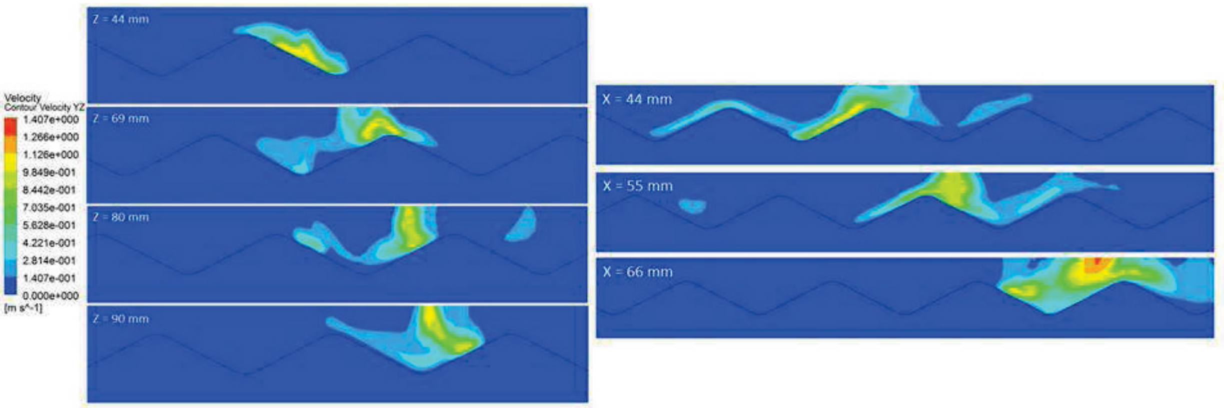

Figure C.2 Velocity contours for water-glycerol along XY and ZY plane for corrugated sheet of packing without perforations.

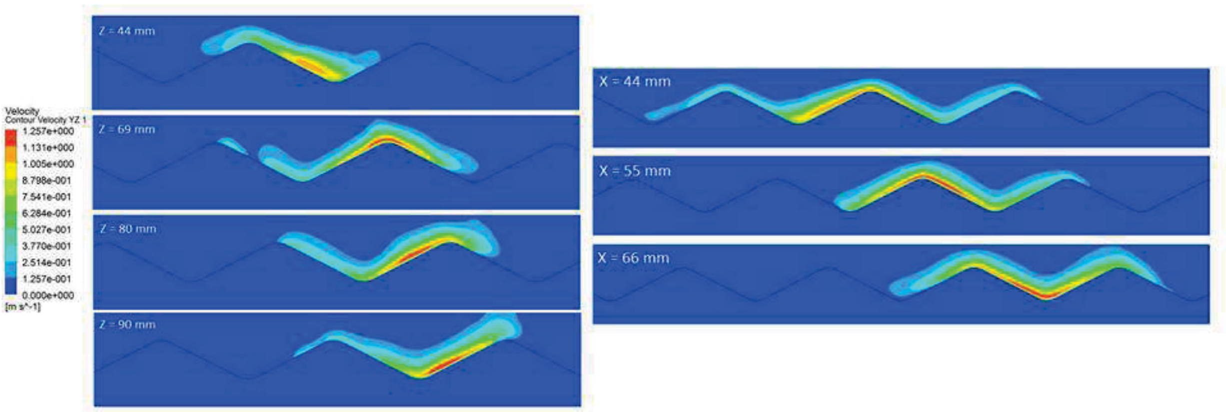

Figure C.3 Velocity contours for silicon-oil along XY and ZY plane for corrugated sheet of packing without perforations.

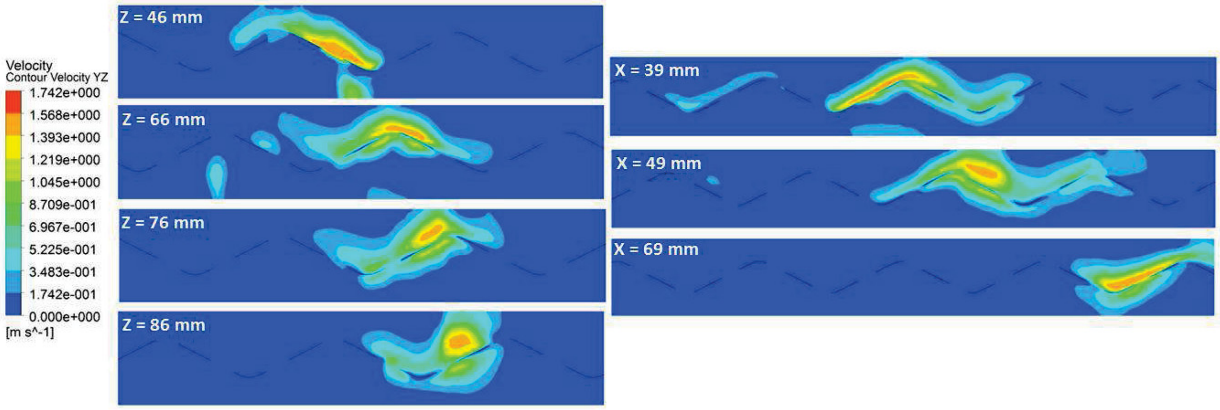

Figure C.4 Velocity contours for water along XY and ZY plane for corrugated sheet of packing with perforations.

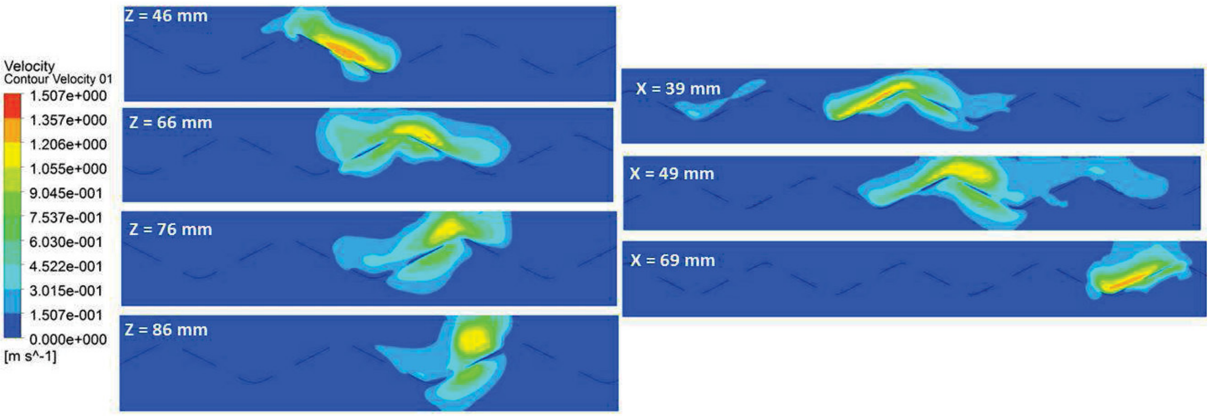

Figure C.5 Velocity contours for water-glycerol along XY and ZY plane for corrugated sheet of packing with perforations.

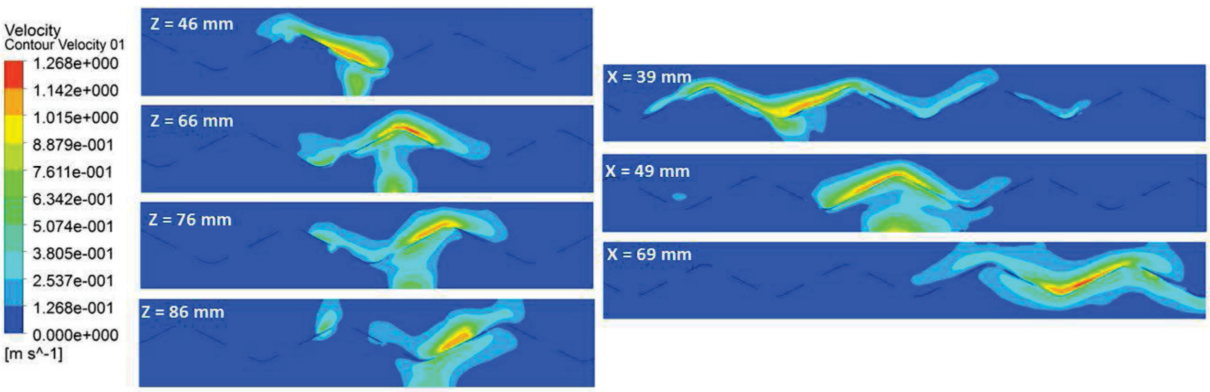

Figure C.6 Velocity contours for silicon-oil along XY and ZY plane for corrugated sheet of packing with perforations.

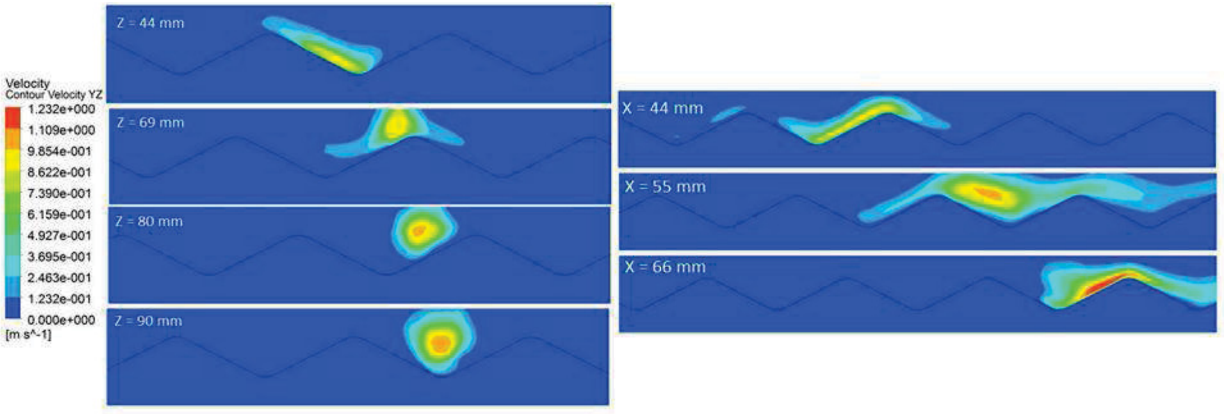

Figure C.7 Velocity contours for water along XY and ZY plane for corrugated sheet of packing without perforations.

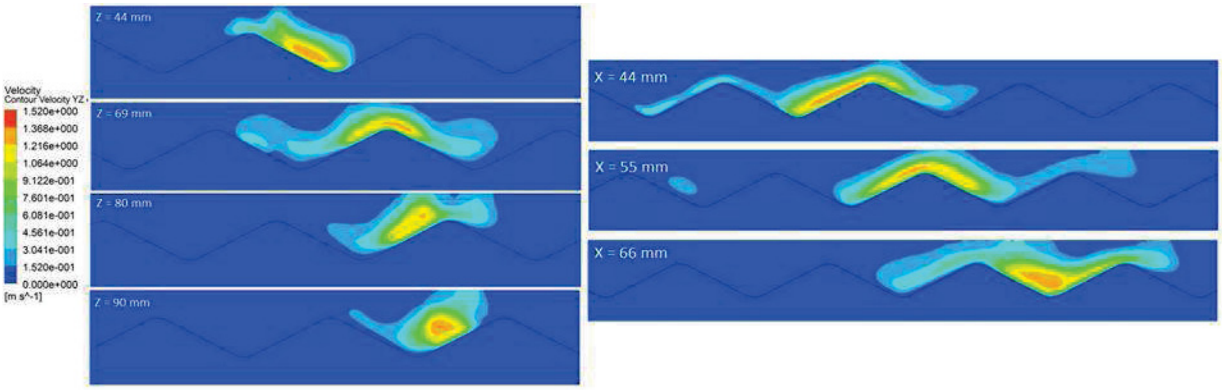

FigureC.8 Velocity contours for water-glycerol along XY and ZY plane for corrugated sheet of packing without perforations.

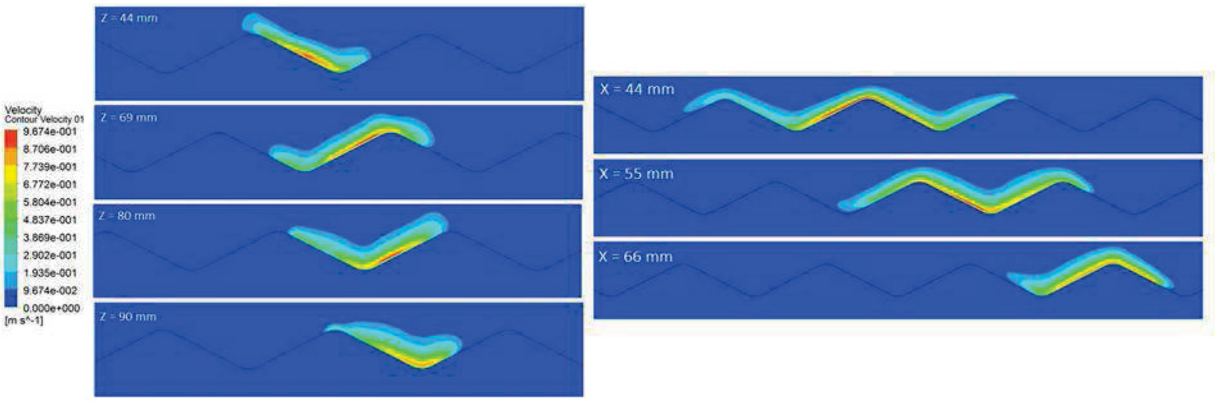

Figure C.9 Velocity contours for silicon-oil along XY and ZY plane for corrugated sheet of packing without perforations.

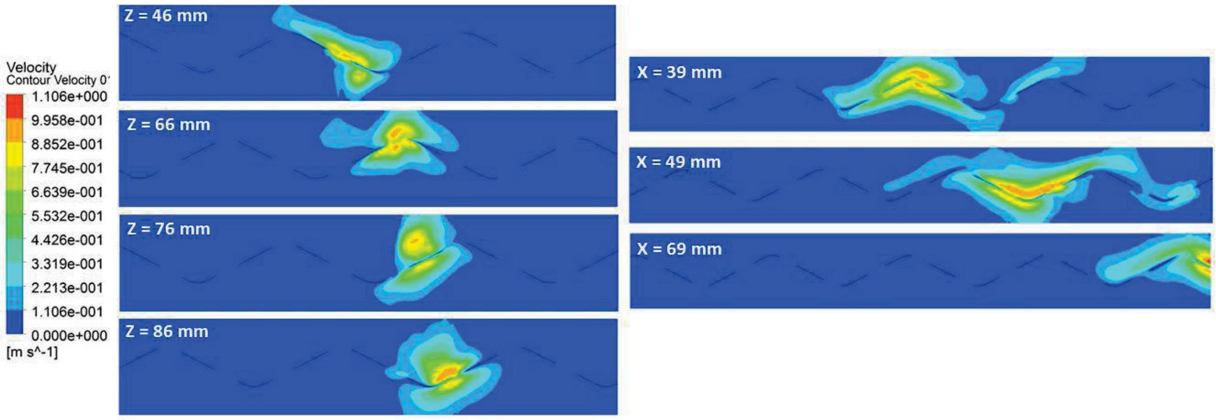

Figure C.10 Velocity contours for water along XY and ZY plane for corrugated sheet of packing with perforations.

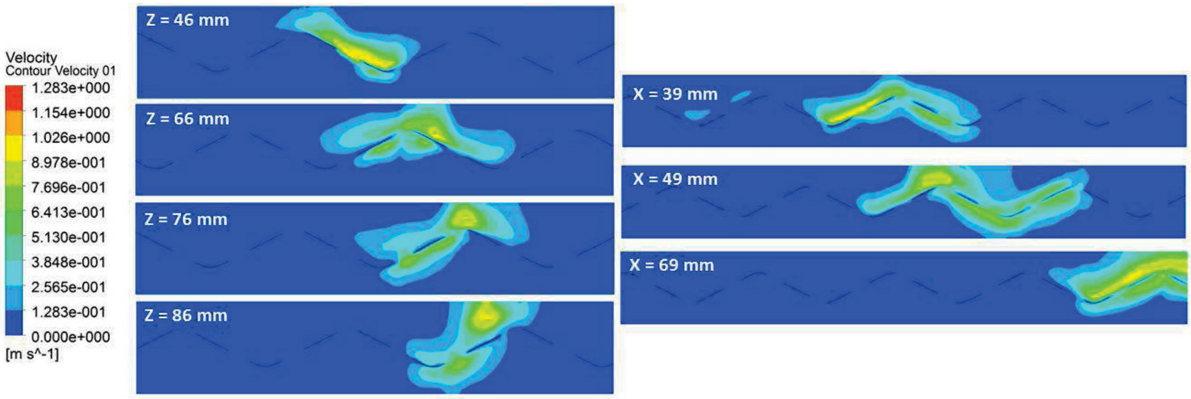

Figure C.11 Velocity contours for water-glycerol along XY and ZY plane for corrugated sheet of packing with perforations.

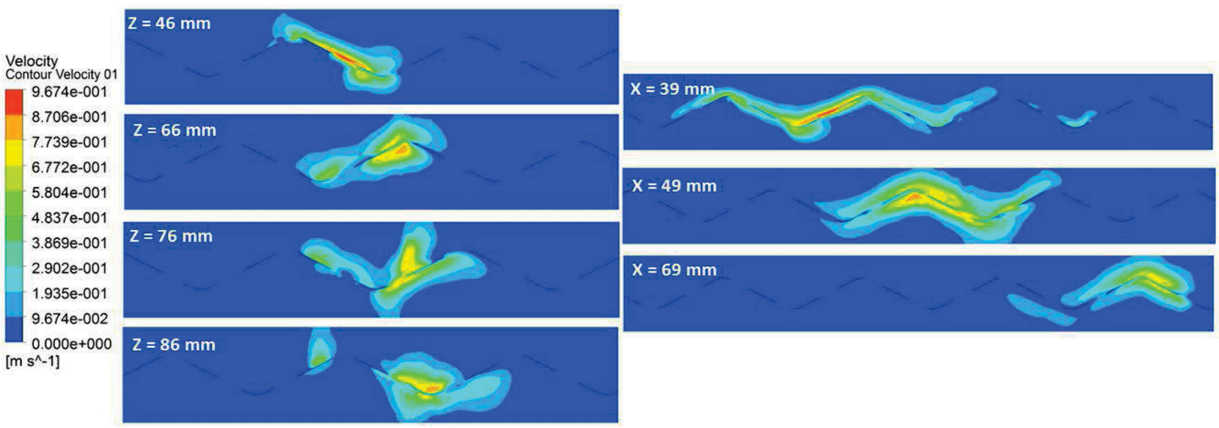

Figure C.12 Velocity contours for silicon-oil along XY and ZY plane for corrugated sheet of packing with perforations.

APPENDIX.D.INFLUENCE OF PRE-WETTING

The influence of the pre-wetting on the two different types corrugated sheet of packing has been done experimentally using the wetting test. Fig. D.1 and D.2 show the influence of pre-wetting on the wetting characteristics for Montz B1-300 and Mellapak 350Y corrugated sheet of packing. In both the cases, water-glycerol (45 wt.%) solution is used as a testing system. In Fig. D.1, the impact of pre-wetting for two different flow rates can be seen. As expected, increasing the flow rate also increases the wetting area and hence the interfacial area available for transport processes. The increase in wetting area due to pre-wetting is quite high even for the low flow rate and hence the wetting area with pre-wetting for low rate is even more than wetting area from high flow rate without pre-wetting. This is also in accordance with the result from (Raynal et al., 2009). They also recommended that the industrial operations should be run at maximum liquid load before running at nominal conditions to bring the influence of pre-wetting into the real conditions.

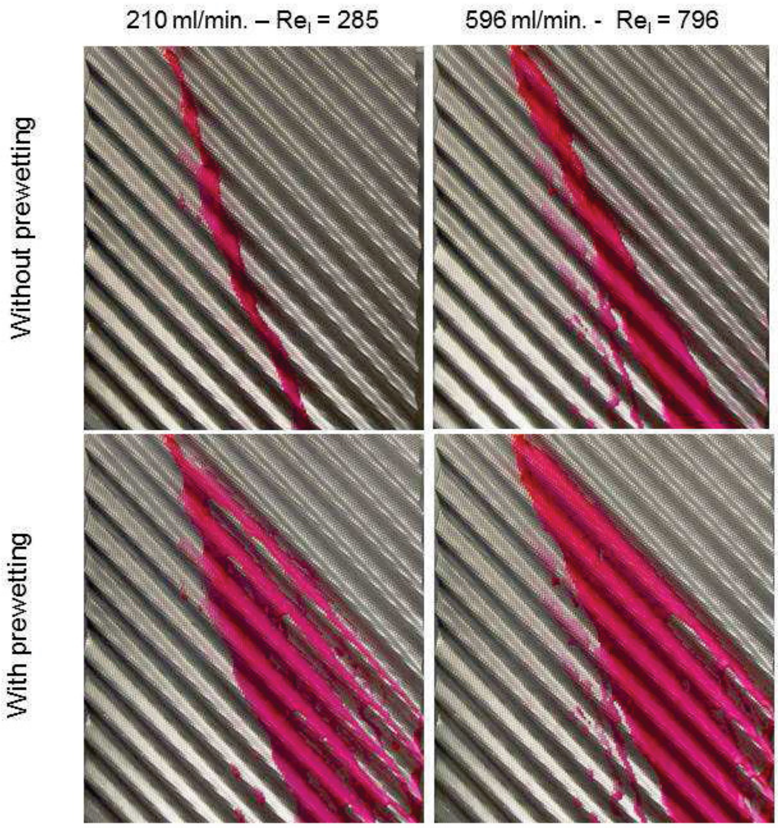

Figure D.1 Comparison of wetting due to pre-wetting for water-glycerol system in corrugated sheet without perforations

In Fig. D.2, the influence of pre-wetting for Mellapak- 250Y is shown. Here, the influence of prewetting along with the perforations can be seen. Even though the trend is similar as seen in Fig. D.2, i.e., wetting area increases with pre-wetting but the influence is considerably less in comparison to Montz pak without perforations. The influence is only due to the perforations. Perforations reduce the influence of pre-wetting on one side of the packing. Nevertheless, the major influence of perforations as mentioned in earlier chapter is also to wet the back side of the packing which also plays a crucial role in transport processes. While considering the corrugated sheet with perforations but without microstructures, former gives better wetting and more stable film than the later.

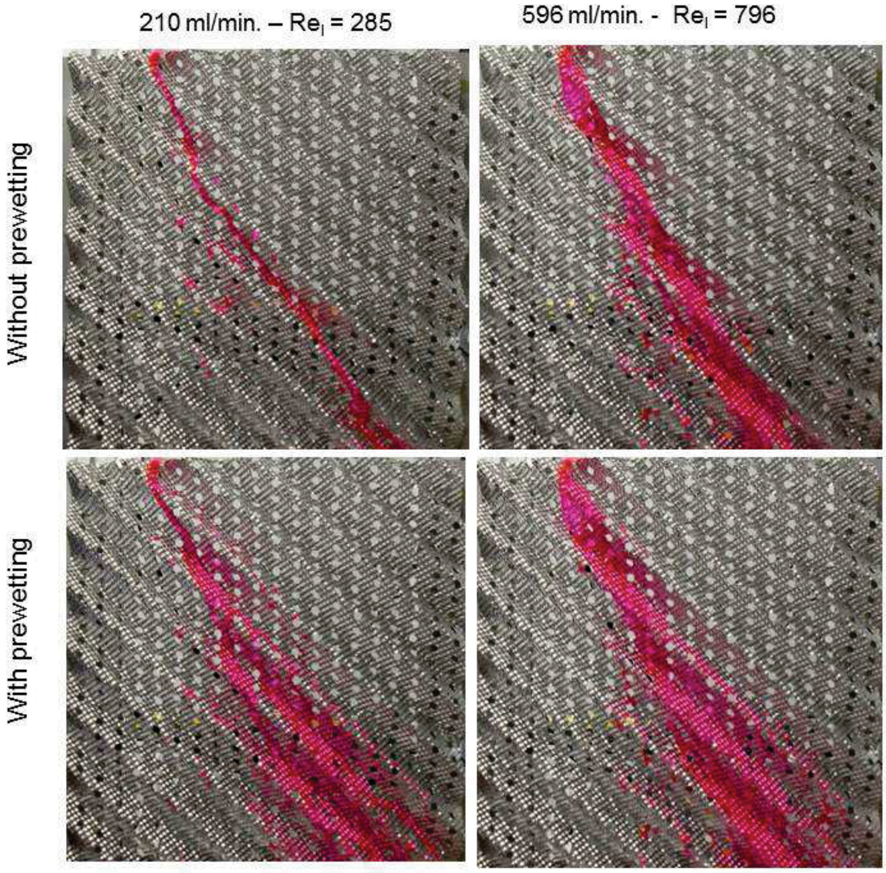

Figure D.2 Comparison of wetting due to pre-wetting for water-glycerol in corrugated sheet with perforations.

APPENDIX.E. INFLUENCE OF MICRO TEXTURES

Fig. E.1 and E.2 shows the wetting characteristics of three different testing liquids such as water and water-glycerol on two different kinds of packing namely Mellapak 350Y which has no microstructures on the surface and Mellapak 350.YB which has microstructures on the surface of the packings. Also the comparison is presented for three different liquid flow rates in all the cases. The trend of wetting for the packing with and without microstructure can be clearly seen in these figures. It is obvious that the packing with microstructures has slightly more wetting than the packing without microstructure. As all the packing studied experimentally has holes, the wetting on the back side of the packing need to be considered and it is technically difficult to capture the picture on the back side of the packing. Hence, we are restricted to present pictures of front side of the packing alone. Liquid spreads homogenous in the case of packing with microstructure which is also noted while performing the experiments.

Figure E.1 Wetting behaviour for water in two different corrugated sheets with and without microstructures. Top – Mellapak 350Y without microstructures ; Bottom – Mellapak 350Y B with microstructures.

Figure E.1

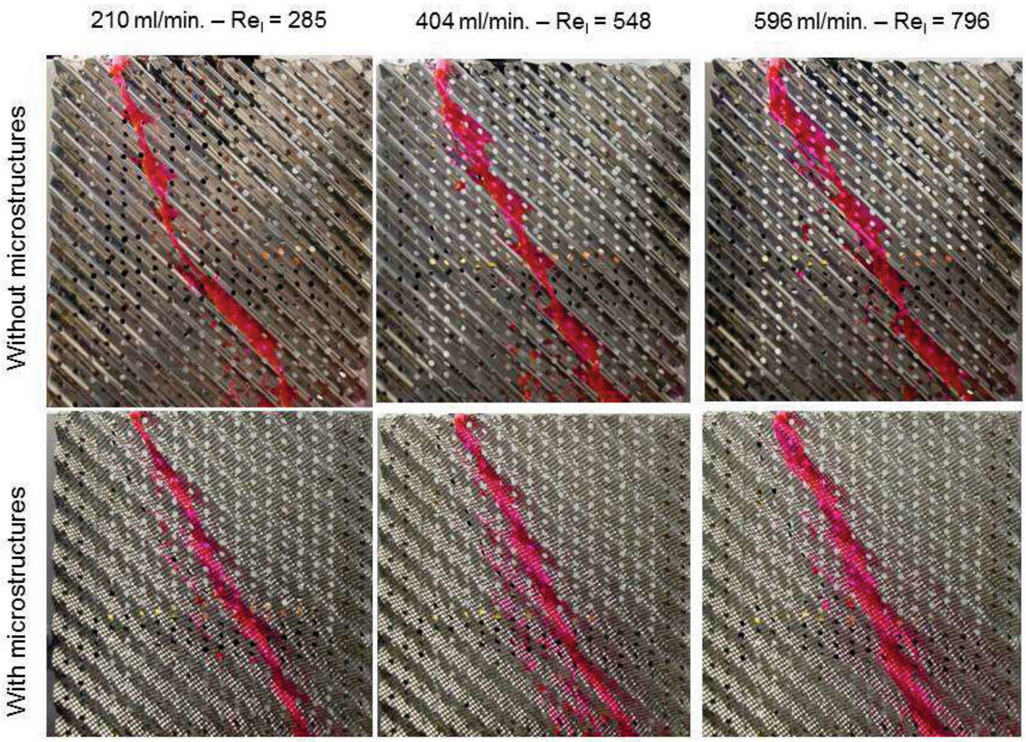

Figure E.2 Wetting behaviour for water-glycerol in two different Corrugated sheets with and without microstructures. Top – Mellapak 350Y without microstructures ; Bottom – Mellapak 350Y B with microstructures.

REFERENCES

ADOMEIT, P. 1996. *Experimentelle Untersuchung der Strömung laminar-welliger Rieselfilme.* Dissertation, RWTH Aachen.

ADOMEIT, P. & RENZ, U. 2000. Hydrodynamics of three-dimensional waves in laminar falling films. *International Journal of Multiphase Flow,* 26**,** 1183-1208.

AFERKA, S., VIVA, A., BRUNAZZI, E., MARCHOT, P., CRINE, M. & TOYE, D. 2011. Tomographic measurement of liquid hold up and effective interfacial area distributions in a column packed with high performance structured packings. *Chemical Engineering Science,* 66**,** 3413-3422.

AL-SIBAI, F. 2005. *Experimentelle Untersuchung des Wärme- und Impulstransports in welligen Rieselfilmen.* Dissertation, RWTH Aachen.

AL-SIBAI, F., LEEFKEN, A., LEL, V. & RENZ, U. 2003. Measurements of Transport Phenomena in Thin Wavy Films. *Conference on Transport Phenomena with Moving Boundaries.* Berlin.

ALEKSEENKO, S. V., BOBYLEV, A. V., EVSEEV, A. R., KARSTEN, V. M., MARKOVICH, D. M. & TARASOV, B. V. 2003. Measurements of the Liquid-Film Thickness by a Fiber-Optic Probe. *Instruments and Experimental Techniques,* 46**,** 260-264.

ALEKSEENKO, S. V., MARKOVICH, D. M., EVSEEV, A. R., BOBYLEV, A. V., TARASOV, B. V. & KARSTEN, V. M. 2008. Experimental investigation of liquid distribution over structured packing. *AIChE Journal,* 54**,** 1424-1430.

ALEKSEENKO, S. V., NAKORYAKOV, V. E. & POKUSAEV, B. G. 1985. Wave formation on vertical falling liquid films. *International Journal of Multiphase Flow,* 11**,** 607-627.

ALIX, P. & RAYNAL, L. 2008. Liquid distribution and liquid hold-up in modern high capacity packings. *Chemical Engineering Research and Design,* 86**,** 585-591.

ALIX, P., RAYNAL, L., ABBE, F., MEYER, M., PREVOST, M. & ROUZINEAU, D. 2011. Mass transfer and hydrodynamic characteristics of new carbon carbon packing: Application to CO2 post-combustion capture. *Chemical Engineering Research and Design,* 89**,** 1658-1668.

ANSYS INC. 2009a. Ansys Fluent 12.0 User Guide.

ANSYS INC. 2009b. ICEM CFD 12.1 User Guide.

ARBOGAST, T., DOUGHLAS, J. & HORNUNG, U. 1990. Derivation of the double porousity model of single phase flow via homogenization theory. *SIAM J Math Anal.,* 21**,** 823-836.

AROONWILAS, A., TONTIWACHWUTHIKUL, P. & CHAKMA, A. 2001. Effects of operating and design parameters on CO2 absorption in columns with structured packings. *Separation and Purification Technology,* 24**,** 403-411.

ATAKI, A. 2006. *Wetting of Structured Packing Elements - CFD and Experiment.* Dissertation, Technischen Universität Kaiserslautern.

ATAKI, A. & BART, H.-J. 2006. Experimental and CFD Simulation Study for the Wetting of a Structured Packing Element with Liquids. *Chem. Eng. Techn.,* 29**,** 336-347.

ATAKI, A., KOLB, P., BÜHLMANN, U. & BART, H.-J. Wetting Performance and Pressure Drop of Structured Packings: CFD and Experiment. IChemE Symp. Series No., 2006.

AUSNER, I. 2006. *Experimentelle Untersuchungen mehrphasiger Filmströmungen.* Dissertation, TU Berlin.

BATTISTA, J. & BÖHM, U. 2003. Mass Transfer In Trickle-Bed Reactors With Structured Packing. *Chemical Engineering & Technology,* 26**,** 1061-1067.

BEHRENS, M., SARABER, P. P., JANSEN, H. & OLUJIC, Z. 2001. Performance Characteristics of a Monolith-like Structured Packing. *Chem. Biochem. Eng. Q,* 15**,** 8.

BENDER, P. & MOLL, A. 2003. Modifications to Structured Packings to Increase Their Capacity. *Chemical Engineering Research and Design,* 81**,** 58-67.

BESSOU, V., ROUZINEAU, D., PRÉVOST, M., ABBÉ, F., DUMONT, C., MAUMUS, J. & MEYER, M. 2010. Performance characteristics of a new structured packing. *Chemical Engineering Science,* 65**,** 4855-4865.

BILLET, R. & SCHULTES, M. 1999. Prediction of Mass Transfer Columns with Dumped and Arranged Packings: Updated Summary of the Calculation Method of Billet and Schultes. *Chemical Engineering Research and Design,* 77**,** 498-504.

BLYTH, M. G. 2006. Film flow down an inclined plane over a three-dimensional obstacle. *Phys. Fluids,* 18**,** 052104.

BRACKBILL, J. U., KOTHE, D. B. & ZEMACH, C. 1992. A continuum method for modeling surface tension. *J. Comput. Phys.,* 100**,** 335-354.

BRAUER, H. 1971. Grundlagen der Einphasen- und Mehrphasenströmung. *Sauerländer Verlag*.

BRAVO, J. L., ROCHA, J. A. & FAIR, J. R. 1985. Mass transfer in gauze packings. *Hydrocarbon Processing,* 64 (1)**,** 91-95.

BRINKMANN, U., SCHILDHAUER, T. J. & KENIG, E. Y. 2010. Hydrodynamic analogy approach for modelling of reactive stripping with structured catalyst supports. *Chemical Engineering Science,* 65**,** 298-303.

BRUNAZZI, E., NARDINI, G., PAGLIANTI, A. & PETARCA, L. 1995. Interfacial area of mellapak packing: Absorption of 1,1,1-trichloroethane by Genosorb 300. *Chemical Engineering & Technology,* 18**,** 248-255.

CASSIE, A. B. D. 1948. Contact angles. *Discussions of the Faraday Society,* 3**,** 11-16.

CASSIE, A. B. D. & BAXTER, S. 1944. Wettability of porous surfaces. *Transactions of the Faraday Society,* 40**,** 546-551.

CHEN, J., LIU, C., LI, Y., HUANG, Y., YUAN, X. & YU, G. 2007. Experimental Investigation of Single-phase Flow in Structured Packing by LDV. *Chinese Journal of Chemical Engineering,* 15**,** 821-827.

CHEN, J., LIU, C., YUAN, X. & YU, G. 2009. CFD Simulation of Flow and Mass Transfer in Structured Packing Distillation Columns. *Chinese Journal of Chemical Engineering,* 17**,** 381-388.

DANCKWERTS, P. V. 1970. *Gas-Liquid Reactions*, Mc-Graw Hill Ed., New York.

DAVIES, J. T. & WARNER, K. V. 1969. The effect of large-scale roughness in promoting gas absorption. *Chemical Engineering Science,* 24**,** 231-240.

DE BRITO, M. H., VON STOCKAR, U., BANGERTER, A. M., BOMIO, P. & LASO, M. 1994. Effective Mass-Transfer Area in a Pilot Plant Column Equipped with Structured Packings and with Ceramic Rings. *Industrial & Engineering Chemistry Research,* 33**,** 647-656.

DETTRE, R. H. & JOHNSON, R. E. 1964. Contact Angle Hysteresis. *Contact Angle, Wettability, and Adhesion.* AMERICAN CHEMICAL SOCIETY.

DETTRE, R. H. & JOHNSON, R. E. 1965. Contact Angle Hysteresis. IV. Contact Angle Measurements on Heterogeneous Surfaces1. *The Journal of Physical Chemistry,* 69**,** 1507-1515.

DIETZE, G. 2010. *Flow Separation in Falling Liquid Films.* Dissertation, RWTH Aachen.

DUSS, M., MEIERHOFER, H. & BOMIO, P. Comparison between random and structured packings and a model to predict the efficiency of structured packing in distillation and absorption applications. Distillation and Absorption '97, 1997 Maastrict, the Netherlands. Inst. Chem. Eng. Symp. Ser. No. 142, 439 - 452.

FAIR, J. R. & BRAVO, J. L. 1990. Distillation columns containing structured packing. *Chemical Engineering Progress,* 86(1).

GREEN, C. W., FARONE, J., BRILEY, J. K., ELDRIDGE, R. B., KETCHAM, R. A. & NIGHTINGALE, B. 2007. Novel Application of X-ray Computed Tomography: Determination of Gas/Liquid Contact Area and Liquid Holdup in Structured Packing. *Industrial & Engineering Chemistry Research,* 46**,** 5734-5753.

GU, F., LIU, C. J., YUAN, X. G. & YU, G. C. 2004. CFD Simulation of Liquid Film Flow on Inclined Plates. *Chemical Engineering & Technology,* 27**,** 1099-1104.

GUALITO, J. J., CERINO, F. J., CARDENAS, J. C. & ROCHA, J. A. 1997. Design Method for Distillation Columns Filled with Metallic, Ceramic, or Plastic Structured Packings. *Industrial & Engineering Chemistry Research,* 36**,** 1747-1757.

HAROUN, Y., LEGENDRE, D. & RAYNAL, L. 2010a. Direct numerical simulation of reactive absorption in gas-liquid flow on structured packing using interface capturing method. *Chemical Engineering Science,* 65**,** 351-356.

HAROUN, Y., LEGENDRE, D. & RAYNAL, L. 2010b. Volume of fluid method for interfacial reactive mass transfer: Application to stable liquid film. *Chemical Engineering Science,* 65**,** 2896-2909.

HIGLER, A. P., KRISHNA, R., ELLENBERGER, J. & TAYLOR, R. 1999. Counter-current operation of a structured catalytically packed-bed reactor:: Liquid phase mixing and mass transfer. *Chemical Engineering Science,* 54**,** 5145-5152.

HIRT, C. W. & NICHOLS, B. D. 1981. Volume of fluid (VOF) method for the dynamics of free boundaries. *Journal of Computational Physics,* 39**,** 201-225.

HOFFMANN, A., AUSNER, I., REPKE, J.-U. & WOZNY, G. 2005. Fluid dynamics in multiphase distillation processes in packed towers. *Computers & Chemical Engineering,* 29**,** 1433-1437.

HOFFMANN, A., AUSNER, I., REPKE, J. U. & WOZNY, G. 2006. Detailed Investigation of Multiphase (Gas-Liquid and Gas-Liquid-Liquid) Flow Behaviour on Inclined Plates. *Chemical Engineering Research and Design,* 84**,** 147-154.

ILIUTA, I. & LARACHI, F. 2001. Mechanistic Model for Structured-Packing-Containing Columns: Irrigated Pressure Drop, Liquid Holdup, and Packing Fractional Wetted Area. *Industrial & Engineering Chemistry Research,* 40**,** 5140-5146.

ILIUTA, I., PETRE, C. F. & LARACHI, F. 2004. Hydrodynamic continuum model for two-phase flow structured-packing-containing columns. *Chemical Engineering Science,* 59**,** 879-888.

IVANOVA, S., LOUIS, B., MADANI, B., TESSONNIER, J. P., LEDOUX, M. J. & PHAM-HUU, C. 2007. ZSM-5 Coatings on β-SiC Monoliths: Possible New Structured Catalyst for the Methanol-to-Olefins Process. *The Journal of Physical Chemistry C,* 111**,** 4368-4374.

JOHNSON, R. E. & DETTRE, R. H. 1964a. Contact Angle Hysteresis. *Contact Angle, Wettability, and Adhesion.* AMERICAN CHEMICAL SOCIETY.

JOHNSON, R. E. & DETTRE, R. H. 1964b. Contact Angle Hysteresis. III. Study of an Idealized Heterogeneous Surface. *The Journal of Physical Chemistry,* 68**,** 1744-1750.

KISTER, H. 1992. *Distillation Design*, McGraw-Hill.

KOHRT, M. 2011. *Experimentelle Untersuchung von Stoff transport und Fluiddynamik bei Riesellmströmungen auf mikrostrukturierten Oberflächen.* Dissertation, TU Berlin.

KOHRT, M., AUSNER, I., WOZNY, G. & REPKE, J.-U. 2011. Texture influence on liquid-side mass transfer. *Chemical Engineering Research and Design,* 89**,** 1405-1413.

LARACHI, F., PETRE, C. F., ILIUTA, I. & GRANDJEAN, B. 2003. Tailoring the pressure drop of structured packings through CFD simulations. *Chemical Engineering and Processing,* 42**,** 535-541.

LOSER, T. 2002. *Berechnung der zweiphasigen Strömung in Schichtungen.* Dissertation, Leibnitz Universität Hannover.

LUO, H. 2006. Effect of inertia on film flow over oblique and three-dimensional corrugations. *Phys. Fluids,* 18**,** 078107.

LUO, H. & POZRIKIDIS, C. 2007. Gravity-driven film flow down an inclined wall with three-dimensional corrugations. *Acta Mechanica,* 188**,** 209-225.

LUO, S. J., FEI, W. Y., SONG, X. Y. & LI, H. Z. 2008. Effect of channel opening angle on the performance of structured packings. *Chemical Engineering Journal,* 144**,** 227-234.

MAHR, B. 2007. *Numerisches Berechnen und tomographisches Messen zwei-phasiger Strömugsfelder in geordneten Schichtungen.* Dissertation, Leibnitz Universität Hannover.

MAHR, B. & MEWES, D. Modelling and measurement of macroscopic flow fields in structured packings. Distillation and Absorption, 2006a London, UK.

MAHR, B. & MEWES, D. X-ray tomographic visualization of liquid spreading in structured packings using contrast-agent tracer. International Heat Transfer Conference IHTC-13, 2006b Australia.

MAHR, B. & MEWES, D. 2007. CFD Modelling and Calculation of Dynamic Two-Phase Flow in Columns Equipped with Structured Packing. *Chemical Engineering Research and Design,* 85**,** 1112-1122.

MCGLAMERY, G. G. 1988. *Liquid Film Transport Characteristics of Textured metal Surfaces.* Dissertatino, The University of Texas at Austin.

MEWES, D., LOSER, T. & MILLIES, M. 1999. Modelling of two-phase flow in packings and monoliths. *Chem. Eng. Sci.,* 54**,** 4729-4747.

NICOLAIEWSKY, E. M. A. & FAIR, J. R. 1998. Liquid Flow over Textured Surfaces. 1. Contact Angles. *Industrial & Engineering Chemistry Research,* 38**,** 284-291.

NICOLAIEWSKY, E. M. A., TAVARES, F. W., RAJAGOPAL, K. & FAIR, J. R. 1999. Liquid film flow and area generation in structured packed columns. *Powder Technology,* 104**,** 84-94.

NUSSELT, W. 1916a. Die Oberflächenkondensation des Wasserdampfes. *Vereines deutscher Ingenieure-Zs,* 60**,** 541-546.

NUSSELT, W. 1916b. Die Oberflächenkondensation des Wasserdampfes. *Vereines deutscher Ingenieure-Zs,* 60**,** 569-575.

OLIVER, J. P., HUH, C. & MASON, S. G. 1980. An experimental study of some effects of solid surface roughness on wetting. *Colloids and Surfaces,* 1**,** 79-104.

OLUJIC, Z., BEHRENS, M., COLLI, L. & PAGLIANTI, A. 2004. Predicting the Efficiency of Corrugated Sheet Structured packings with large specific surface area. *Chem. Biochem. Eng. Q,* 18**,** 89.

OLUJIC, Z., KAMERBEEK, A. B. & DE GRAAUW, J. 1999. A corrugation geometry based model for efficiency of structured distillation packing. *Chemical Engineering and Processing,* 38**,** 683-695.

OLUJIC, Z., SEIBERT, A. F. & FAIR, J. R. 2000. Influence of corrugation geometry on the performance of structured packings: an experimental study. *Chemical Engineering and Processing,* 39**,** 335-342.

ONDA, K., TAKEUCHI, H. & OKUMOTO, Y. 1968. Mass transfer Coefficients between Gas and Liquid phases in packed columns. *J. Chem. Eng. Jpn.,* 1**,** 56.

PANGARKAR, K., SCHILDHAUER, T. J., VAN OMMEN, J. R., NIJENHUIS, J., KAPTEIJN, F. & MOULIJN, J. A. 2008. Structured Packings for Multiphase Catalytic Reactors. *Industrial & Engineering Chemistry Research,* 47**,** 3720-3751.

PASCHKE, S. 2011. *Experimentelle Analyse ein- und zweiphasiger Filmströmungen auf glatten und strukturierten Oberflächen.* Dissertation, TU Berlin.

PASCHKE, S., REPKE, J. U. & WOZNY, G. 2007. Analyse heterogener Filmströmungen auf Packungsmaterialien mittels einer neuen microPIV- Methode. *Chem. Ing. Tech. 79*.

PATENT, S. 2005. *SPS Patent*.

PETRE, C. F., LARACHI, F., ILIUTA, I. & GRANDJEAN, B. P. A. 2003. Pressure drop through structured packings: Breakdown into the contributing mechanisms by CFD modeling. *Chemical Engineering Science,* 58**,** 163-177.

PONTER, A. B. & AU-YEUNG, P. H. 1984. Influence of Liquid Viscosity on Effective Interfacial Area in Packed Columns. *Chemie Ingenieur Technik,* 56**,** 701-703.

PONTER, A. B., DAVIES, G. A., BEATON, W. & ROSS, T. K. 1967. The measurement of contact angles under equilibrium and mass-transfer conditions. *International Journal of Heat and Mass Transfer,* 10**,** 733-736.

RAYNAL, L., BALLAGUET, J.-P. & BARRERE-TRICCA, C. 2004a. Determination of mass transfer characteristics of co-current two-phase flow within structured packing. *Chemical Engineering Science,* 59**,** 5395-5402.

RAYNAL, L., BEN RAYANA, F. & ROYON-LEBEAUD, A. 2009. Use of CFD for CO2 absorbers optimum design : from local scale to large industrial scale. *Energy Procedia,* 1**,** 917-924.

RAYNAL, L., BOYER, C. & BALLAGUET, J.-P. 2004b. Liquid Holdup and Pressure Drop Determination in Structured Packing with CFD Simulations. *The Canadian Journal of Chemical Engineering,* 82**,** 871-879.

REPKE, J. U., AUSNER, I., PASCHKE, S., HOFFMANN, A. & WOZNY, G. 2007. On the Track to Understanding Three Phases in One Tower. *Chemical Engineering Research and Design,* 85**,** 50-58.

REPKE, J. U. & WOZNY, G. 2002. Experimental Investigations of Three-Phase Distillation in a Packed Column. *Chemical Engineering & Technology,* 25**,** 513-519.

ROCHA, J. A., BRAVO, J. L. & FAIR, J. R. 1993. Distillation columns containing structured packings: a comprehensive model for their performance. 1. Hydraulic models. *Industrial & Engineering Chemistry Research,* 32**,** 641-651.

ROCHA, J. A., BRAVO, J. L. & FAIR, J. R. 1996. Distillation Columns Containing Structured Packings: A Comprehensive Model for Their Performance. 2. Mass-Transfer Model. *Industrial & Engineering Chemistry Research,* 35**,** 1660-1667.

SAID, W., NEMER, M. & CLODIC, D. 2011. Modeling of dry pressure drop for fully developed gas flow in structured packing using CFD simulations. *Chemical Engineering Science,* 66**,** 2107-2117.

SHETTY, S. & CERRO, R. L. 1993. Flow of a thin fiom over a periodic surface. *International Journal of Multiphase Flow,* 19**,** 1013-1027.

SHETTY, S. & CERRO, R. L. 1997. Fundamental Liquid Flow Correlations for the Computation of Design Parameters for Ordered Packings. *Industrial & Engineering Chemistry Research,* 36**,** 771-783.

SHETTY, S. & CERRO, R. L. 1998. Spreading of a Liquid Point Source over a Complex Surface. *Industrial & Engineering Chemistry Research,* 37**,** 626-635.

SHI, M. G. & MERSMANN, A. 1985. *Effective interfacial area in packed columns,* Weinheim, ALLEMAGNE, VCH.

SHILKIN, A., HEINEN, K., GROßMANN, C., LAUTENSCHLEGER, A., JANZEN, A. & KENIG, E. Y. On the development of an energy efficient packing for vacuum distillation. *In:* DE HAAN, A. B., KOOIJMAN, H. & GORAK, A., eds. Distillation and Absorption 2010, 2010 Eindhoven, The Netherlands. 653 - 658.

SHILKIN, A. & KENIG, E. Y. 2005. A new approach to fluid separation modelling in the columns equipped with structured packings. *Chemical Engineering Journal,* 110**,** 87-100.

SHILKIN, A., KENIG, E. Y. & OLUJIC, Z. 2006. Hydrodynamic-analogy-based model for efficiency of structured packing columns. *AIChE Journal,* 52**,** 3055-3066.

SHOJAEE, S., HOSSEINI, S. H., RAFATI, A. & AHMADI, G. 2011. Prediction of the Effective Area in Structured Packings by Computational Fluid Dynamics. *Industrial & Engineering Chemistry Research,* 50**,** 10833-10842.

SPEKULJAK, Z. 1986. *Modelacion de Rellenos Regullares de Alta Eficienca Para la Transferencia de Materia.* Ph.D. , Universidad Nacional del Litoral.

SPIEGEL, L. & MEIER, W. Correlations of the performance characteristics of the various Mellapak types. Distillation and Absorption 1987, 1988 Brighton, UK. Inst. Chem. Symp. Ser. 104, A203 - A215.

STEPHAN, M. & MAYINGER, F. 1992. Experimental and Analytical Study on Countercurrent Flow Limitation in Vertical Gas/Liquid Flows. *Chem. Eng. Tech.,* 15**,** 51 - 62.

STOTER, F. 1993. *Modeling of maldistribution in structured packings: from detail to column design.* Dissertation Delft University of Technology.

STOTER, F., OLUJIC, Z. & DE GRAAUW, J. 1993. Modelling and measurement of gas flow distribution in corrugated sheet structured packings. *The Chemical Engineering Journal and the Biochemical Engineering Journal,* 53**,** 55-66.

SUBAWALLA, H., GONZÁLEZ, J. C., SEIBERT, A. F. & FAIR, J. R. 1997. Capacity and Efficiency of Reactive Distillation Bale Packing: Modeling and Experimental Validation. *Industrial & Engineering Chemistry Research,* 36**,** 3821-3832.

SUESS, P. & SPIEGEL, L. 1992. Hold-up of mellapak structured packings. *Chemical Engineering and Processing,* 31**,** 119-124.

SZULCZEWSKA, B., ZBICINSKI, I. & GÓRAK, A. 2003. Liquid Flow on Structured Packing: CFD Simulation and Experimental Study. *Chemical Engineering & Technology,* 26**,** 580-584.

TSAI, R. E., SCHULTHEISS, P., KETTNER, A., LEWIS, J. C., SEIBERT, A. F., ELDRIDGE, R. B. & ROCHELLE, G. T. 2008. Influence of Surface Tension on Effective Packing Area. *Industrial & Engineering Chemistry Research,* 47**,** 1253-1260.

VALLURI, P. 2004. *Multiphase Fluid Dynamics in Structured Packings.* Imperial College London.

VALLURI, P., MATAR, O. K., HEWITT, G. F. & MENDES, M. A. 2005. Thin film flow over structured packings at moderate Reynolds numbers. *Chemical Engineering Science,* 60**,** 1965-1975.

VALLURI, P., MATAR, O. K., MENDES, M. A. & HEWITT, G. F. 2002. Modelling Hydrodynamics and Mass Transfer in Structured Packings - A Review. *Multiphase Science and Technology,* 14.

VAN BATEN, J. M., ELLENBERGER, J. & KRISHNA, R. 2001a. Hydrodynamics of reactive distillation tray column with catalyst containing envelopes: experiments vs. CFD simulations. *Catalysis Today,* 66**,** 233-240.

VAN BATEN, J. M., ELLENBERGER, J. & KRISHNA, R. 2001b. Radial and axial dispersion of the liquid phase within a KATAPAK-S® structure: experiments vs. CFD simulations. *Chemical Engineering Science,* 56**,** 813-821.

VAN BATEN, J. M. & KRISHNA, R. 2001. Liquid-phase mass transfer within KATAPAK-S® structures studied using computational fluid dynamics simulations. *Catalysis Today,* 69**,** 371-377.

VAN BATEN, J. M. & KRISHNA, R. 2002. Gas and liquid phase mass transfer within KATAPAK-S® structures studied using CFD simulations. *Chemical Engineering Science,* 57**,** 1531-1536.

VIVA, A., AFERKA, S., BRUNAZZI, E., MARCHOT, P., CRINE, M. & TOYE, D. 2011a. Processing of X-ray tomographic images: A procedure adapted for the analysis of phase distribution in MellapakPlus 752.Y and Katapak-SP packings. *Flow Measurement and Instrumentation,* 22**,** 279-290.

VIVA, A., AFERKA, S., TOYE, D., MARCHOT, P., CRINE, M. & BRUNAZZI, E. 2011b. Determination of liquid hold-up and flow distribution inside modular catalytic structured packings. *Chemical Engineering Research and Design,* 89**,** 1414-1426.

WEN, X., AKHTER, S., AFACAN, A., NANDAKUMAR, K. & CHUANG, K. T. 2007. CFD modeling of columns equipped with structured packings: I. Approach based on detailed packing geometry. *Asia-Pacific Journal of Chemical Engineering,* 2**,** 336-344.

WENZEL, R. N. 1936. Resistance of Solid surfaces to wetting by water. *Industrial & Engineering Chemistry,* 28**,** 988-994.

WIERSCHEM, A. & AKSEL, N. 2003. Instability of a liquid film flowing down an inclined wavy plane. *Physica D: Nonlinear Phenomena,* 186**,** 221-237.

WIERSCHEM, A., BONTOZOGLOU, V., HEINING, C., UECKER, H. & AKSEL, N. 2008. Linear resonance in viscous films on inclined wavy planes. *International Journal of Multiphase Flow,* 34**,** 580-589.

WOERLEE, G. F., BERENDS, J., OLUJIC, Z. & DE GRAAUW, J. 2001. A comprehensive model for the pressure drop in vertical pipes and packed columns. *Chemical Engineering Journal,* 84**,** 367-379.

XU, Y. Y., PASCHKE, S., REPKE, J. U., YUAN, J. Q. & WOZNY, G. 2008. Portraying the Countercurrent Flow on Packings by Three-Dimensional Computational Fluid Dynamics Simulations. *Chemical Engineering & Technology,* 31**,** 1445-1452.

YOUNG, T. 1805. An Essay on the Cohesion of Fluids. *Philosophical Transactions of the Royal Society of London,* 95**,** 65-87.

YUAN, Y., HAN, M., CHENG, Y., WANG, D. & JIN, Y. 2005. Experimental and CFD analysis of two-phase cross/countercurrent flow in the packed column with a novel internal. *Chemical Engineering Science,* 60**,** 6210-6216.

ZHAO, L. & CERRO, R. L. 1992. Experimental characterization of viscous film flows over complex surfaces. *International Journal of Multiphase Flow,* 18**,** 495-516.

ZUIDERWEG, F. J. & HARMENS, A. 1958. The influence of surface phenomena on the performance of distillation columns. *Chemical Engineering Science,* 9**,** 89-103.

LIST OF PUBLICATIONS/CONFERENCES AND WORKSHOP ATTENDED/WORK SUPERVISED

List of Publications

Subramanian, K.; Paschke, S.; Repke, J.-U.; Wozny, G.; Drag Modelling in CFD Simulation to gain insight of Packed Columns, In: Chemical Engineering Transactions, 17, 561 – 566, doi: 10.3303/CET0917094.

Paschke , S.; **Subramanian, K.;** Repke, J.-U.; Wozny, G.; Effect of Countercurrent Gas Flow on Liquid Films, 5th International Berlin Workshop on Transport Phenomena with moving boundaries; ISBN : 978 – 3 – 18 – 392003 -7.

Subramanian, K.; Wozny, G.; Analysis of Hydrodynamics of Fluid flow in Corrugated Sheets of Packing, International Journal of Chemical Engineering, Volume 2012 (2012), doi: 10.1155/2012/838965.

Conference and Workshop Attended

Subramanian, K.; Paschke, S.; Repke, J.-U.; Wozny, G.; Drag Modelling in CFD Simulation to gain insight of Packed Columns, 9th International Conference on Chemical and Process Engineering (Icheap9); Rome, Italy ; 10th – 13th May 2009.

Subramanian,K.; Multiphase Flow- Simulation, Experiment and Applications**;** Dresden; 26th – 28th May 2009.

Paschke , S.; **Subramanian, K.;** Repke, J.-U.; Wozny, G.; Effect of Countercurrent Gas Flow on Liquid Films, 5th International Berlin Workshop on Transport Phenomena with moving boundaries; Berlin; 8th – 9th October 2009.

Subramanian, K.; Paschke, S.; Repke, J.-U.; Wozny, G.; Computational Analysis of Corrugated Sheets of Packing, 10AIChE - 2010 AIChE Annual Meeting, Salt Lake City, Utah; 7th – 12th November 2010.

Works Supervised

Sommerwerk, T.; Woltmann, P.; Benetzungsexperimente an komplexen Oberflachen; Praktikum (2011).

Vogt, A.; Lepenies, E.; Drescher, A.; Benetzungsexperimente an komplexen Oberflachen; Praktikum (2011).

DECLARATION

I hereby declare that I completed this work without any improper help from a third party and without using any aids other than those cited. All ideas derived directly or indirectly from other sources are identified as such.

I did not seek the help of a professional doctorate-consultant. Only persons identified as having done so received any financial payment from me for any work done for me.

This thesis has not previously been submitted to another examination authority in the same or similar form in Germany or abroad.

April 15, 2015 **Kumar Subramanian**